EFFICIENT COMPUTING OF POTENTIAL FIELDS INDUCED BY POINT SOURCES IN THIN PERFORATED SHELL STRUCTURES

by

Volodymyr Borodin

A Dissertation Submitted in Partial Fulfillment

of the Requirements for the Degree of

Doctor of Philosophy in Computational Sciences

Middle Tennessee State University

December 2014

Dissertation Committee:

Dr. Yuri Melnikov, Chair

Dr. Abdul Khaliq

Dr. Tibor Koritsanszky

Dr. William Robertson

Dr. John Wallin

ACKNOWLEDGEMENTS

I would like to express my deepest gratitude to my advisor, Dr. Yuri Afanasievich Melnikov, for his remarkable guidance, caring, and providing me with an excellent atmosphere for doing research. His professionalism and tendency to perfectness in every aspect of work truly inspired me to do my best in achieving goals. Dr. Melnikov showed his unlimited patience and support every time I asked for help. Thank you, Yuri Afanasievich, for the perfect example of what a real teacher and man should be like.

I would also like to thank Dr. John Wallin, the director of Computational Sciences Program at Middle Tennessee State University, for the valuable advices and financial support through all my study.

ABSTRACT

Potential fields of various physical nature might significantly affect viability of structures in automobiles, aircraft, and other areas of contemporary engineering. That is why accurate analysis of potential fields, occurring in elements of structures, is required for the exploration of conditions of their predetermined functioning. Thermoelasticity, for example, is a specific branch of natural sciences where information about thermal fields is especially critical. Fields induced by point sources represent an important particular case quite often occurring in reality.

The present project aims at the investigation of potential fields in thin shell structures made of conductive materials. Our manual is conditionally viewed as consisting of three segments, the first of which deals with point sources in single shell fragments of standard geometry (cylindrical, spherical, toroidal, etc.). The second segment is devoted to joint shell structures composed of fragments of different geometries, whilst single fragments and joint structures weakened with apertures are considered in the last segment.

The Green's function formalism constitutes theoretical background of our work. Exploring potential fields generated by point sources in single shell fragments, we use the Green's function method, possibility of which implementation had been advocated, for this class of problems, a few decades ago. We have further developed this approach by obtaining computer-friendly representations of Green's functions for a broad variety of boundary-value problems stated for the Laplace equation written in geographical coordinates.

In approaching solid joint shell structures, the classical Green's function formalism fails. We turn therefore to the matrix of Green's type notion also introduced awhile ago, and our focus is on obtaining readily computable matrices for a score of structures.

A Green's function-based algorithm, that allows an accurate computation of potential fields induced in shell structures weakened with apertures, is developed.

TABLE OF CONTENTS

LIST OF TABLES

LIST OF FIGURES

1 Introduction

Study of potential fields had traditionally attracted researchers who worked in nearly every branch of natural science and engineering, and it continues to remain in the sphere of their interest in nowadays. This is so because a vast number of phenomena and processes that are going on in real life are potential in nature. The most important among those are: steady-state heat conduction in solids [25, 45, 86, 91], magneto- and electrostatics [2, 23, 34, 35, 82], gravitation [29, 51, 62], steady-state concentration of substance in the media [41, 85], and so on. Mathematically, potential phenomena and processes reduce to boundary-value problems stated for Laplace and Poisson equation. Simplest of those problems allow analytical solutions, for most others – numerical methods appear efficient.

The heat transfer, in particular, represents one of the significant phenomena that requires professional treatment in engineering. This phenomenon is crucial in the decision making for experts who work on either construction of new or modification of modern machines and devices. To name just some of the engineering sciences, where the heat conduction should be taken into account, one might recall the heat insulation [42], laser welding [7], drilling [87], geodesy [27], plasma study [17], etc. The most recent area of interest for the heat transfer is in the nano-engineering [61, 71, 78].

Three different types of the heat transfer problems are distinguished in applications based on their spatial dimensionality. One-dimensional problems occur when one of the spatial dimensions of the considered object is significantly larger compared to the other two, which allows to neglect the heat flow in their directions. Examples of such objects could be long and thin beams, tubes, spiral-shaped heating elements, and so on [63, 80]. Two-dimensional heat transfer occurs, when only one of the dimensions of the object is negligibly small, but two others must be taken into consideration. Such problems arise, when we consider heat transfer in different plates, shells, jackets, etc. [54, 70, 72] If none of the dimensional sizes of the considered object is negligible, we have to stay within the scope of three-dimensional heat conduction scenario. It occurs, for example, when one evaluates the heat conduction inside fluid or gas containing reservoirs [59], or if the heat distribution must be found in thick walls weakened with some cavities or holes [84]. Three-dimensional problem statements are also unavoidable if the air conditioning system is developed to cool down industrial or residential rooms [60].

Another approach to the classification of heat transfer problems touches upon the time variable. If the heat distribution in a system depends not only on spatial variables but on time as well, then the heat transfer is transient, if the heat distribution is only the spatial variables dependent function and does not depend on time, then the process reaches the so-called steady-state phase. Transient heat transfer is studied, when we are interested in actual heat distribution through the space within the time period prior to the steady state is reached, if ever [8, 36, 76].

If the heat in solids is distributed due to the heat conduction mechanism, then this is where the classical heat equation [19, 31] comes to the picture. In the case of a steady-state situation, the heat equation degenerates to either Laplace (if there are no internal sources of energy available) or Poisson equation.

Two different types of problems are distinguished for the heat equation. If the shape of the object under consideration, the initial and boundary conditions, the thermal coefficients of the material of which the object is made (we will refer to all of these as the initial data) all are given, then we face the so-called direct problem formulation. Direct problems have traditionally been considered and solved in science and engineering for centuries. If, in contrast to the direct formulation, the solution of a heat conduction problem is available, but some of the initial data are missed, then the so-called inverse or semi-inverse problems take place. This type of problems attracts more and more attention nowadays. Many scientists devoted their efforts to this subject using methods based on various techniques, such as finite-difference method [65], fundamental solution method [33], Green's function-based methods [28], genetic algorithms [64], and so on. Other scientists focus on estimating the heat transfer coefficients using iterative regularization method [69], input estimation approach [77], or other techniques. Inverse problems for potential fields also arise in other fields of science, for example, medicine and geophysics [3], where the electrostatic potential around cardio-stimulators, or gravitational forces within different Earth layers are studied.

Theory of inverse problems [5, 57, 72, 83] is much more complex compared to the theory of direct problems, because inverse problems are generally speaking ill-posed, which implies that their solution must not necessarily vary a small amount if the initial data are slightly changed. As to the selection of numerical methods, that have to be used to obtain the solution of inverse problems, engineers have to be very delicate, because rounding up initial data, which is practically unavoidable, might result in large errors in the solution. That is why various regularization procedures are usually recommended [57, 72, 74] to provide reliable results for inverse problems.

There is no (and could not be) a general consensus on which particular method is the best for all heat conduction problems. Many scientists put their effort to find the analytical solution for some simple or specific cases [4, 43, 46]. The fundamental work, which has been done in this field, is efficiently summarized in [79], which provides a score of efficient analytic techniques for solving heat conduction problems. The key emphasis of the study of Wang et al. [79] is made on the wave equation, steady-state heat conduction equation, mixed problems and Cauchy problems for the hyperbolic heat conduction equation, dual-phase-lagging heat conduction equation, and other potential phenomena related equations. However that remarkable work does not consider important class of problems posed in multi-layer structures, where some analytical approaches have later been proven to be efficient. See [52] for more information on heat conduction in one-dimensional composite slabs, or [39] for multi-layer heat conduction problems posed on a sphere.

Another popular in applied mathematical approach is to design a general numerical algorithm which would be capable to solve a certain class of problems. There exist a vast number of numerical methods to solve partial differential equations in general and heat conduction equation in particular. In some of them the uniform mesh over the domain is used to calculate values at grid-points [1, 55], while in others the mesh is nonuniform [60]. In order to achieve higher accuracy and low computational cost, the entire class of the so-called meshless method was developed (see, for example, [6, 67, 88]). Though, numerical methods enable us to solve a wide range of problems compare to analytic approaches, their vulnerability is oscillations, which occur at points of discontinuity. To overcome this phenomenon, a number of methods have been proposed and is referred to as Gibb's phenomenon. To name a few, Laplace transform-based control-volume special schemes [20], characteristics-based total variation diminishing scheme [81], hybrid Green's function-based method [21], and some others.

Many authors combine the knowledge and experience from other fields of science to come up with the solution for yet unsolved problems. For example, in [3] the moment theory was successfully applied for a score of problems dealing with potential fields; machine-learning schemes based on generic algorithms were summoned to solve inverse problems in heat conduction in [64]; Cheng and Wu [22] combined body-fitted grid generation and conjugate gradient methods to achieve high accuracy in solving heat conduction problems.

Mostly recommended for engineers numerical approaches to the solution of direct heat conduction problems are based on either the finite difference method (FDM) [7, 38, 65] or the finite element method (FEM) [40, 44, 56]. These methods reduce the original initial-boundary-value problem (transient formulation) or boundary-value problem (steady-state case) to some linear algebra problems for which well-established computer friendly routines are available in most contemporary software. The main advantage of the finite difference schemes is their formal ease, but practical implementation of them meets many constraints coming up, in particular, from convergence requirements, shape irregularity of the region, and enormous computer time consumption. For the FEM, the region's shape does not represent an important issue, because a proper mesh pattern can quite accurately approximate the region. But practical creation of such a mesh is very individual for each region and could significantly drop the method's efficiency.

An alternative to the FDM and FEM, that was quite recently introduced [18] into industrial applications, is the so-called boundary element method (BEM). It reduces boundary-value problem for a partial differential equation to some integral or integral-type functional equations. The numerical algorithm, based on a semi-analytical approach developed in the present study, is relevant to the BEM.

The present work is devoted to potential fields induced in thin-walled structures, implying that some two-dimensional boundary-value problems should be considered for second order partial differential equations in regions representing fragments of middle surfaces of those structures. We are going to develop computationally efficient semi-analytical techniques for obtaining potential fields generated by point-concentrated sources in assemblies of thin-walled shells. The assemblies of shells to be considered are composed of fragments representing standard shells of revolution (cylindrical, spherical, toroidal, and so on), each of which is made of an individual homogeneous isotropic conductive material, contains some foreign inclusions, and might be weakened with apertures. This results in an intricate situation where we arrive at some boundary-value problems for sets of two-dimensional Laplace equations written in geographical coordinates specific for each shell fragment.

Among other factors, building up complexity of the problems considered in the present study, is, in particular, the fact that the problems are set up in inhomogeneous multiply-connected regions of irregular configuration. This factor makes merely impossible application of pure analytical methods for their solution. The semi-analytical approach, which is developed instead in this study and whose efficiency is demonstrated herein, belongs to the classical [53, 75] boundary integral equation (BIE) group of methods, which are predecessors of the BEM. The key point of those methods is that they are meshless [24, 68, 89] in nature, implying that the solution of the original boundary-value problem for a governing partial differential equation is expressed in a form of an integral representation whose kernel is the fundamental solution of the considered PDE. This reduces the original problem to a boundary integral equation which is to solve numerically. This approach provides the users with two significant advantages. First, the dimensionality of the original boundary-value problem reduces, and, second, not differential but integral operators require some numerical approximation.

To further modify the classical BIE approach to boundary-value problems, its Green's function version (see, for example, [48]) had been proposed. The key idea of this version is the use of some Green's functions as kernels of boundary integrals representing the problem's solution. This further elevates the computational effectiveness of the BIE method, because some of the boundary conditions in the original problem formulation are supposed to be exactly satisfied prior to a computational phase of the solution process. But, on another hand, a notable drawback of this version of the BIE method is the necessity for the user to have a required Green's function available. Note that a vast number of Green's functions for a variety of boundary-value problems can, for instance, be found in [26, 48, 50].

Since many of the problems considered in the present study do not deal with a single PDE but rather with sets of equations, neither the classical BIE methods nor their Green's function version can be directly implemented. With this in mind, to properly treat such complex problems, we make use of the extension of the Green's function formalism proposed earlier in [48]. This gives birth to the notion of matrix of Green's type. Specific matrices of Green's type, required for present work, are constructed for solid shell assemblies. Either compact analytical expressions for those matrices or some of their compact computer-friendly series representations are obtained.

So, in the present study we are going to focus on the boundary element method, with an emphasis on one of its Green's function modifications. We feel necessity to show the step-by-step algorithm for the construction of Green's functions for a number of boundary-value problems to be considered. Our construction procedure for required Green's functions is based on the classical [31] separation of variables method whose essential component is a Green's function for a corresponding ordinary differential equation. That is why we begin our presentation with the latter subject, limiting ourself to the case of second order equations. Two standard [49] approaches are reviewed in necessary detail. We will frequently refer to the results presented here and implement them later in this manual.

Consider a linear second order homogeneous ordinary differential equation with variable coefficients on the interval $[a, b]$, which is not supposed to be necessarily finite,

$$L\left[y\left(x\right)\right] \equiv p_0\left(x\right) y''\left(x\right) + p_1\left(x\right) y'\left(x\right) + p_2\left(x\right) y\left(x\right) = 0 \tag{1.1}$$

and subject it to the homogeneous boundary conditions

$$M_k\left(y; a, b\right) \equiv \sum_{j=0}^{1} \left[\alpha_j^k y^{(j)}\left(a\right) + \beta_j^k y^{(j)}\left(b\right)\right] = 0, \quad k = 1, 2 \tag{1.2}$$

where $p_i\left(x\right)$ $(i = 0, 1, 2)$ are continuous functions on $[a, b]$, with $p_0\left(x\right) \neq 0$. Let M_k be linearly independent operators, with α_j^k, β_j^k representing constants. The superscript (j) stands for the derivative order. It worth noting that each standard boundary condition (Dirichlet, Neumann, and Robin) follows from (1.2) as a particular case. The form in (1.2) includes also the case of periodic boundary conditions.

If the boundary-value problem in (1.1)-(1.2) is well-posed, providing only the trivial solution, then its unique Green's function $g(x, s)$ exists possessing the following four properties, for any arbitrarily fixed point $s \in (a, b)$:

1. $g(x, s)$ satisfies the governing equation in (1.1) everywhere except for $x = s$, i.e.:

$$L\left[g\left(x, s\right)\right] = 0, \quad x \in \left(a, s\right) \cup \left(s, b\right), \tag{1.3}$$

2. $g(x, s)$ is continuous at $x = s$

$$\lim_{x \to s^+} g\left(x, s\right) = \lim_{x \to s^-} g\left(x, s\right), \tag{1.4}$$

3. the first derivative of $g(x, s)$ has removable discontinuity at $x = s$, to satisfy the relation

$$\lim_{x \to s^+} \frac{\partial g\left(x, s\right)}{\partial x} - \lim_{x \to s^-} \frac{\partial g\left(x, s\right)}{\partial x} = -\frac{1}{p_0\left(s\right)}, \tag{1.5}$$

where $p_0(x)$ is the leading coefficient of the equation in (1.1), and

4. $g(x,s)$ satisfies the boundary conditions in (1.2), that is

$$M_k\left(g;a,b\right)=0,\quad k=1,2. \tag{1.6}$$

To prove the existence of the Green's function for the boundary-value problem in (1.1)-(1.2), we follow the classical [31] straightforward procedure. In doing so assume that $y_1(x)$ and $y_2(x)$ are two linearly independent particular solutions of the equation in (1.1), and look for the Green's function in the form

$$g(x,s)=\begin{cases} y_1\left(x\right)A_1\left(s\right)+y_2\left(x\right)A_2\left(s\right), & x\leq s \\ y_1\left(x\right)B_1\left(s\right)+y_2\left(x\right)B_2\left(s\right), & x\geq s \end{cases} \tag{1.7}$$

automatically satisfying the first defining property in (1.3).

Indeed, both branches of (1.7) are linear combinations of $y_1(x)$ and $y_2(x)$, and each of them is therefore a solution of (1.1). In order to find the unknown functions $A_i(s)$, and $B_i(s)$ we refer to the remaining properties. By satisfying the property in (1.4) one comes up with the following equation:

$$y_1\left(s\right)C_1\left(s\right)+y_2\left(s\right)C_2\left(s\right)=0 \tag{1.8}$$

where

$$C_i\left(s\right)=B_i\left(s\right)-A_i\left(s\right),\quad i=1,2 \tag{1.9}$$

From the property in (1.5) it follows that

$$y_1'\left(s\right)C_1\left(s\right)+y_2'\left(s\right)C_2\left(s\right)=-\frac{1}{p_0\left(s\right)} \tag{1.10}$$

Relations in (1.8) and (1.10) form a system of linear algebraic equations in two unknown functions $C_1(s)$ and $C_2(s)$. This system has a unique solution since its determinant represents Wronskian for the fundamental set of solutions $y_i(x)$, and is therefore nonzero. Before we turn to property 4 we split up the operator $M_k(y)$ in two parts as

$$M_k\left(y\right)=P_k\left(y\right)+Q_k\left(y\right),$$

where

$$P_k\left(y\right)=\sum_{j=0}^{1}\alpha_j^k y^{(j)}\left(a\right),\quad Q_k\left(y\right)=\sum_{j=0}^{1}\beta_j^k y^{(j)}\left(b\right).$$

To continue let us introduce a shorthand notation for the two pieces of the piecewise defined Green's function in (1.7). From now on, the piece that corresponds to the interval $[a,s]$ will be called the upper branch of the Green's function and denoted as $g^+(x,s)$, whilst the piece defined on the interval $[s,b]$ will be referred to as the lower branch $g^-(x,s)$.

Since $g(a,s)$ corresponds to the upper branch of the Green's function in (1.7) and $g(b,s)$ corresponds to the lower branch, the relations in (1.6) could be rewritten as

$$M_k\left(g\left(x,s\right)\right)\equiv P_k\left(g^+\left(x,s\right)\right)+Q_k\left(g^-\left(x,s\right)\right)=0,\quad k=1,2$$

Or in other words, because of the linearity of the operators $P_k(y)$ and $Q_k(y)$, the above expressions read

$$\sum_{i=1}^{2}P_k\left(y_i\left(a\right)\right)A_i\left(s\right)+\sum_{i=1}^{2}Q_k\left(y_i\left(b\right)\right)B_i\left(s\right)=0,\quad k=1,2 \tag{1.11}$$

Expressing then the functions $A_i(s)$ in terms of $C_i(s)$ and $B_i(s)$ from (1.9), we obtain the 2×2 system of linear algebraic equations in $B_i(s)$

$$\sum_{i=1}^{2}P_k\left(y_i\left(a\right)\right)\left(B_i\left(s\right)-C_i\left(s\right)\right)+\sum_{i=1}^{2}Q_k\left(y_i\left(b\right)\right)B_i\left(s\right)=0,\quad k=1,2$$

which can be written in a more compact form as

$$\sum_{i=1}^{2}M_k\left(y_i\left(b\right)\right)B_i\left(s\right)=\sum_{i=1}^{2}P_k\left(y_i\left(a\right)\right)C_i\left(s\right),\quad k=1,2 \tag{1.12}$$

The system in (1.12) has a unique solution, because the operators $M_k(y)$ are linearly independent. And once $B_i(s)$ are found, the corresponding $A_i(s)$ follow from (1.9).

So, observing the derivation just completed, we outline that it does not only prove the existence and uniqueness of the Green's function of the problem in (1.1) and (1.2), but also gives us a straightforward procedure for its obtaining.

Note that for some of boundary-value problems of the type in (1.1) and (1.2), the construction procedure for their Green's functions, that we just described, can be notably modified [49]. Namely, if the boundary conditions in (1.2) are point-split, meaning that one of them is imposed at $x = a$

$$\alpha_0 y(a) + \alpha_1 y'(a) = 0, \tag{1.13}$$

whilst another is imposed at $x = b$

$$\beta_0 y(b) + \beta_1 y'(b) = 0, \tag{1.14}$$

then, instead of taking any pair of linearly independent particular solutions of the governing differential equation in (1.1) and proceeding with them as earlier suggested, we choose the first component $y_1(x)$ of the fundamental set of solutions as the solution to the initial-value problem

$$\alpha_0 y_1(a) + \alpha_1 y_1'(a) = 0 \tag{1.15}$$

and

$$\alpha_0^* y_1(a) + \alpha_1^* y_1'(a) = 0 \tag{1.16}$$

for equation (1.1). The second component $y_2(x)$ of the fundamental set of solutions is chosen as the solution to another initial-value problem

$$\beta_0 y_1(b) + \beta_1 y_1'(b) = 0 \tag{1.17}$$

and

$$\beta_0^* y_1(b) + \beta_1^* y_1'(b) = 0 \tag{1.18}$$

Clearly, to make the initial-value problem in (1.1), (1.15) and (1.16) well-posed, the coefficients α_0^* and α_1^* in (1.16) must be chosen in the way making the determinant of the matrix

$$\begin{pmatrix} \alpha_0 & \alpha_1 \\ \alpha_0^* & \alpha_1^* \end{pmatrix}$$

non-zero. By similar reasoning, the choice of β_0^* and β_1^* in (1.18) must be predetermined by the condition

$$\begin{vmatrix} \beta_0 & \beta_1 \\ \beta_0^* & \beta_1^* \end{vmatrix} \neq 0.$$

Now, in light of the proposed specific choice of the components $y_1(x)$ and $y_2(x)$ of the fundamental set of solution, the Green's function of the boundary-value problem in (1.1), (1.13), and (1.14) can be expressed in the form

$$g(x,s) = \begin{cases} y_1(x)\,A(s)\,, & \alpha \le x \le s \\ y_2(x)\,B(s)\,, & s \le x \le b \end{cases} \tag{1.19}$$

It is evident that the above form satisfies the defining properties 1 and 4 in the definition of the Green's function. To find the functions $A(s)$ and $B(s)$, we take advantage of the continuity properties 2 and 3 which results in the system of linear algebraic equations

$$\begin{aligned} y_1(s)\,A(s) - y_2(s)\,B(s) &= \quad 0 \\ y_1'(s)\,A(s) - y_2'(s)\,B(s) &= -p_0^{-1}(s) \end{aligned} \tag{1.20}$$

the well-posedness of which follows from the fact that the coefficient matrix of (1.20) is not singular (indeed, it is the Wronskian of the fundamental set of solutions whose components are $y_1(x)$ and $y_2(x)$). So, once the functions $A(s)$ and $B(s)$ are available, they go to where they belong to, that is to equation (1.19). This completes the construction of the Green's function that we are looking for.

Before turning to the second of the classical ways [49] usually used to practically construct the Green's function for the boundary-value problem of the type (1.1) and (1.2), we will consider the non-homogeneous equation

$$p_0(x)\,y''(x) + p_1(x)\,y'(x) + p_2(x)\,y(x) = -f(x) \tag{1.21}$$

subject to the boundary conditions in (1.2). It can be shown that the solution of the boundary-value problem in (1.21) and (1.2) can be expressed in terms of the Green's function $g(x,s)$ of the setting in (1.1) and (1.2) in the form

$$y(x) = \int_a^b g(x,s)\,f(s)\,ds \tag{1.22}$$

This implies that our objective is to show that the function in (1.22) does make the equation in (1.21) true and satisfies the boundary conditions in (1.2). To proceed with this endeavour, note that since the Green's function $g(x,s)$ is defined in two pieces, the form in (1.22) can be split as

$$y(x) = \int_a^x g^-(x,s) f(s) \, ds + \int_x^b g^+(x,s) f(s) \, ds \tag{1.23}$$

To substitute the above expression for $y(x)$ into (1.21) we recall the differentiation rule for the integral with variable limits. It reads

$$\frac{d}{dx}\left(\int_{a(x)}^{b(x)} h(x,s)\, ds\right) = \int_{a(x)}^{b(x)} h_x(x,s)\, ds + h(x, b(x))\, b'(x) - h(x, a(x))\, a'(x).$$

Differentiation of the expression for $y(x)$ in (1.23) yields

$$y'(x) = \int_a^x g_x^+(x,s) f(s)\, ds + \int_x^b g_x^-(x,s) f(s)\, ds$$
$$+ g(x, x-0) f(x) - g(x, x+0) f(x)$$

which reduces, due to the second property of the Green's function, to

$$y'(x) = \int_a^b g_x(x,s) f(s)\, ds \tag{1.24}$$

This implies that the boundary conditions in (1.2) are satisfied with $y(x)$ expressed by (1.22), since all the differentiations in $M_k(y; a, b)$ can be brought under the integration sign. Following the same logic as for the first derivative and keeping in mind the third property of the Green's function, the expression for the second derivative of $y(x)$ could be found as

$$y''(x) = \int_a^b g_{xx}(x,s) f(s)\, ds - \frac{1}{p_0(x)} f(x) \tag{1.25}$$

By substituting (1.22), (1.24), and (1.25) into (1.21) it can be shown that the latter reduces to

$$\int_a^x L\left[g^+(x,s)\right] f(s)\, ds + \int_x^b L\left[g^-(x,s)\right] f(s)\, ds - f(x) = -f(x)$$

which is an identity, because of the first property of the Green's function,

$$L\left[g\left(x,s\right)\right]=0, \quad x\in\left(a,s\right)\cup\left(s,b\right).$$

So, an important practical observation follows from what we have done. That is, if the solution to a boundary-value problem posed for a non-homogeneous differential equation subject to homogeneous boundary conditions could be expressed in the integral form of (1.22), then the kernel of that integral is the Green's function for the corresponding homogeneous problem. This fact gives rise to another approach for the construction of Green's functions which is described below in detail by means of the Lagrange's method of variation of parameters [31]. In doing so, assume that $y_1(x)$ and $y_2(x)$ are two linearly independent particular solutions of the equation in (1.1). Then the general solution of the non-homogeneous equation could be written as

$$y\left(x\right)=C_1\left(x\right)y_1\left(x\right)+C_2\left(x\right)y_2\left(x\right) \tag{1.26}$$

Differentiating the above yields

$$y'\left(x\right)=C_1'\left(x\right)y_1\left(x\right)+C_2'\left(x\right)y_2\left(x\right)+C_1\left(x\right)y_1'\left(x\right)+C_2\left(x\right)y_2'\left(x\right).$$

Making the assumption

$$C_1'\left(x\right)y_1\left(x\right)+C_2'\left(x\right)y_2\left(x\right)=0, \tag{1.27}$$

the second derivative of (1.26) reads

$$y''\left(x\right)=C_1'\left(x\right)y_1'\left(x\right)+C_2'\left(x\right)y_2'\left(x\right)+C_1\left(x\right)y_1''\left(x\right)+C_2\left(x\right)y_2''\left(x\right)$$

Substituting the above expressions for $y'\left(x\right)$ and $y''\left(x\right)$ into (1.21), one obtains

$$p_0(x)C_1'\left(x\right)y_1'\left(x\right)+p_0(x)C_2'\left(x\right)y_2'\left(x\right)=-f\left(x\right) \tag{1.28}$$

The relations in (1.27) and (1.28) form a system of linear algebraic equations in $C_1'\left(x\right)$ and $C_2'\left(x\right)$ which reads as

$$\begin{aligned} &C_1'\left(x\right)y_1\left(x\right)+C_2'\left(x\right)y_2\left(x\right)=0\\ &C_1'\left(x\right)y_1'\left(x\right)+C_2'\left(x\right)y_2'\left(x\right)=-f\left(x\right)/p_0\left(x\right)\end{aligned} \tag{1.29}$$

The system in (1.29) has a unique solution since its determinant is Wronskian

$$W(x) = y_1(x)\, y_2'(x) - y_1'(x)\, y_2(x) \neq 0$$

of the two linearly independent functions $y_1(x)$ and $y_2(x)$.

The solution of the above system is obtained in the form

$$C_1'(x) = -\frac{y_2(x) f(x)}{p_0(x) W(x)}, \quad C_2'(x) = \frac{y_1(x) f(x)}{p_0(x) W(x)}$$

which after straightforward integration yields

$$C_1(x) = -\int_a^x \frac{y_2(s) f(s)}{p_0(s) W(s)} ds + D_1, \quad C_2(x) = \int_a^x \frac{y_1(s) f(s)}{p_0(s) W(s)} ds + D_2 \tag{1.30}$$

Substituting the above expressions into (1.26), we obtain the general solution of the non-homogeneous equation in (1.21) as

$$y(x) = \int_a^x \frac{y_1(s)\, y_2(x) - y_1(x)\, y_2(s)}{p_0(s) W(s)} f(s)\, ds + D_1 y_1(x) + D_2 y_2(x) \tag{1.31}$$

The constants of integration D_1 and D_2 in (1.31) are to be determined from the boundary conditions in (1.2). To complete the derivation procedure let us consider the simplest case of the boundary conditions as

$$y(a) = 0, \quad y(b) = 0 \tag{1.32}$$

Satisfying these conditions yields the system of linear algebraic equations

$$\begin{aligned} D_1 y_1(a) + D_2 y_2(a) &= 0 \\ D_1 y_1(b) + D_2 y_2(b) &= P \end{aligned} \tag{1.33}$$

in D_1 and D_2, where

$$P = -\int_a^b \frac{H(b,s) f(s)}{p_0(s) W(s)} ds$$

and

$$H(b,s) = y_1(s)\, y_2(b) - y_1(b)\, y_2(s)$$

Solving the above system results in

$$D_1 = -\int_a^b \frac{y_2(a) H(b,s) f(s)}{p_0(s) H(a,b) W(s)} ds, \quad D_2 = \int_a^b \frac{y_1(a) H(b,s) f(s)}{p_0(s) H(a,b) W(s)} ds$$

which upon substitution into (1.31) provides us with the solution of the problem in (1.21) and (1.32) as

$$y(x) = \int_a^x \frac{H(x,s) f(s)}{p_0(s) W(s)} ds - \int_a^b \frac{H(a,x) H(b,s) f(s)}{p_0(s) H(a,b) W(s)} ds$$

Combining the above integrals in a single integral form, we finally obtain

$$y(x) = \int_a^b K(x,s) f(s) ds \tag{1.34}$$

with the kernel being defined in two pieces as

$$K(x,s) = \frac{1}{p_0(s) H(a,b) W(s)} \begin{cases} -H(a,x) H(b,s), & \text{if } a \leq x \leq s \\ H(a,b) H(x,s) - H(a,x) H(b,s), & \text{if } s \leq x \leq b \end{cases} \tag{1.35}$$

Thus, the function in (1.35) does indeed represent the Green's function for the boundary-value problem in (1.1) and (1.32) that we are looking for.

The present manual is organized in five chapters. Chapter 1 is actually the Introduction. In Chapter 2, we provide a detailed description of the method that we use for the construction of Green's functions for boundary-value problems stated for the Laplace equation written in geographical coordinates for single shell fragment. We consider different fragments of spherical, cylindrical, and toroidal shape as regions over which actual boundary-value problems are formulated. For each of these regions a score of Green's functions are provided in Chapter 2. Chapter 3 is devoted to the construction of matrices of Green's type for a number of thin shell assemblies. A special attention is paid to the obtaining of computer-friendly forms of the elements of such matrices.

Most complicated problem statements, considered in this study, are discussed in Chapter 4 where perforated single shell fragments and assemblies of fragments undergoing point sources are considered. The last Chapter provides some verification of the efficiency of the proposed semi-analytic algorithms. The computational cost and the parallelizability of those algorithms are discussed in there. Based on the method of successive approximations approach we also explored in Chapter 5 the possibility of solving some inverse problems, where our algorithms appear efficient if used at each iteration for solution of corresponding direct settings.

The results of the present study have been published [11,13,15] in peer-reviewed journals and presented to a series of regional, national, and international professional conferences (see [10, 12, 14, 16]).

2 Laplace equation on surfaces of revolution

Thin plates and shells represent widely used fragments of structural elements of machines and devices in contemporary engineering and science. If these fragments are made of conductive materials, then potential fields of various origin may occur in them affecting their functional properties and capacity for efficient work. This is why an engineer, who is involved in the design process, is required to accurately compute potential fields generated in thin-walled fragments of machines and devices.

Our objective in this chapter is to develop a reliable background for computing potential fields induced by point-concentrated sources in single shells of standard geometry. Spherical, cylindrical, and toroidal shells will be considered in detail. Mathematically, this requires Green's functions for the two dimensional Laplace equation written in various geographical coordinates. A number of boundary-value problems will be considered.

2.1 Boundary-value problems on sphere

We begin with a boundary-value problem stated in the quadrilateral region (see Figure 1)

$$\Omega = \{\phi, \theta | \phi_1 \leq \phi \leq \phi_2, \theta_1 \leq \theta \leq \theta_2\}$$

on a spherical surface of radius a for the two-dimensional Poisson equation

$$\frac{1}{a^2 \sin\phi} \frac{\partial}{\partial \phi} \left(\sin\phi \frac{\partial u(\phi, \theta)}{\partial \phi} \right) + \frac{1}{a^2 \sin^2\phi} \frac{\partial^2 u(\phi, \theta)}{\partial \theta^2} = -f(\phi, \theta) \quad \phi, \theta \in \Omega \tag{2.1}$$

written in spherical coordinates and subject to the boundary conditions

$$B_1 [u(\phi, \theta_1)] = 0 \quad B_2 [u(\phi, \theta_2)] = 0 \tag{2.2}$$

and

$$B_3 [u(\phi_1, \theta)] = 0 \quad B_4 [u(\phi_2, \theta)] = 0, \tag{2.3}$$

where B_i, $i = \overline{1, 4}$, are the boundary condition operators of one of the three (Dirichlet, Neumann, and Robin) standard types.

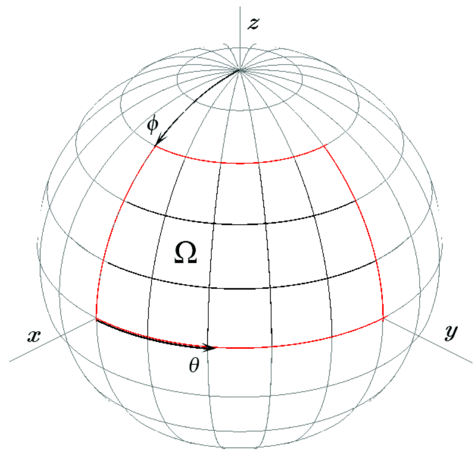

Figure 1: Quadrilateral fragment of a thin spherical shell

If $G(\phi, \theta; \psi, \tau)$ represents the Green's function of the homogeneous boundary-value problem corresponding to (2.1)-(2.3), then the solution to the problem in (2.1)-(2.3) itself can be expressed as the domain integral

$$u(\phi, \theta) = \int\int_{\Omega} G(\phi, \theta; \psi, \tau) f(\psi, \tau) d_{\psi,\tau}\Omega. \tag{2.4}$$

If the boundary-value problem in (2.1)-(2.3) allows analytic separation of variables, implying that B_1 and B_2 represent either Dirichlet or Neumann operators, then we expand the solution $u(\phi, \theta)$ of the original problem and the right-hand side function $f(\phi, \theta)$ of the governing equation in the Fourier series

$$u(\phi, \theta) = \sum_{n=1}^{\infty} u_n(\phi) \sin \nu\theta \tag{2.5}$$

and

$$f(\phi, \theta) = \sum_{n=1}^{\infty} f_n(\phi) \sin \nu\theta, \tag{2.6}$$

where the factor ν is directly proportional to the index of summation n.

Substituting the above trigonometric representations into the boundary-value problem in (2.1)-(2.3), we obtain the set

$$\frac{1}{a^2 \sin\phi} \frac{d}{d\phi}\left(\sin\phi \frac{du_n(\phi)}{d\phi}\right) - \frac{\nu^2}{a^2 \sin^2\phi} u_n(\phi) = -f_n(\phi), \quad n = 1, 2, 3, ... \tag{2.7}$$

$$B_3\left[u_n\left(\phi_1\right)\right]=0 \quad B_4\left[u_n\left(\phi_2\right)\right]=0 \tag{2.8}$$

of boundary-value problems in the coefficients $u_n(\phi)$ of the series in (2.5).

Keeping in mind application of the method of variation of parameters to the boundary-value problem in (2.7)-(2.8), we need two linearly independent particular solutions for the homogeneous equation corresponding to (2.7). While changing the independent variable as

$$\omega=\ln\left(\tan\left(\frac{\phi}{2}\right)\right),$$

we reduce the problem in (2.7)-(2.8) to

$$\frac{d^2u_n\left(\omega\right)}{d\omega^2}-\nu^2u_n\left(\omega\right)=0 \tag{2.9}$$

$$B_3\left[u_n\left(\omega_1\right)\right]=0 \quad B_4\left[u_n\left(\omega_2\right)\right]=0. \tag{2.10}$$

This allows us to express the general solution for (2.9), within the scope of the method of variation of parameters [31], in the form

$$u_n\left(\omega\right)=C_1\left(\omega\right)e^{\nu\omega}+C_2\left(\omega\right)e^{-\nu\omega},$$

or going back to the original independent variable ϕ, we have the solution $u_n\left(\phi\right)$ to (2.7) in the form

$$u_n\left(\phi\right)=C_1\left(\phi\right)\tan^{\nu}\left(\frac{\phi}{2}\right)+C_2\left(\phi\right)\tan^{-\nu}\left(\frac{\phi}{2}\right). \tag{2.11}$$

Following the classical procedure, which was described explicitly in the Introduction, we arrive at the general solution for the non-homogeneous equation in (2.7) as

$$\begin{aligned} u_n\left(\phi\right) &= -\int_{\phi_1}^{\phi}\frac{\tan^{\nu}\left(\phi/2\right)}{2\nu\tan^{\nu}\left(\psi/2\right)}f_n\left(\psi\right)d\psi+D_1\tan^{\nu}\left(\phi/2\right) \\ &\quad +\int_{\phi_1}^{\phi}\frac{\tan^{\nu}\left(\psi/2\right)}{2\nu\tan^{\nu}\left(\phi/2\right)}f_n\left(\psi\right)d\psi+D_2\tan^{-\nu}\left(\phi/2\right), \end{aligned}$$

which transforms into

$$u_n\left(\phi\right)=\frac{1}{2\nu}\int_{\phi_1}^{\phi}\left(\frac{\tan^{\nu}\left(\psi/2\right)}{\tan^{\nu}\left(\phi/2\right)}-\frac{\tan^{\nu}\left(\phi/2\right)}{\tan^{\nu}\left(\psi/2\right)}\right)f_n\left(\psi\right)d\psi$$

$$+D_1 \tan^{\nu}(\phi/2) + D_2 \tan^{-\nu}(\phi/2) . \tag{2.12}$$

Satisfying the boundary conditions in (2.8), we express (2.12) in the form

$$u_n(\phi) = \int_{\phi_1}^{\phi_2} g_n(\phi, \psi) f_n(\psi) \, d\psi, \tag{2.13}$$

where the kernel function $g_n(\phi, \psi)$ is expressed in two pieces. In considering particular problems later in this chapter, we discuss this issue in detail.

To proceed further with our approach, we express the coefficients $f_n(\psi)$ of (2.6) using the Euler-Fourier formula

$$f_n(\phi) = \frac{2}{\theta_2 - \theta_1} \int_{\theta_1}^{\theta_2} f(\phi, \tau) \sin \nu\tau d\tau$$

and substitute $u_n(\phi)$ into (2.5). This yields

$$u(\phi, \theta) = \iint_{\Omega} G(\phi, \theta; \psi, \tau) f(\psi, \tau) \, d_{\psi,\tau}\Omega,$$

where $G(\phi, \theta; \psi, \tau)$ represents the Green's function of the homogeneous boundary-value problem corresponding to (2.1)-(2.3), and appears in the form

$$G(\phi, \theta; \psi, \tau) = \frac{2}{\theta_2 - \theta_1} \sum_{n=1}^{\infty} g_n(\phi, \psi) \sin \nu\theta \sin \nu\tau. \tag{2.14}$$

In what follows, we will consider a score of specific boundary-value problems and obtain explicit expression for their Green's functions.

To be more specific, consider the spherical quadrilateral

$$\Omega = \{\phi, \theta \mid \alpha \le \phi \le \beta; \ 0 \le \theta \le \gamma\},$$

where $0 < \alpha < \beta < \pi$ and $0 < \gamma < 2\pi$, and impose the following boundary conditions on its contour

$$u(\phi, 0) = 0, \qquad \frac{\partial u(\phi, \gamma)}{\partial \theta} = 0, \tag{2.15}$$

and

$$u(\alpha, \theta) = 0, \qquad \frac{\partial u(\beta, \theta)}{\partial \phi} = 0. \tag{2.16}$$

To meet the conditions in (2.15), the summation index ν in the Fourier series expansions of (2.5)-(2.6) must be $\nu = (2n-1)\,\pi/2\gamma$. By satisfying the boundary conditions in (2.16) to determine the constants D_1 and D_2 in (2.12), we come up with the following system of linear algebraic equations in D_1 and D_2

$$\begin{gathered} D_1 A^{\nu} + D_2 A^{-\nu} = 0 \\ D_1 B^{\nu} - D_2 B^{-\nu} = P, \end{gathered}$$

where

$$P = -\frac{1}{2\nu}\int_{\alpha}^{\beta}\left(\frac{B^{\nu}}{\Phi^{\nu}(\psi)} + \frac{\Phi^{\nu}(\psi)}{B^{\nu}}\right)\widetilde{f}_n(\psi)\,d\psi$$

and

$$\Phi(\xi) = \tan^{\pi/\gamma}(\xi/2), \quad A = \tan^{\pi/\gamma}(\alpha/2), \quad \text{and} \quad B = \tan^{\pi/\gamma}(\beta/2).$$

Upon solving the above system, we obtain

$$D_1 = \frac{1}{2\nu\left(A^{2n}+B^{2n}\right)}\int_{\alpha}^{\beta}\frac{B^{2n}+\Phi^{2n}(\psi)}{\Phi^{n}(\psi)}\widetilde{f}_n(\psi)\,d\psi \tag{2.17}$$

and

$$D_2 = -\frac{A^{2n}}{2\nu\left(A^{2n}+B^{2n}\right)}\int_{\alpha}^{\beta}\frac{B^{2n}+\Phi^{2n}(\psi)}{\Phi^{n}(\psi)}\widetilde{f}_n(\psi)\,d\psi \tag{2.18}$$

Substituting expressions from (2.17) and (2.18) into (2.12), one obtains

$$\begin{aligned} u_n(\phi) \quad = \quad & \frac{1}{2\nu\left(A^{2n}+B^{2n}\right)}\left[\int_{\alpha}^{\phi}\frac{\Phi^{2n}(\psi)-A^{2n}}{\Phi^{n}(\psi)}\frac{B^{2n}+\Phi^{2n}(\phi)}{\Phi^{n}(\phi)}\widetilde{f}_n(\psi)\,d\psi\right. \\ & \left.+\int_{\phi}^{\beta}\frac{\Phi^{2n}(\phi)-A^{2n}}{\Phi^{n}(\phi)}\frac{B^{2n}+\Phi^{2n}(\psi)}{\Phi^{n}(\psi)}\widetilde{f}_n(\psi)\,d\psi\right], \end{aligned}$$

which could be interpreted as

$$u_n(\phi) = \int_{\phi_1}^{\phi_2} g_n(\phi,\psi)\,\widetilde{f}_n(\psi)\,d\psi,$$

where

$$g_n(\phi,\psi) = \frac{A^n B^n}{2\nu\left(A^{2n}+B^{2n}\right)}\begin{cases} \left(\frac{\Phi^n(\psi)}{A^n} - \frac{A^n}{\Phi^n(\psi)}\right)\left(\frac{B^n}{\Phi^n(\phi)} + \frac{\Phi^n(\phi)}{B^n}\right), & \alpha \le \psi \le \phi \\ \left(\frac{\Phi^n(\phi)}{A^n} - \frac{A^n}{\Phi^n(\phi)}\right)\left(\frac{B^n}{\Phi^n(\psi)} + \frac{\Phi^n(\psi)}{B^n}\right), & \phi \le \psi \le \beta \end{cases}. \tag{2.19}$$

Now we make use of (2.14) to find the Green's function for the homogeneous boundary-value problem corresponding to that in (2.1), (2.15) and (2.16). Breaking the product of sines into the difference of cosines, using then the standard summation formula [30]

$$\sum_{n=1}^{\infty} \frac{p^{2n-1}}{2n-1} \cos(2n-1)\alpha = \frac{1}{4} \ln \left(\frac{1+2p\cos\alpha + p^2}{1-2p\cos\alpha + p^2} \right),$$

and introducing shorthand notations

$$H_N(x,\alpha,\beta) = \frac{1}{\pi} \ln \left(\frac{1+2x\cos\alpha + x^2}{1-2x\cos\alpha + x^2} \right) - \frac{1}{\pi} \ln \left(\frac{1+2x\cos\beta + x^2}{1-2x\cos\beta + x^2} \right), \tag{2.20}$$

$$\kappa(\theta,\tau) = \frac{\pi}{\gamma}(\theta+\tau), \quad \text{and} \quad \eta(\theta,\tau) = \frac{\pi}{\gamma}(\theta-\tau), \tag{2.21}$$

we appear at the Green's function $G(\phi,\theta;\psi,\tau)$ in the form

$$\begin{aligned} G(\phi,\theta;\psi,\tau) &= H_N\left(\sqrt{\frac{\Phi(\phi)\,\Phi(\psi)}{B^2}}, \frac{\eta}{2}, \frac{\kappa}{2}\right) - H_N\left(\sqrt{\frac{A^2}{\Phi(\phi)\,\Phi(\psi)}}, \frac{\eta}{2}, \frac{\kappa}{2}\right) \\ &+ \left\{ \begin{array}{l} H_N\left(\sqrt{\frac{\Phi(\phi)}{\Phi(\psi)}}, \frac{\eta}{2}, \frac{\kappa}{2}\right) - H_N\left(\sqrt{\frac{\Phi(\phi)A^2}{\Phi(\psi)B^2}}, \frac{\eta}{2}, \frac{\kappa}{2}\right) \\ H_N\left(\sqrt{\frac{\Phi(\psi)}{\Phi(\phi)}}, \frac{\eta}{2}, \frac{\kappa}{2}\right) - H_N\left(\sqrt{\frac{\Phi(\psi)A^2}{\Phi(\phi)B^2}}, \frac{\eta}{2}, \frac{\kappa}{2}\right) \end{array} \right. + R, \end{aligned} \tag{2.22}$$

where $R = R(\phi,\theta;\psi,\tau)$ is the regular part of the original series in (2.14) which converges uniformly and is expressed as

$$R(\phi,\theta;\psi,\tau) = \sum_{n=1}^{\infty} \frac{1}{2\pi\nu} \frac{A^n(\Phi^n(\phi)+B^n)(\Phi^n(\psi)-A^n)}{B^n\sqrt{\Phi^n(\phi)\,\Phi^n(\psi)}\,(B^n+A^n)} \sin\nu\theta \sin\nu\tau,$$

and the upper branch of the third additive component in (2.22) is valid for $\alpha \le \phi \le \psi$, whereas in its lower branch $\psi \le \phi \le \beta$.

Note that the Green's function in (2.22) possesses the logarithmic singularity when $\phi \to \psi$ and $\theta \to \tau$ and represents the solution of the boundary-value problem in (2.1), (2.15) and (2.16) if the right-hand side function $f(\phi,\theta)$ in (2.1) is understood as the Dirack delta-function $\delta(\phi-\psi,\theta-\tau)$. Profile of the Green's function just found is shown in Figure 2 for the domain $\Omega = \{\phi,\theta | 0.15\pi \le \phi \le 0.5\pi, 0 \le \theta \le 0.5\pi\}$ with a point-source location at $(0.35\pi, 035\pi)$.

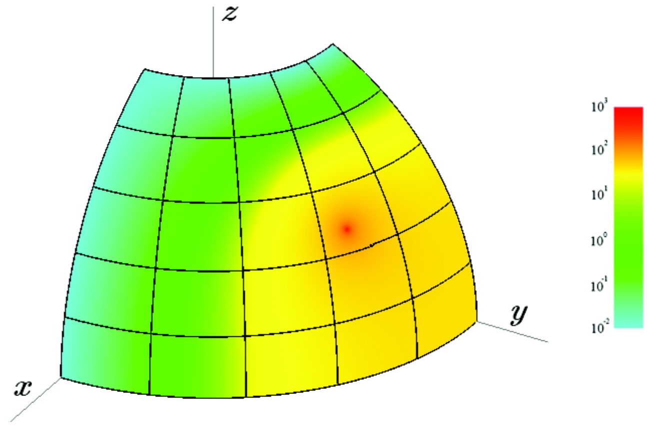

Figure 2: A point source-generated field in the spherical quadrilateral

The described in this section technique can be used to obtain compact representations of Green's functions for a score of boundary-value problems set up for a variety of regions on a spherical surface.

Before proceeding further with our development we introduce some simplifying notations. First a 4-letter abbreviation will be used to specify the boundary conditions, where each letter corresponds to a specific boundary condition operator in (2.2)-(2.3). "D" stays for the Dirichlet condition, "N" means the Neumann condition, while "S" means the boundary condition at a singular point. For example, the boundary conditions in (2.15) and (2.16) could be referred to as DNDN. In addition, along with H_N introduced in (2.20), we use the shorthand notation $H_D(x, \alpha, \beta)$ for the logarithmic function

$$H_D(x, \alpha, \beta) = -\frac{1}{4\pi} \ln \left(\frac{1 - 2x\cos\alpha + x^2}{1 - 2x\cos\beta + x^2} \right). \tag{2.23}$$

Table 1 contains a number of computer-friendly expressions of Green's functions constructed for well-posed boundary-value problems [10, 11]. In cases where the series in (2.14) cannot be completely summed up, we split the logarithmic singularity, and leave the regular components R_i expressed as uniformly convergent series.

In Figure 3, the superposition of three profiles of the Green's function is shown for the Dirichlet boundary-value problem posed in a spherical biangle of radius 1. The domain Ω is chosen as $\{(\phi,\theta)\,|0\le\phi\le\pi, 0\le\theta\le 0.3\pi\}$, the locations of the point sources are $(0.35\pi, 0.06\pi)$, $(0.55\pi, 0.12\pi)$, and $(0.45\pi, 0.27\pi)$

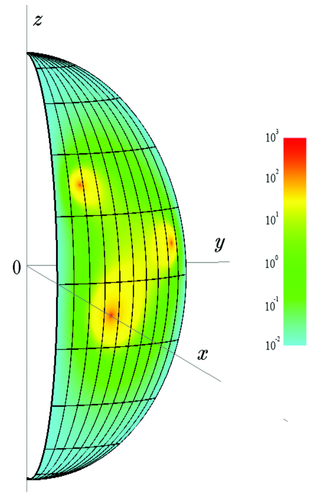

Figure 3: The potential field generated by three point sources in a spherical biangle

Table 1: Green's functions for boundary-value problems posed on a sphere

#	Boundary conditions	$G(\phi,\theta;\psi,\tau)$
1	DDSD	$H_D\left(\frac{\Phi(\phi)\Phi(\psi)}{B^2},\kappa,\eta\right)-H_D\left(\frac{\Phi(\phi)}{\Phi(\psi)},\kappa,\eta\right)$
2	DDSN	$-H_D\left(\frac{\Phi(\phi)\Phi(\psi)}{B^2},\kappa,\eta\right)-H_D\left(\frac{\Phi(\phi)}{\Phi(\psi)},\kappa,\eta\right)$
3	DNSD	$H_N\left(\sqrt{\frac{\Phi(\phi)\Phi(\psi)}{B^2}},\frac{\kappa}{2},\frac{\eta}{2}\right)-H_N\left(\sqrt{\frac{\Phi(\phi)}{\Phi(\psi)}},\frac{\kappa}{2},\frac{\eta}{2}\right)$
4	DNSN	$-H_N\left(\sqrt{\frac{\Phi(\phi)\Phi(\psi)}{B^2}},\frac{\kappa}{2},\frac{\eta}{2}\right)-H_N\left(\sqrt{\frac{\Phi(\phi)}{\Phi(\psi)}},\frac{\kappa}{2},\frac{\eta}{2}\right)$
5	DDSS	$-H_D\left(\frac{\Phi(\phi)}{\Phi(\psi)},\kappa,\eta\right)$
6	DNSS	$-H_N\left(\sqrt{\frac{\Phi(\phi)}{\Phi(\psi)}},\frac{\kappa}{2},\frac{\eta}{2}\right)$

Table 1 (cont.): Green's functions for boundary-value problems posed on a sphere

#	Boundary conditions	$G(\phi,\theta;\psi,\tau)$
7	DDDD	$H_D\left(\frac{\Phi(\phi)\Phi(\psi)}{B^2},\kappa,\eta\right)-H_D\left(\frac{\Phi(\phi)A^2}{\Phi(\psi)B^2},\kappa,\eta\right)$ $-H_D\left(\frac{\Phi(\phi)}{\Phi(\psi)},\kappa,\eta\right)+H_D\left(\frac{A^2}{\Phi(\phi)\Phi(\psi)},\kappa,\eta\right)+R_7$
8	DDDN	$-H_D\left(\frac{\Phi(\phi)\Phi(\psi)}{B^2},\kappa,\eta\right)+H_D\left(\frac{\Phi(\phi)A^2}{\Phi(\psi)B^2},\kappa,\eta\right)$ $-H_D\left(\frac{\Phi(\phi)}{\Phi(\psi)},\kappa,\eta\right)+H_D\left(\frac{A^2}{\Phi(\phi)\Phi(\psi)},\kappa,\eta\right)+R_8$
9	DDND	$H_D\left(\frac{\Phi(\phi)\Phi(\psi)}{B^2},\kappa,\eta\right)+H_D\left(\frac{\Phi(\phi)A^2}{\Phi(\psi)B^2},\kappa,\eta\right)$ $-H_D\left(\frac{\Phi(\phi)}{\Phi(\psi)},\kappa,\eta\right)-H_D\left(\frac{A^2}{\Phi(\phi)\Phi(\psi)},\kappa,\eta\right)+R_9$
10	DDNN	$-H_D\left(\frac{\Phi(\phi)\Phi(\psi)}{B^2},\kappa,\eta\right)-H_D\left(\frac{\Phi(\phi)A^2}{\Phi(\psi)B^2},\kappa,\eta\right)$ $-H_D\left(\frac{\Phi(\phi)}{\Phi(\psi)},\kappa,\eta\right)-H_D\left(\frac{A^2}{\Phi(\phi)\Phi(\psi)},\kappa,\eta\right)+R_{10}$
11	DNDD	$H_N\left(\sqrt{\frac{\Phi(\phi)\Phi(\psi)}{B^2}},\frac{\kappa}{2},\frac{\eta}{2}\right)-H_N\left(\sqrt{\frac{\Phi(\phi)A^2}{\Phi(\psi)B^2}},\frac{\kappa}{2},\frac{\eta}{2}\right)$ $-H_N\left(\sqrt{\frac{\Phi(\phi)}{\Phi(\psi)}},\frac{\kappa}{2},\frac{\eta}{2}\right)+H_N\left(\sqrt{\frac{A^2}{\Phi(\phi)\Phi(\psi)}},\frac{\kappa}{2},\frac{\eta}{2}\right)+R_{11}$
12	DNDN	$-H_N\left(\sqrt{\frac{\Phi(\phi)\Phi(\psi)}{B^2}},\frac{\kappa}{2},\frac{\eta}{2}\right)+H_N\left(\sqrt{\frac{\Phi(\phi)A^2}{\Phi(\psi)B^2}},\frac{\kappa}{2},\frac{\eta}{2}\right)$ $-H_N\left(\sqrt{\frac{\Phi(\phi)}{\Phi(\psi)}},\frac{\kappa}{2},\frac{\eta}{2}\right)+H_N\left(\sqrt{\frac{A^2}{\Phi(\phi)\Phi(\psi)}},\frac{\kappa}{2},\frac{\eta}{2}\right)+R_{12}$
13	DNND	$H_N\left(\sqrt{\frac{\Phi(\phi)\Phi(\psi)}{B^2}},\frac{\kappa}{2},\frac{\eta}{2}\right)+H_N\left(\sqrt{\frac{\Phi(\phi)A^2}{\Phi(\psi)B^2}},\frac{\kappa}{2},\frac{\eta}{2}\right)$ $-H_N\left(\sqrt{\frac{\Phi(\phi)}{\Phi(\psi)}},\frac{\kappa}{2},\frac{\eta}{2}\right)-H_N\left(\sqrt{\frac{A^2}{\Phi(\phi)\Phi(\psi)}},\frac{\kappa}{2},\frac{\eta}{2}\right)+R_{13}$
14	DNNN	$-H_N\left(\sqrt{\frac{\Phi(\phi)\Phi(\psi)}{B^2}},\frac{\kappa}{2},\frac{\eta}{2}\right)-H_N\left(\sqrt{\frac{\Phi(\phi)A^2}{\Phi(\psi)B^2}},\frac{\kappa}{2},\frac{\eta}{2}\right)$ $-H_N\left(\sqrt{\frac{\Phi(\phi)}{\Phi(\psi)}},\frac{\kappa}{2},\frac{\eta}{2}\right)-H_N\left(\sqrt{\frac{A^2}{\Phi(\phi)\Phi(\psi)}},\frac{\kappa}{2},\frac{\eta}{2}\right)+R_{14}$

Three different domain shapes are considered in Table 1, that is:

1. spherical triangle: $\{\phi,\theta\mid 0\le\phi\le\beta;\ 0\le\theta\le\gamma\}$ in rows 1-4;
2. spherical biangle: $\{\phi,\theta\mid 0\le\phi\le\pi;\ 0\le\theta\le\gamma\}$ in rows 5-6;

3. spherical rectangle: $\{\phi, \theta \mid \alpha \leq \phi \leq \beta;\ 0 \leq \theta \leq \gamma\}$ in rows 7-14.

The regular components R_i, $i = \overline{7,14}$ for the Green's functions which cannot be summed up are obtained as

$$R_7 = \sum_{n=1}^{\infty} \frac{1}{2\pi\nu} \frac{A^{2n}\left(\Phi^{2n}(\phi) - B^{2n}\right)\left(\Phi^{2n}(\psi) - A^{2n}\right)}{B^{2n}\Phi^{n}(\phi)\,\Phi^{n}(\psi)\left(B^{2n} - A^{2n}\right)} \left(\cos n\eta - \cos n\kappa\right),$$

$$R_8 = \sum_{n=1}^{\infty} \frac{1}{2\pi\nu} \frac{A^{2n}\left(\Phi^{2n}(\phi) + B^{2n}\right)\left(\Phi^{2n}(\psi) - A^{2n}\right)}{B^{2n}\Phi^{n}(\phi)\,\Phi^{n}(\psi)\left(B^{2n} + A^{2n}\right)} \left(\cos n\eta - \cos n\kappa\right),$$

$$R_9 = \sum_{n=1}^{\infty} \frac{1}{2\pi\nu} \frac{A^{2n}\left(B^{2n} - \Phi^{2n}(\phi)\right)\left(\Phi^{2n}(\psi) + A^{2n}\right)}{B^{2n}\Phi^{n}(\phi)\,\Phi^{n}(\psi)\left(B^{2n} + A^{2n}\right)} \left(\cos n\eta - \cos n\kappa\right),$$

$$R_{10} = \sum_{n=1}^{\infty} \frac{1}{2\pi\nu} \frac{A^{2n}\left(\Phi^{2n}(\phi) + B^{2n}\right)\left(\Phi^{2n}(\psi) + A^{2n}\right)}{B^{2n}\Phi^{n}(\phi)\,\Phi^{n}(\psi)\left(B^{2n} - A^{2n}\right)} \left(\cos n\eta - \cos n\kappa\right),$$

$$R_{11} = \sum_{n=1}^{\infty} \frac{1}{2\pi\nu} \frac{A^{n}\left(\Phi^{n}(\phi) - B^{n}\right)\left(\Phi^{n}(\psi) - A^{n}\right)}{B^{n}\sqrt{\Phi^{n}(\phi)\,\Phi^{n}(\psi)}\left(B^{n} - A^{n}\right)} \left(\cos\frac{n\eta}{2} - \cos\frac{n\kappa}{2}\right),$$

$$R_{12} = \sum_{n=1}^{\infty} \frac{1}{2\pi\nu} \frac{A^{n}\left(\Phi^{n}(\phi) + B^{n}\right)\left(\Phi^{n}(\psi) - A^{n}\right)}{B^{n}\sqrt{\Phi^{n}(\phi)\,\Phi^{n}(\psi)}\left(B^{n} + A^{n}\right)} \left(\cos\frac{n\eta}{2} - \cos\frac{n\kappa}{2}\right),$$

$$R_{13} = \sum_{n=1}^{\infty} \frac{1}{2\pi\nu} \frac{A^{n}\left(B^{n} - \Phi^{n}(\phi)\right)\left(\Phi^{n}(\psi) + A^{n}\right)}{B^{n}\sqrt{\Phi^{n}(\phi)\,\Phi^{n}(\psi)}\left(B^{n} + A^{n}\right)} \left(\cos\frac{n\eta}{2} - \cos\frac{n\kappa}{2}\right),$$

and

$$R_{14} = \sum_{n=1}^{\infty} \frac{1}{2\pi\nu} \frac{A^{n}\left(\Phi^{n}(\phi) + B^{n}\right)\left(\Phi^{n}(\psi) + A^{n}\right)}{B^{n}\sqrt{\Phi^{n}(\phi)\,\Phi^{n}(\psi)}\left(B^{n} - A^{n}\right)} \left(\cos\frac{n\eta}{2} - \cos\frac{n\kappa}{2}\right).$$

Recall another type of boundary conditions for the problem in (2.1)-(2.3), which is of a practical importance. It simulates the 2π-periodicity for the coordinate θ, when in (2.2) $\theta_2 = \theta_1 + 2\pi$. This takes place, for example, in the case of boundary conditions written as

$$u(\phi, \theta_1) - u(\phi, \theta_2) = 0 \tag{2.24}$$

and

$$\frac{\partial u(\phi, \theta_1)}{\partial \theta} - \frac{\partial u(\phi, \theta_2)}{\partial \theta} = 0. \tag{2.25}$$

In this case, the complete Fourier series expansions for $u(\phi,\theta)$ and $f(\phi,\theta)$ are used as

$$u(\phi,\theta)=\frac{1}{2}u_0(\phi)+\sum_{n=1}^{\infty}u_n^{(c)}(\phi)\cos n\theta+\sum_{n=1}^{\infty}u_n^{(s)}(\phi)\sin n\theta \tag{2.26}$$

and

$$f(\phi,\theta)=\frac{1}{2}f_0(\phi)+\sum_{n=1}^{\infty}f_n^{(c)}(\phi)\cos n\theta+\sum_{n=1}^{\infty}f_n^{(s)}(\phi)\sin n\theta. \tag{2.27}$$

And the Green's function for the boundary-value problem in (2.1), (2.3), (2.24), and (2.25) appears in the form

$$\begin{aligned} G(\phi,\theta;\psi,\tau) &= \frac{1}{2}g_0(\phi,\psi)+\sum_{n=1}^{\infty}g_n^{(c)}(\phi,\psi)\cos n\theta\cos n\tau \\ &+\sum_{n=1}^{\infty}g_n^{(s)}(\phi,\psi)\sin n\theta\sin n\tau. \end{aligned} \tag{2.28}$$

The derivation of the above function will be given in detail only for the boundary-value problem posed on a spherical belt $\Omega=\{\phi,\theta \mid \alpha\le\phi\le\beta;\ 0\le\theta\le 2\pi\}$ with boundary conditions imposed on boundary lines $\phi=\alpha$ and $\phi=\beta$ as

$$u(\alpha,\theta)=0 \quad \frac{\partial u(\beta,\theta)}{\partial\phi}=0. \tag{2.29}$$

Green's functions for other problems with 2π-periodic boundary conditions for θ coordinate could be found in a similar way.

Note that the derivation of the Fourier coefficients $g_n^{(c)}(\phi,\psi)$ and $g_n^{(s)}(\phi,\psi)$ is indifferent to the type of the series, that is why we will omit the superscripts (s) and (c) in what follows. Following the standard separation of variables procedure one reduces the boundary-value problem in (2.1), (2.24), (2.25), and (2.29) to

$$\frac{1}{a^2\sin\phi}\frac{d}{d\phi}\left(\sin\phi\frac{du_n(\phi)}{d\phi}\right)-\frac{n^2}{a^2\sin^2\phi}u_n(\phi)=-f_n(\phi), \quad n=1,2,3,... \tag{2.30}$$

$$u_n(\alpha)=0 \quad \text{and} \quad \frac{\partial u_n(\beta)}{\partial\phi}=0. \tag{2.31}$$

which results in the following expression of the Green's function in (2.28)

$$G(\phi,\theta;\psi,\tau)=\frac{1}{2}g_0(\phi,\psi)+\sum_{n=1}^{\infty}g_n(\phi,\psi)\cos n(\theta-\tau). \tag{2.32}$$

The cases $n = 0$ and $n \geq 1$ should be considered individually. Note, that for the case $n \geq 1$, the boundary-value problem in (2.30)-(2.31) is identical to one in (2.7), (2.16), if the parameter ν is replaced with n. This allows us to state that

$$g_n(\phi, \psi) = \frac{A^n B^n}{2n\left(A^{2n} + B^{2n}\right)} \begin{cases} \left(\frac{\Phi_0^n(\psi)}{A_0^n} - \frac{A_0^n}{\Phi_0^n(\psi)}\right)\left(\frac{B_0^n}{\Phi_0^n(\phi)} + \frac{\Phi_0^n(\phi)}{B_0^n}\right), & \alpha \leq \psi \leq \phi \\ \left(\frac{\Phi_0^n(\phi)}{A_0^n} - \frac{A_0^n}{\Phi_0^n(\phi)}\right)\left(\frac{B_0^n}{\Phi_0^n(\psi)} + \frac{\Phi_0^n(\psi)}{B_0^n}\right), & \phi \leq \psi \leq \beta \end{cases}, \tag{2.33}$$

where

$$\Phi_0(\xi) = \tan(\xi/2), \quad A_0 = \tan(\alpha/2), \quad \text{and } B_0 = \tan(\beta/2). \tag{2.34}$$

To derive the component $g_0(\phi, \psi)$ in (2.32) we find the general solution $u_0(\phi)$ of the homogeneous equation corresponding to (2.8) for $n = 0$

$$\frac{1}{a^2 \sin\phi} \frac{d}{d\phi}\left(\sin\phi \frac{du_0(\phi)}{d\phi}\right) = 0,$$

as

$$u_0(\phi) = C_1 \ln\left(\tan\left(\frac{\phi}{2}\right)\right) + C_2.$$

Using the method of variation of parameters, one finds the general solution to the corresponding non-homogeneous equation with the right-hand side function $f_0(\phi)$ as

$$u_0(\phi) = \int_\alpha^\phi \ln \frac{\Phi_0(\psi)}{\Phi_0(\phi)} \widetilde{f}_0(\psi)\, d\psi + D_1 \ln \Phi_0(\phi) + D_2, \tag{2.35}$$

where $\widetilde{f}_0(\psi) = a^2 \sin\psi f_0(\psi)$.

The constants of integration D_1 and D_2 could be found by satisfying the boundary conditions in (2.29) as

$$D_1 = \int_\alpha^\beta \widetilde{f}_0(\psi)\, d\psi \quad \text{and} \quad D_2 = -\int_\alpha^\beta \ln(A_0)\, \widetilde{f}_0(\psi)\, d\psi.$$

Substituting the above into (2.35), $u_0(\phi)$ reads as

$$u_0(\phi) = \int_\alpha^\phi \ln \frac{\Phi_0(\psi)}{A_0} \widetilde{f}_0(\psi)\, d\psi + \int_\phi^\beta \ln \frac{\Phi_0(\phi)}{A_0} \widetilde{f}_0(\psi)\, d\psi,$$

providing us with

$$g_0(\phi, \psi) = \begin{cases} \ln \frac{\Phi_0(\phi)}{A_0} & \text{if } \alpha \leq \phi \leq \psi \\ \ln \frac{\Phi_0(\psi)}{A_0} & \text{if } \psi \leq \phi \leq \beta \end{cases}. \tag{2.36}$$

To sum up the series in (2.32) with the coefficients defined in (2.33), we recall another standard summation formula [30]

$$\sum_{n=1}^{\infty} \frac{p^n}{n} \cos n\alpha = -\frac{1}{2} \ln\left(1 - 2p\cos\alpha + p^2\right) \tag{2.37}$$

and introduce the shorthand notation of the logarithmic function $H_P(x, \alpha)$

$$H_P(x, \alpha) = \frac{1}{4\pi} \ln\left(1 - 2x\cos\alpha + x^2\right) \tag{2.38}$$

The ultimate representation for the Green's function of the problem in (2.1), (2.24), 2.25), and (2.29) appears as

$$\begin{aligned} G(\phi, \theta; \psi, \tau) &= H_P\left(\frac{A_0^2}{\Phi_0(\phi)\,\Phi_0(\psi)}, \theta - \tau\right) - H_P\left(\frac{\Phi_0(\phi)\,\Phi_0(\psi)}{B_0^2}, \theta - \tau\right) \\ &+ \left\{ \begin{array}{l} \ln \frac{\Phi_0(\phi)}{A_0} - H_P\left(\frac{\Phi_0(\phi)}{\Phi_0(\psi)}, \theta - \tau\right) + H_P\left(\frac{\Phi_0(\psi) A_0^2}{\Phi_0(\phi) B_0^2}, \theta - \tau\right) \\ \ln \frac{\Phi_0(\psi)}{A_0} - H_P\left(\frac{\Phi_0(\psi)}{\Phi_0(\phi)}, \theta - \tau\right) + H_P\left(\frac{\Phi_0(\phi) A_0^2}{\Phi_0(\psi) B_0^2}, \theta - \tau\right) \end{array} \right. + R \end{aligned} \tag{2.39}$$

where the upper branch of the third additive component is valid for the case $\alpha \leq \phi \leq \psi$, while the lower branch represents the case $\psi \leq \phi \leq \beta$, and the last additive component $R = R(\phi, \theta; \psi, \tau)$ is expressed as the series

$$R(\phi, \theta; \psi, \tau) = \sum_{n=1}^{\infty} \frac{1}{2\pi n} \frac{A_0^{2n}\left(\Phi_0^{2n}(\phi) + B_0^{2n}\right)\left(\Phi_0^{2n}(\psi) - A_0^{2n}\right)}{B_0^{2n}\Phi_0^n(\phi)\,\Phi_0^n(\psi)\left(B_0^{2n} + A_0^{2n}\right)} \cos n(\theta - \tau) \tag{2.40}$$

that converges uniformly.

Applying the technique just described, one finds Green's functions for some other boundary-value problems posed on a 2π-periodic spherical region. That is, for the spherical cap $\Omega = \{\phi, \theta \mid 0 \leq \phi \leq \beta;\ 0 \leq \theta \leq 2\pi\}$, with the Dirichlet conditions imposed on $\phi = \beta$, we obtain

$$G(\phi, \theta; \psi, \tau) = \frac{1}{4\pi} \ln\left(\frac{B_0^2\left(\Phi_0^2(\phi) - 2\Phi_0(\phi)\,\Phi_0(\psi)\cos(\theta - \tau) + \Phi_0^2(\psi)\right)}{B_0^4 - 2B_0^2\Phi_0(\phi)\,\Phi_0(\psi)\cos(\theta - \tau) + \Phi_0^2(\phi)\,\Phi_0^2(\psi)}\right). \tag{2.41}$$

The case of spherical belt, $\Omega = \{\phi, \theta \mid \alpha \leq \phi \leq \beta;\ 0 \leq \theta \leq 2\pi\}$, with the Dirichlet conditions imposed on both edges, results in

$$\begin{aligned} G(\phi, \theta; \psi, \tau) &= H_P\left(\frac{A_0^2}{\Phi_0(\phi)\Phi_0(\psi)}, \theta - \tau\right) + H_P\left(\frac{\Phi_0(\phi)\Phi_0(\psi)}{B_0^2}, \theta - \tau\right) \\ &+ \begin{cases} \ln\frac{\Phi_0(\phi)}{B_0}\ln\frac{\Phi_0(\psi)}{A_0} - H_P\left(\frac{\Phi_0(\phi)}{\Phi_0(\psi)}, \theta - \tau\right) - H_P\left(\frac{\Phi_0(\psi)A_0^2}{\Phi_0(\phi)B_0^2}, \theta - \tau\right) \\ \ln\frac{\Phi_0(\psi)}{B_0}\ln\frac{\Phi_0(\phi)}{A_0} - H_P\left(\frac{\Phi_0(\psi)}{\Phi_0(\phi)}, \theta - \tau\right) - H_P\left(\frac{\Phi_0(\phi)A_0^2}{\Phi_0(\psi)B_0^2}, \theta - \tau\right) \end{cases} \\ &+ R_{DD} \end{aligned} \tag{2.42}$$

where

$$R_{DD} = R_{DD}(\phi, \theta; \psi, \tau) = \sum_{n=1}^{\infty} \frac{1}{2\pi n} \frac{A_0^{2n}\left(\Phi_0^{2n}(\phi) - B_0^{2n}\right)\left(\Phi_0^{2n}(\psi) - A_0^{2n}\right)}{B_0^{2n}\Phi_0^n(\phi)\Phi_0^n(\psi)\left(B_0^{2n} - A_0^{2n}\right)} \cos n(\theta - \tau),$$

The spherical belt $\Omega = \{\phi, \theta \mid \alpha \leq \phi \leq \beta;\ 0 \leq \theta \leq 2\pi\}$, with the Neumann-Dirichlet conditions, yields

$$\begin{aligned} G(\phi, \theta; \psi, \tau) &= -H_P\left(\frac{A_0^2}{\Phi_0(\phi)\Phi_0(\psi)}, \theta - \tau\right) + H_P\left(\frac{\Phi_0(\phi)\Phi_0(\psi)}{B_0^2}, \theta - \tau\right) \\ &+ \begin{cases} \ln\frac{\Phi_0(\phi)}{B_0} - H_P\left(\frac{\Phi_0(\phi)}{\Phi_0(\psi)}, \theta - \tau\right) + H_P\left(\frac{\Phi_0(\psi)A_0^2}{\Phi_0(\phi)B_0^2}, \theta - \tau\right) \\ \ln\frac{\Phi_0(\psi)}{B_0} - H_P\left(\frac{\Phi_0(\psi)}{\Phi_0(\phi)}, \theta - \tau\right) + H_P\left(\frac{\Phi_0(\phi)A_0^2}{\Phi_0(\psi)B_0^2}, \theta - \tau\right) \end{cases} + R_{ND} \end{aligned} \tag{2.43}$$

where

$$R_{ND} = R_{ND}(\phi, \theta; \psi, \tau) = \sum_{n=1}^{\infty} \frac{1}{2\pi n} \frac{A_0^{2n}\left(B_0^{2n} - \Phi_0^{2n}(\phi)\right)\left(\Phi_0^{2n}(\psi) + A_0^{2n}\right)}{B_0^{2n}\Phi_0^n(\phi)\Phi_0^n(\psi)\left(B_0^{2n} + A_0^{2n}\right)} \cos n(\theta - \tau)$$

An illustrative example for the 2π-periodic problem setting is shown below.

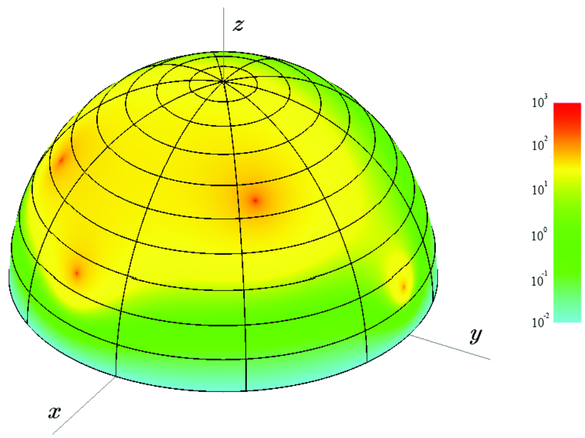

Figure 4: Potential field generated by multiple point sources in a spherical cap

In Figure 4 we depict the potential field generated by four point sources in the spherical cap

$$\Omega = \{(\phi, \theta)\,|0 \leq \phi \leq 0.5\pi, 0 \leq \theta < 2\pi\}$$

This potential field is simulated by superposition of four profiles of the Green's function from (2.41) with point sources located at $(0.22\pi, 0.24\pi)$, $(0.42\pi, 0.5\pi)$, $(0.27\pi, 1.7\pi)$, and $(0.37\pi, 1.9\pi)$.

2.2 Problems on 2π-periodic cylindrical surface

The list of surfaces that allow application of our approach is not limited to those we touched upon so far. To illustrate this point, we consider a boundary-value problem posed on a fragment $\Omega = \{z, \theta \mid 0 \leq z \leq h;\ 0 \leq \theta \leq 2\pi\}$ of a cylindrical surface of radius a, shown in Figure 5.

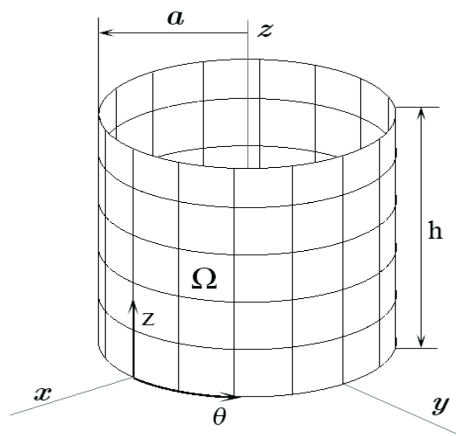

Figure 5: Closed cylindrical shell of a finite height

Let the two-dimensional Poisson equation

$$\frac{\partial^2 u(z,\theta)}{\partial z^2} + \frac{1}{a^2}\frac{\partial^2 u(z,\theta)}{\partial \theta^2} = -f(z,\theta), \quad \text{in } \Omega \tag{2.44}$$

written in cylindrical coordinates be subject to the boundary conditions

$$u(z,0) = u(z,2\pi), \quad \frac{\partial u(z,0)}{\partial \theta} = \frac{\partial u(z,2\pi)}{\partial \theta} \tag{2.45}$$

and

$$u(0,\theta) = 0, \quad \frac{\partial u(h,\theta)}{\partial z} = 0 \tag{2.46}$$

To obtain the solution to the above boundary-value problem in terms of the Green's function of the homogeneous problem corresponding to (2.44)-(2.46), we refer to the Fourier series expansions in (2.26) and (2.27), reducing the governing partial differential equation in (2.44) to the set of ordinary differential equations

$$\frac{d^2 u_n(z)}{dz^2} - \frac{n^2}{a^2} u_n(z) = -f_n(z) \tag{2.47}$$

subject to the boundary conditions

$$u_n(0) = 0, \quad \text{and} \quad \frac{du_n(h)}{dz} = 0 \tag{2.48}$$

Note that the case of $n = 0$ should be considered separately, and we will do it later. A fundamental set of solutions of the homogeneous equation, corresponding to (2.47), for the case of $n \geq 1$, could be chosen as

$$e^{nz/a} \quad \text{and} \quad e^{-nz/a}$$

Applying the standard method of variation of parameters, one obtains the general solution of the non-homogeneous equation in (2.47) as

$$\begin{aligned} u_n(z) = \frac{a}{2n} \int_0^z & \left[e^{n(z-s)/a} - e^{-n(z-s)/a} \right] f_n(s)\, ds \\ & + D_1 e^{nz/a} + D_2 e^{-nz/a} \end{aligned} \tag{2.49}$$

The first boundary condition in (2.48) yields

$$D_1 + D_2 = 0 \tag{2.50}$$

while the second condition in (2.48) results in

$$D_1 e^{nh/a} - D_2 e^{-nh/a} = -\frac{a}{2n} \int_0^h \left[e^{n(h-s)/a} - e^{-n(h-s)/a} \right] f_n(s)\, ds \tag{2.51}$$

The equations in (2.50) and (2.51) form a system of linear algebraic equations in D_1 and D_2. Solving for the latter we find then the solution for the boundary-value problem in (2.47)-(2.48) as

$$\begin{aligned} u_n(z) = & -\frac{a}{n} \int_0^z \frac{\sinh(ns/a) \sinh(n(h-z)/a)}{\cosh(nh/a)} f_n(s)\, ds \\ & -\frac{a}{n} \int_z^h \frac{\sinh(nz/a) \sinh(n(h-s)/a)}{\cosh(nh/a)} f_n(s)\, ds \end{aligned} \tag{2.52}$$

which, according to (1.22) (see Chapter 1), provides us with the Green's function of the homogeneous boundary-value problem corresponding to (2.47)-(2.48) in the form

$$g_n(z, s) = -\frac{a}{n \cosh(nh/a)} \begin{cases} \sinh(nz/a) \sinh(n(h-s)/a), & \text{if } 0 \leq z \leq s \\ \sinh(ns/a) \sinh(n(h-z)/a), & \text{if } s \leq z \leq h \end{cases} \tag{2.53}$$

At this point we turn back to the problem setting in (2.47)-(2.48), and consider the case of $n = 0$ for which the governing equation reduces to

$$\frac{d^2 u_0(z)}{dz^2} = -f_0(z) \tag{2.54}$$

Using our customary variation of parameters procedure, one finds the Green's function for the boundary value problem in (2.54), (2.48) as

$$g_0(z,s) = \begin{cases} z, & \text{if } 0 \le z \le s \\ s, & \text{if } s \le z \le h \end{cases} \tag{2.55}$$

So, with the explicit expressions just obtained for $g_0(z,s)$ and $g_n(z,s)$, the Green's function of the boundary-value problem in (2.44)-(2.46) reads as

$$G(z,\theta;s,\tau) = \frac{1}{2}g_0(z,s) + \sum_{n=1}^{\infty} g_n(z,s)\cos n(\theta-\tau) \tag{2.56}$$

The above series converges non-uniformly due to the logarithmic singularity of the Green's function. To enhance the series computability, we split off its singular and regular components. But before going any further with this, introduce the function

$$\widetilde{g}_n(z,s) = -\frac{a}{n}\begin{cases} \sinh(nz/a)\sinh(n(h-s)/a), & \text{if } 0 \le z \le s \\ \sinh(ns/a)\sinh(n(h-z)/a), & \text{if } s \le z \le h \end{cases}$$

which reads, in terms of the coefficients $g_n(z,s)$ of the series in (2.56), as

$$\widetilde{g}_n(z,s) = g_n(z,s)\cosh(nh/a)$$

Thus, the series in (2.56) can be transformed as

$$\begin{aligned}
&\sum_{n=1}^{\infty} g_n(z,s)\cos n(\theta-\tau) = 2\sum_{n=1}^{\infty}\frac{\widetilde{g}_n(z,s)}{e^{nh/a}+e^{-nh/a}}\cos n(\theta-\tau)\\
=\;& 2\sum_{n=1}^{\infty}\frac{\widetilde{g}_n(z,s)}{e^{nh/a}+e^{-nh/a}}\cos n(\theta-\tau) + 2\sum_{n=1}^{\infty}\frac{\widetilde{g}_n(z,s)}{e^{nh/a}}\cos n(\theta-\tau)\\
&-2\sum_{n=1}^{\infty}\frac{\widetilde{g}_n(z,s)}{e^{nh/a}}\cos n(\theta-\tau)\\
=\;& 2\sum_{n=1}^{\infty}\frac{\widetilde{g}_n(z,s)}{e^{nh/a}}\cos n(\theta-\tau) - 2\sum_{n=1}^{\infty}\frac{\widetilde{g}_n(z,s)}{e^{3nh/a}+e^{nh/a}}\cos n(\theta-\tau)
\end{aligned}$$

Notice that while the second of the two series above converges uniformly (allowing by the way a direct truncation), the first one appears summable. Indeed, application of the standard formula shown in (2.37) yields

$$\begin{aligned}
&\sum_{n=1}^{\infty}\frac{\widetilde{g}_n(z,s)}{e^{nh/a}}\cos n(\theta-\tau)\\
=\;& a\left[H_P\left(e^{(z+s-2h)/a},\theta-\tau\right)+H_P\left(e^{(-z-s)/a},\theta-\tau\right)\right.\\
&\left.-H_P\left(e^{(z-s)/a},\theta-\tau\right)-H_P\left(e^{(-z+s-2h)/a},\theta-\tau\right)\right] \qquad (2.57)
\end{aligned}$$

where $H_P(x,\alpha)$ was introduced earlier in (2.38).

Hence, we finally arrived at an ultimate computer-friendly representation of the Green's function that we are looking for. That is

$$\begin{aligned}
G(z,\theta;s,\tau) \;=\;& a\left[H_P\left(e^{(z+s-2h)/a},\theta-\tau\right)+H_P\left(e^{(-z-s)/a},\theta-\tau\right)\right]+R(z,\theta;s,\tau)\\
&+\begin{cases} z/2-a\left[H_P\left(e^{(z-s)/a},\theta-\tau\right)+H_P\left(e^{(-z+s-2h)/a},\theta-\tau\right)\right]\\ s/2-a\left[H_P\left(e^{(-z+s)/a},\theta-\tau\right)+H_P\left(e^{(z-s-2h)/a},\theta-\tau\right)\right]\end{cases} \qquad (2.58)
\end{aligned}$$

where

$$R(z,\theta;s,\tau)=-2\sum_{n=1}^{\infty}\frac{\widetilde{g}_n(z,s)}{e^{3nh/a}+e^{nh/a}}\cos n(\theta-\tau).$$

and the $z/2$ containing branch of the last additive component in (2.58) is valid for $0\le z\le s$, while the $s/2$ containing branch stays for $s\le z\le h$.

In Figure 6 we show superposition of five Green's function profiles for the boundary-value problem posed in (2.44)-(2.46). The region Ω is chosen to be

$$\{z,\theta|0\le z\le 3.0, 0\le\theta<2\pi\}$$

and the point sources are located at $(0.8,0.12\pi)$, $(0.8,0.48\pi)$, $(1.6,0.07\pi)$, $(1.6,0.53\pi)$, and $(2.4,0.35\pi)$.

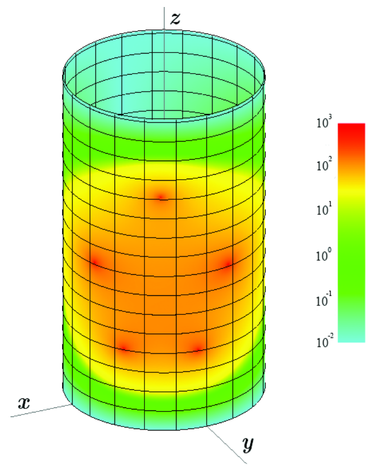

Figure 6: Field generated by multiple point sources in thin closed cylindrical shell

The described technique was used to find Green's functions for a number of boundary-value problems posed in various regions on a cylindrical shell. Table 2 summarizes all the results we obtained. We use the 4-letter abbreviation similar to that introduced earlier in the previous section to specify the boundary conditions: "D" stays for the Dirichlet condition, while "N" stays for the Nuemann condition, "I" is used, when the boundedness condition is imposed at infinity. In the case of 2π-periodicity, the "P" character is used. We present only the branches valid for $0 \leq z \leq s$, and the other branches could be obtained by interchanging the variables z and s. The functions H_D, H_N, and H_P, as well as the parameters κ and η were introduced earlier (see (2.23), (2.20), (2.38), and (2.21)).

Table 2: Green's functions for problems posed on a cylinder

#	Boundary conditions	Green's function
1	DDII	$-aH_D\left(e^{\pi(z-s)/a\gamma}, \kappa, \eta\right)$
2	DNII	$-aH_N\left(e^{\pi(z-s)/2a\gamma}, \frac{\kappa}{2}, \frac{\eta}{2}\right)$
3	DDDI	$aH_D\left(e^{-\pi(z+s)/a\gamma}, \kappa, \eta\right) - aH_D\left(e^{\pi(z-s)/a\gamma}, \kappa, \eta\right)$
4	DNDI	$aH_N\left(e^{-\pi(z+s)/2a\gamma}, \frac{\kappa}{2}, \frac{\eta}{2}\right) - aH_N\left(e^{\pi(z-s)/2a\gamma}, \frac{\kappa}{2}, \frac{\eta}{2}\right)$
5	DDDD	$aH_D\left(e^{\pi(z+s-2h)/a\gamma}, \kappa, \eta\right) - aH_D\left(e^{\pi(z-s)/a\gamma}, \kappa, \eta\right)$ $-aH_D\left(e^{\pi(-z+s-2h)/a\gamma}, \kappa, \eta\right) + aH_D\left(e^{-\pi(z+s)/a\gamma}, \kappa, \eta\right) + R_5$
6	DNDD	$aH_N\left(e^{\pi(z+s-2h)/2a\gamma}, \frac{\kappa}{2}, \frac{\eta}{2}\right) - aH_N\left(e^{\pi(z-s)/2a\gamma}, \frac{\kappa}{2}, \frac{\eta}{2}\right)$ $-aH_N\left(e^{\pi(-z+s-2h)/2a\gamma}, \frac{\kappa}{2}, \frac{\eta}{2}\right) + aH_N\left(e^{-\pi(z+s)/2a\gamma}, \frac{\kappa}{2}, \frac{\eta}{2}\right) + R_6$
7	DDDN	$-aH_D\left(e^{\pi(z+s-2h)/a\gamma}, \kappa, \eta\right) - aH_D\left(e^{\pi(z-s)/a\gamma}, \kappa, \eta\right)$ $+aH_D\left(e^{\pi(-z+s-2h)/a\gamma}, \kappa, \eta\right) + aH_D\left(e^{-\pi(z+s)/a\gamma}, \kappa, \eta\right) + R_7$
8	DNDN	$-aH_D\left(e^{\pi(z+s-2h)/2a\gamma}, \frac{\kappa}{2}, \frac{\eta}{2}\right) - aH_D\left(e^{\pi(z-s)/2a\gamma}, \frac{\kappa}{2}, \frac{\eta}{2}\right)$ $+aH_D\left(e^{\pi(-z+s-2h)/2a\gamma}, \frac{\kappa}{2}, \frac{\eta}{2}\right) + aH_D\left(e^{-\pi(z+s)/2a\gamma}, \frac{\kappa}{2}, \frac{\eta}{2}\right) + R_8$
9	PDD	$aH_P\left(e^{(z+s-2h)/a}, \theta-\tau\right) - aH_P\left(e^{(z-s)/a}, \theta-\tau\right)$ $-aH_P\left(e^{(-z+s-2h)/a}, \theta-\tau\right) + aH_P\left(e^{-(z+s)/a}, \theta-\tau\right) + R_9$
10	PDN	$z - aH_P\left(e^{(z+s-2h)/a}, \theta-\tau\right) - aH_P\left(e^{(z-s)/a}, \theta-\tau\right)$ $+aH_P\left(e^{(-z+s-2h)/a}, \theta-\tau\right) + aH_P\left(e^{-(z+s)/a}, \theta-\tau\right) + R_{10}$
11	PDI	$aH_P\left(e^{-(z+s)/a}, \theta-\tau\right) - aH_P\left(e^{(z-s)/a}, \theta-\tau\right)$

Table 2 provides the Green's functions for problems posed on five different cylindrical fragments:

1. Infinite cylindrical shell $\{z, \theta \mid -\infty \le z \le \infty;\ 0 \le \theta \le \gamma\}$ for problems in rows 1-2;

2. Semi-infinite cylindrical shell $\{z, \theta \mid 0 \le z \le \infty;\ 0 \le \theta \le \gamma\}$ in rows 3-4;

3. Cylindrical rectangle $\{z, \theta \mid 0 \le z \le h;\ 0 \le \theta \le \gamma\}$ in rows 5-8;

4. Finite cylindrical shell $\{z, \theta \mid 0 \le z \le h;\ 0 \le \theta \le 2\pi\}$ in rows 9-10;

5. Semi-infinite cylindrical shell $\{z, \theta \mid 0 \le z \le \infty;\ 0 \le \theta \le 2\pi\}$ in row 11.

The regular components $R_i = R_i\,(z, \theta; s, \tau)$, $i = \overline{5, 10}$ are found as

$$R_5 = \sum_{n=1}^{\infty} \frac{a}{2\pi n} \frac{\sinh\left(n\pi z/\gamma a\right) \sinh\left(n\pi (s-h)/\gamma a\right)}{e^{2\pi n h/\gamma a} \sinh\left(n\pi h/\gamma a\right)} \left(\cos n\eta - \cos n\kappa\right),$$

$$R_6 = \sum_{n=1}^{\infty} \frac{a}{2\pi n} \frac{\sinh\left(n\pi z/2\gamma a\right) \sinh\left(n\pi (s-h)/2\gamma a\right)}{e^{n\pi h/\gamma a} \sinh\left(n\pi h/2\gamma a\right)} \left(\cos \frac{n\eta}{2} - \cos \frac{n\kappa}{2}\right),$$

$$R_7 = \sum_{n=1}^{\infty} \frac{a}{2\pi n} \frac{\sinh\left(n\pi z/\gamma a\right) \cosh\left(n\pi (s-h)/\gamma a\right)}{e^{2n\pi h/\gamma a} \cosh\left(n\pi h/\gamma a\right)} \left(\cos n\eta - \cos n\kappa\right),$$

$$R_8 = \sum_{n=1}^{\infty} \frac{a}{2\pi n} \frac{\sinh\left(n\pi z/2\gamma a\right) \cosh\left(n\pi (s-h)/2\gamma a\right)}{e^{n\pi h/\gamma a} \cosh\left(n\pi h/2\gamma a\right)} \left(\cos \frac{n\eta}{2} - \cos \frac{n\kappa}{2}\right),$$

$$R_9 = \sum_{n=1}^{\infty} \frac{a}{2\pi n} \frac{\sinh\left(nz/a\right) \sinh\left(n(s-h)/a\right)}{e^{2nh/a} \sinh\left(nh/a\right)} \cos n\left(\theta - \tau\right),$$

and

$$R_{10} = \sum_{n=1}^{\infty} \frac{a}{2\pi n} \frac{\sinh\left(nz/a\right) \cosh\left(n(s-h)/a\right)}{e^{2nh/a} \cosh\left(nh/a\right)} \cos n\left(\theta - \tau\right).$$

As another illustrative example, the potential field generated by three point sources in a cylindrical rectangle, with Dirichlet boundary conditions, is shown in Figure 7. The Green's function presented in row 5 of Table 2 is employed. A half of cylindrical shell of radius $a = 1.0$, and height $h = 2.0$ is considered. The locations of the point sources are $(0.9, 0.07\pi)$, $(0.7, 0.65\pi)$, and $(1.5, 0.75\pi)$.

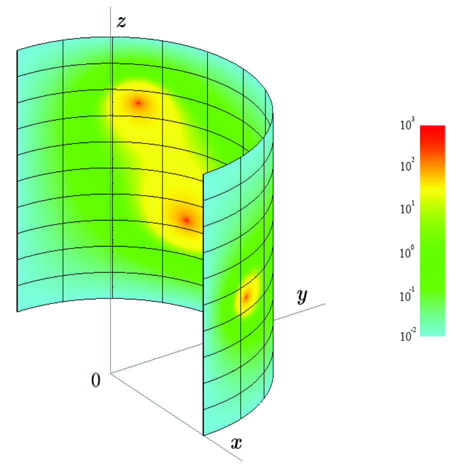

Figure 7: Three point sources in a cylindrical quadrilateral

The results obtained so far are for problems with Dirichlet and Neumann boundary conditions imposed on different fragments of regions' boundaries. In what follows, the derivation of Green's functions for boundary-value problems with Robin conditions are presented.

Consider the two-dimensional Poisson equation in (2.44) posed on a closed cylindrical region of height h, subject to the boundary condition

$$u\left(0,\theta\right)-\lambda\frac{\partial u\left(0,\theta\right)}{\partial z}=0,\quad u\left(h,\theta\right)=0 \tag{2.59}$$

where λ is a positive constant representing the thermal conductivity of the material of which the shell is made. We aim at finding the Green's function for the boundary-value problem in (2.44), (2.45), and (2.59). Since the region is closed ($0\leq\theta\leq2\pi$), the Green's function is looked for in the form of (2.56). Following the standard separation of variables procedure, we use the series expansions in (2.26) and (2.27). This reduces the governing boundary-value problem to

$$\frac{d^2u_n\left(z\right)}{dz^2}-\frac{n^2}{a^2}u_n\left(z\right)=-f_n\left(z\right) \tag{2.60}$$

$$u_n\left(0\right)-\lambda\frac{du_n\left(0\right)}{dz}=0,\quad u_n\left(h\right)=0 \tag{2.61}$$

in the coefficients $u_n(z)$ of the trigonometric Fourier series.

Consider the case of $n > 0$, while the case $n = 0$ is to be treated separately. The general solution of the above equation is already found in (2.49) as

$$u_n(z) = \frac{a}{2n} \int_0^z \left[e^{n(z-s)/a} - e^{-n(z-s)/a} \right] f_n(s)\, ds + D_1 e^{nz/a} + D_2 e^{-nz/a} \tag{2.62}$$

Satisfying the boundary conditions in (2.61) one comes up with the system of linear algebraic equations

$$\begin{pmatrix} 1 - \lambda n/a & 1 + \lambda n/a \\ e^{nh/a} & e^{-nh/a} \end{pmatrix} \begin{pmatrix} D_1 \\ D_2 \end{pmatrix} = \begin{pmatrix} 0 \\ -aI/n \end{pmatrix}$$

in D_1 and D_2, which results in

$$D_1 = \frac{a}{n\Delta}\left(1 + \frac{\lambda}{a} n\right) I, \quad D_1 = -\frac{a}{n\Delta}\left(1 - \frac{\lambda}{a} n\right) I$$

where

$$I = \int_0^h \sinh\left(n\left(h - s\right)/a\right) f_n(s)\, ds$$

and

$$\Delta = \left(1 - \frac{\lambda}{a} n\right) e^{-nh/a} - \left(1 + \frac{\lambda}{a} n\right) e^{nh/a}$$

Substituting the above into (2.62) one obtains

$$\begin{aligned} u_n(z) &= \frac{a}{n\Delta} \int_0^z \sinh\left(n\left(h - z\right)/a\right) \left[\left(1 + \frac{\lambda}{a} n\right) e^{ns/a} - \left(1 - \frac{\lambda}{a} n\right) e^{-ns/a} \right] f_n(s)\, ds \\ &\quad + \frac{a}{n\Delta} \int_z^h \sinh\left(n\left(h - s\right)/a\right) \left[\left(1 + \frac{\lambda}{a} n\right) e^{nz/a} - \left(1 - \frac{\lambda}{a} n\right) e^{-nz/a} \right] f_n(s)\, ds \end{aligned}$$

The Green's function for the homogeneous boundary-value problem corresponding to that in (2.60) and (2.61) is found as

$$g_n(z, s) = \frac{a}{n\Delta} \begin{cases} \sinh\left(n(h - s)/a\right) \left[\left(1 - n\lambda/a\right) e^{-nz/a} - \left(1 + n\lambda/a\right) e^{nz/a} \right], & \text{if } 0 \le z \le s \\ \sinh\left(n(h - z)/a\right) \left[\left(1 - n\lambda/a\right) e^{-ns/a} - \left(1 + n\lambda/a\right) e^{ns/a} \right], & \text{if } s \le z \le h \end{cases} \tag{2.63}$$

For the case of $n = 0$, the equation in (2.60) reduces to

$$\frac{d^2 u_0(z)}{dz^2} = -f_0(z) \tag{2.64}$$

Applying the standard method of variation of parameters, one finds the solution for the problem in (2.61) and (2.64) as

$$u_0(z) = \int_0^z \frac{(\lambda+s)(h-z)}{\lambda+h} f_0(s)\,ds + \int_z^h \frac{(\lambda+z)(h-s)}{\lambda+h} f_0(s)\,ds$$

which results in

$$g_0(z,s) = \frac{1}{\lambda+h}\begin{cases} (\lambda+z)(h-s), & \text{if } 0 \le z \le s \\ (\lambda+s)(h-z), & \text{if } s \le z \le h \end{cases} \tag{2.65}$$

Note, that the two branches of the Green's functions in (2.63) and (2.65) are symmetric, hence, the further analysis may be provided only for the case $z \le s$, since the other case could be treated by formal interchange of the variables z and s. After the substitution of (2.63) and (2.65) into (2.56) we obtain the series which converges non-uniformly and cannot be completely summed up. Following the procedure described earlier, we set apart its logarithmic and regular components as

$$G(z,\theta;s,\tau) = \frac{1}{2}g_0(z,s) + L(z,\theta;s,\tau) + P(z,\theta;s,\tau)$$

where

$$L(z,\theta;s,\tau) = \sum_{n=1}^{\infty}\frac{a}{2\pi n}\Big[\frac{1-n\lambda/a}{1+n\lambda/a}e^{n(-z-s)/a} - \frac{1-n\lambda/a}{1+n\lambda/a}e^{n(-z+s-2h)/a}$$
$$+e^{n(z+s-2h)/a} - e^{n(z-s)/a}\Big]\cos n(\theta-\tau) \tag{2.66}$$

and

$$P(z,\theta;s,\tau) = \sum_{n=1}^{\infty}\frac{a}{2\pi n}\frac{a-n\lambda}{a+n\lambda}P_n(z,s)\cos n(\theta-\tau) \tag{2.67}$$

with

$$P_n(z,s) = \frac{\sinh(n(h-s)/a)\left[(a-n\lambda)e^{-nz/a} - (a+n\lambda)e^{nz/a}\right]}{(a+n\lambda)e^{3nh/a} - (a-n\lambda)e^{nh/a}}$$

It appears that, the last two of the four additive components in (2.66) allow a complete summation. In order to achieve high computational efficiency for the first two components, some algebra should be applied. We show in detail the transformations for just one of them implying that the second component can be transformed in a similar way. That is

$$\begin{aligned}
&\frac{a}{2\pi n}\frac{1-n\lambda/a}{1+n\lambda/a}e^{n(-z-s)/a} = \frac{a}{2\pi n}e^{n(-z-s)/a} - \frac{\lambda}{\pi\left(1+n\lambda/a\right)}e^{n(-z-s)/a} \\
= \;& \frac{a}{2\pi n}e^{n(-z-s)/a} - \frac{\lambda}{\pi\left(1+n\lambda/a\right)}e^{n(-z-s)/a} + \frac{a}{\pi n}e^{n(-z-s)/a} - \frac{a}{\pi n}e^{n(-z-s)/a} \\
= \;& -\frac{a}{2\pi n}e^{n(-z-s)/a} + \frac{a}{\pi n\left(1+n\lambda/a\right)}e^{n(-z-s)/a}
\end{aligned}$$

If we substitute the above into (2.66), the second component of the above has the convergence rate of $1/n^2$ while the first one falls into the standard summation formula in (2.37) territory. With all this in mind, we ultimately obtain a computer-friendly form of the Green's function for the boundary-value problem in (2.44), (2.45), and (2.59) as

$$\begin{aligned}
G\left(z,\theta;s,\tau\right) = \frac{\left(\lambda+z\right)\left(h-s\right)}{\lambda+h} &+ aH_P\left(e^{(z+s-2h)/a},\theta-\tau\right) - aH_P\left(e^{(-z-s)/a},\theta-\tau\right) \\
&+aH_P\left(e^{(-z+s-2h)/a},\theta-\tau\right) - aH_P\left(e^{(z-s)/a},\theta-\tau\right) + R\left(z,\theta;s,\tau\right)
\end{aligned}$$

where

$$R\left(z,\theta;s,\tau\right) = \sum_{n=1}^{\infty}\frac{a}{\pi n}\frac{e^{n(-z-s)/a} - e^{n(-z+s-2h)/a}}{\left(1+n\lambda/a\right)}\cos n\left(\theta-\tau\right) + P\left(z,\theta;s,\tau\right)$$

and the term $P\left(z,\theta;s,\tau\right)$ is presented in (2.67).

To illustrate the computability of the representation of the Green's function to the problem setting in (2.44), (2.45), and (2.59) (that we just obtained), we depict in Figure 8 the potential fields generated by a point source located at $(0.66, 0.42\pi)$ in the closed cylindrical shell of radius $a = 1.0$ and height $h = 1.0$. Three different values 0.0, 1.0, and 10.0 have been chosen for the parameter λ in (2.59).

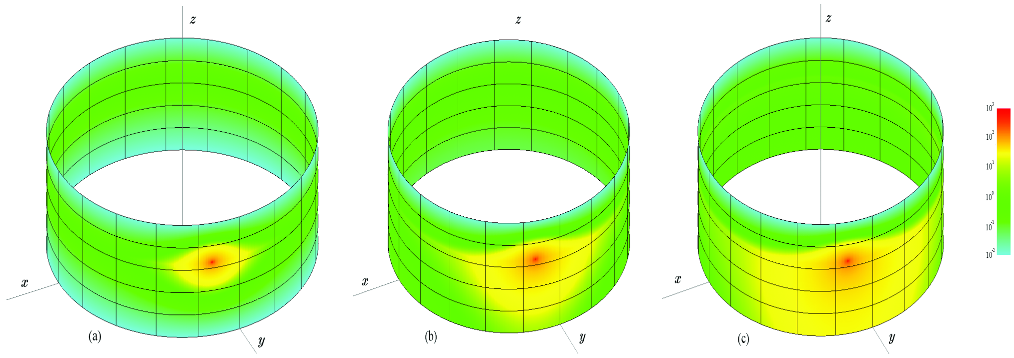

Figure 8: A point source in a cylindrical shell with Dirichlet and Robin boundary conditions imposed

Note that in the case of $\lambda = 0.0$ (fragment (a)), the first of the boundary conditions in (2.59) reduces to the Dirichlet type, whilst the fragment (c) reduces practically to the Neumann type condition.

2.3 Problem posed on a toroidal surface

For another problem setting, illustrating our approach, consider the quadrilateral

$$\Omega = \{\varphi, \theta \mid \varphi_0 \leq \varphi \leq \varphi_1;\ 0 \leq \theta \leq \gamma\},$$

on a toroidal surface with radii R and r (see Figure 9).

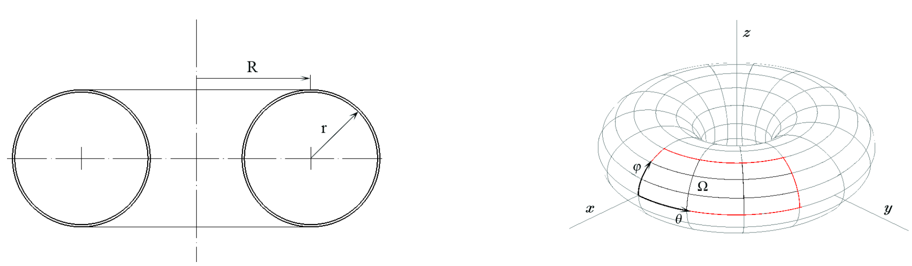

Figure 9: The toroidal surface (axial cross-section and a quadrilateral Ω)

The nonhomogeneous equation that simulates potential-type phenomenon in a fragment Ω of a toroidal shell reads as

$$\frac{1}{D(\varphi)}\frac{\partial}{\partial\varphi}\left(D(\varphi)\frac{\partial u(\varphi,\theta)}{\partial\varphi}\right)+\frac{r^2}{D^2(\varphi)}\frac{\partial^2 u(\varphi,\theta)}{\partial\theta^2}=-f(\varphi,\theta) \tag{2.68}$$

which we subject to the Dirichlet boundary conditions

$$u(\varphi,0)=0,\quad u(\varphi,\gamma)=0 \tag{2.69}$$

and

$$u(\varphi_0,\theta)=0,\quad u(\varphi_1,\theta)=0 \tag{2.70}$$

The function $D(\varphi)$ in (2.68) is defined in terms of the radii R and r of the considered toroidal surface as

$$D(\varphi)=R+r\sin\varphi.$$

To construct the Green's function for the homogeneous boundary-value problem corresponding to (2.68)-(2.70) we follow the strategy implemented earlier in Sections 2.1 and 2.2, and express the solution $u(\varphi,\theta)$ of the problem in (2.68)-(2.70) and the right-hand side $f(\varphi,\theta)$ of the governing equation in the Fourier series

$$u(\phi,\theta)=\sum_{n=1}^{\infty}u_n(\phi)\sin\nu\theta \tag{2.71}$$

and

$$f(\phi,\theta)=\sum_{n=1}^{\infty}f_n(\phi)\sin\nu\theta \tag{2.72}$$

where $\nu=n\pi/\gamma$. This reduces the partial differential equation in (2.68) to the set of ordinary differential equations

$$\frac{1}{r}\frac{d}{d\varphi}\left(D(\varphi)\frac{du_n(\varphi)}{d\varphi}\right)-\frac{r\nu^2}{D(\varphi)}u_n(\varphi)=-\widetilde{f}_n(\varphi) \tag{2.73}$$

subject to the boundary conditions

$$u_n(\varphi_0)=0,\quad u_n(\varphi_1)=0 \tag{2.74}$$

in the coefficients $u_n(\varphi)$ of the series in (2.71), where

$$\widetilde{f}_n(\varphi) = \frac{D(\varphi)}{r} f_n(\varphi).$$

The fundamental set of solutions of the homogeneous equation corresponding to (2.73) could be chosen [31] as

$$e^{\nu\omega(\varphi)} \quad \text{and} \quad e^{-\nu\omega(\varphi)}$$

where

$$\omega(\varphi) = \frac{2r}{\sqrt{R^2 - r^2}} \arctan\left(\frac{r + R\tan(\varphi/2)}{\sqrt{R^2 - r^2}}\right) \tag{2.75}$$

Proceeding with the standard variation of parameter routine, we arrive at the general solution to (2.73) as

$$u_n(\varphi) = \frac{1}{2\nu} \int_{\varphi_0}^{\varphi} \left(e^{\nu(\omega(\varphi)-\omega(\xi))} - e^{-\nu(\omega(\varphi)-\omega(\xi))}\right) \widetilde{f}_n(\xi)\, d\xi + D_1 e^{\nu\omega(\varphi)} + D_2 e^{-\nu\omega(\varphi)}$$

The following system of linear algebraic equations in D_1 and D_2

$$\begin{pmatrix} e^{\nu\omega(\varphi_0)} & e^{-\nu\omega(\varphi_0)} \\ e^{\nu\omega(\varphi_1)} & e^{-\nu\omega(\varphi_1)} \end{pmatrix} \begin{pmatrix} D_1 \\ D_2 \end{pmatrix} = \begin{pmatrix} 0 \\ F(\varphi_0, \varphi_1) \end{pmatrix}$$

where

$$F(\varphi_0, \varphi_1) = -\frac{1}{\nu} \int_{\varphi_0}^{\varphi_1} \sinh \nu (\omega(\varphi_1) - \omega(\xi))\, \widetilde{f}_n(\xi)\, d\xi$$

appears when the boundary conditions in (2.74) are recalled. It reveals the constants D_1 and D_2 in the form

$$D_1 = \frac{e^{-\nu\omega(\varphi_0)}}{2\nu\Delta} \int_{\varphi_0}^{\varphi_1} \sinh \nu (\omega(\varphi_1) - \omega(\xi))\, \widetilde{f}_n(\xi)\, d\xi$$

and

$$D_2 = -\frac{e^{\nu\omega(\varphi_0)}}{2\nu\Delta} \int_{\varphi_0}^{\varphi_1} \sinh \nu (\omega(\varphi_1) - \omega(\xi))\, \widetilde{f}_n(\xi)\, d\xi$$

where

$$\Delta = \sinh \nu (\omega(\varphi_0) - \omega(\varphi_1))$$

After substituting the above expressions for D_1 and D_2 into (2.73), we present the solution of the boundary-value problem in (2.73)-(2.74) as

$$\begin{aligned} u_n(\varphi) &= \frac{2}{\nu\Delta}\left[\int_{\varphi_0}^{\varphi} \sinh\left(\nu\left(\omega(\xi)-\omega(\varphi_0)\right)\right)\sinh\left(\nu\left(\omega(\varphi_1)-\omega(\varphi)\right)\right)\widetilde{f}_n(\xi)\,d\xi\right. \\ &\quad \left. + \int_{\varphi}^{\varphi_1} \sinh\left(\nu\left(\omega(\varphi)-\omega(\varphi_0)\right)\right)\sinh\left(\nu\left(\omega(\varphi_1)-\omega(\xi)\right)\right)\widetilde{f}_n(\xi)\,d\xi\right] \end{aligned}$$

from which the kernel function $g_n(\varphi,\xi)$ of the above representation

$$u_n(\varphi) = \int_{\varphi_0}^{\varphi_1} g_n(\varphi,\xi)\,\widetilde{f}_n(\xi)\,d\xi$$

follows as

$$g_n(\varphi,\xi) = \frac{2}{\nu\Delta}\begin{cases} \sinh\left(\nu\left(\omega(\xi)-\omega(\varphi_0)\right)\right)\sinh\left(\nu\left(\omega(\varphi_1)-\omega(\varphi)\right)\right) & \varphi_0 \le \xi \le \varphi \\ \sinh\left(\nu\left(\omega(\varphi)-\omega(\varphi_0)\right)\right)\sinh\left(\nu\left(\omega(\varphi_1)-\omega(\xi)\right)\right) & \varphi \le \xi \le \varphi_1 \end{cases} \tag{2.76}$$

With this, the Green's function for the homogeneous boundary-value problem corresponding to (2.68)-(2.70) appears as

$$G(\phi,\theta;\psi,\tau) = \frac{2}{\gamma}\sum_{n=1}^{\infty} g_n(\varphi,\xi)\sin\nu\theta\sin\nu\tau$$

We partially sum up the above series with the coefficients shown in (2.76). In doing so we use the standard summation formula [30]

$$\sum_{n=1}^{\infty}\frac{p^n}{n}\cos n\alpha = -\frac{1}{2}\ln\left(1-2p\cos\alpha+p^2\right) \tag{2.77}$$

that is valid for $p<1$ and $0 \le \alpha < 2\pi$.

After setting apart the logarithmic and the regular components of the series representing the Green's function, the latter appears as

$$\begin{aligned} G(\varphi,\theta;\xi,\tau) &= -\begin{cases} H_D\left(e^{\frac{\pi}{\gamma}(\omega(\varphi)-\omega(\xi)+2\omega(\varphi_0)-2\omega(\varphi_1))},\eta,\kappa\right) + H_D\left(e^{\frac{\pi}{\gamma}(\omega(\xi)-\omega(\varphi))},\eta,\kappa\right) \\ H_D\left(e^{\frac{\pi}{\gamma}(\omega(\xi)-\omega(\varphi)+2\omega(\varphi_0)-2\omega(\varphi_1))},\eta,\kappa\right) + H_D\left(e^{\frac{\pi}{\gamma}(\omega(\varphi)-\omega(\xi))},\eta,\kappa\right) \end{cases} \\ &\quad + H_D\left(e^{\frac{\pi}{\gamma}(\omega(\varphi)+\omega(\xi)-2\omega(\varphi_1))},\eta,\kappa\right) + H_D\left(e^{\frac{\pi}{\gamma}(2\omega(\varphi_0)-\omega(\varphi)-\omega(\xi))},\eta,\kappa\right) + R \end{aligned} \tag{2.78}$$

where η and κ have earlier been defined in (2.21), while the function $H_D\left(x,\alpha,\beta\right)$ can be found in (2.23). The upper branch corresponds to the case $\varphi_0 \leq \varphi \leq \xi$, whilst the lower branch represents the case $\xi \leq \varphi \leq \varphi_1$. The regular component $R = R\left(\varphi,\theta;\xi,\tau\right)$ is presented in the series form as

$$R\left(\varphi,\theta;\xi,\tau\right) = \sum_{n=1}^{\infty} \frac{g_n\left(\varphi,\xi\right)\Delta}{2\nu\left(e^{3\nu(\omega(\varphi_1)-\omega(\varphi_0))} - e^{\nu(\omega(\varphi_1)-\omega(\varphi_0))}\right)} \sin\nu\theta \sin\nu\tau$$

Illustrating the computational efficiency of the form in (2.78), we present in Figure 10 a field generated by two point sources in the region representing a quarter of the closed toroidal shell. The field is obtained as superposition of two Green's function profiles, with the sources located at $(0.33\pi, 0.22\pi)$ and $(0.67\pi, 0.77\pi)$.

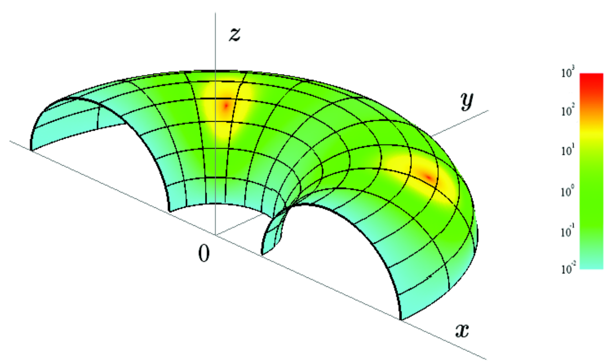

Figure 10. The field generated in a fragment of the toroidal shell

In Table 3 we present the list of Green's functions obtained for different boundary-value problems stated in regions on toroidal surface. The Table is organized a manner similar to that of Tables 1 and 2, with the functions H_D, H_N, H_P, as well as parameters η and κ introduced earlier in (2.23), (2.20), (2.38), and (2.21).

Table 3: Green's functions for problems posed on a toroidal surfaces

#	Boundary conditions	Green's function
1	DDDD	$H_D\left(e^{\pi(2\omega(\varphi_0)-\omega(\varphi)-\omega(\xi))/\gamma},\kappa,\eta\right)+H_D\left(e^{\pi(\omega(\varphi)+\omega(\xi)-2\omega(\varphi_1))/\gamma},\kappa,\eta\right)$ $-H_D\left(e^{\pi(\omega(\varphi)-\omega(\xi))/\gamma},\kappa,\eta\right)-H_D\left(e^{\pi(\omega(\xi)-\omega(\varphi)+2\omega(\varphi_0)-2\omega(\varphi_1))/\gamma},\kappa,\eta\right)+R_1$
2	DNDD	$H_N\left(e^{\pi(2\omega(\varphi_0)-\omega(\varphi)-\omega(\xi))/2\gamma},\frac{\kappa}{2},\frac{\eta}{2}\right)+H_N\left(e^{\pi(\omega(\varphi)+\omega(\xi)-2\omega(\varphi_1))/2\gamma},\frac{\kappa}{2},\frac{\eta}{2}\right)$ $-H_N\left(e^{\pi(\omega(\varphi)-\omega(\xi))/2\gamma},\frac{\kappa}{2},\frac{\eta}{2}\right)-H_N\left(e^{\pi(\omega(\xi)-\omega(\varphi)+2\omega(\varphi_0)-2\omega(\varphi_1))/2\gamma},\frac{\kappa}{2},\frac{\eta}{2}\right)+R_2$
3	DDDN	$H_D\left(e^{\pi(2\omega(\varphi_0)-\omega(\varphi)-\omega(\xi))/\gamma},\kappa,\eta\right)-H_D\left(e^{\pi(\omega(\varphi)+\omega(\xi)-2\omega(\varphi_1))/\gamma},\kappa,\eta\right)$ $-H_D\left(e^{\pi(\omega(\varphi)-\omega(\xi))/\gamma},\kappa,\eta\right)+H_D\left(e^{\pi(\omega(\xi)-\omega(\varphi)+2\omega(\varphi_0)-2\omega(\varphi_1))/\gamma},\kappa,\eta\right)+R_3$
4	DNDN	$H_N\left(e^{\pi(2\omega(\varphi_0)-\omega(\varphi)-\omega(\xi))/2\gamma},\frac{\kappa}{2},\frac{\eta}{2}\right)-H_N\left(e^{\pi(\omega(\varphi)+\omega(\xi)-2\omega(\varphi_1))/2\gamma},\frac{\kappa}{2},\frac{\eta}{2}\right)$ $-H_N\left(e^{\pi(\omega(\varphi)-\omega(\xi))/2\gamma},\frac{\kappa}{2},\frac{\eta}{2}\right)+H_N\left(e^{\pi(\omega(\xi)-\omega(\varphi)+2\omega(\varphi_0)-2\omega(\varphi_1))/2\gamma},\frac{\kappa}{2},\frac{\eta}{2}\right)+R_4$
5	PDD	$H_P\left(e^{2\omega(\varphi_0)-\omega(\varphi)-\omega(\xi)},\theta-\tau\right)+H_P\left(e^{\omega(\varphi)+\omega(\xi)-2\omega(\varphi_1)},\theta-\tau\right)$ $-H_P\left(e^{\omega(\varphi)-\omega(\xi)},\theta-\tau\right)-H_P\left(e^{\omega(\xi)-\omega(\varphi)+2\omega(\varphi_0)-2\omega(\varphi_1)},\theta-\tau\right)+R_5$
6	PDN	$H_P\left(e^{2\omega(\varphi_0)-\omega(\varphi)-\omega(\xi)},\theta-\tau\right)-H_P\left(e^{\omega(\varphi)+\omega(\xi)-2\omega(\varphi_1)},\theta-\tau\right)$ $-H_P\left(e^{\omega(\varphi)-\omega(\xi)},\theta-\tau\right)+H_P\left(e^{\omega(\xi)-\omega(\varphi)+2\omega(\varphi_0)-2\omega(\varphi_1)},\theta-\tau\right)+R_6$

Two toroidal regions are present in Table 3. For the first four rows, the toroidal rectangle $\Omega=\{\varphi,\theta \mid \varphi_0\leq\varphi\leq\varphi_1;\ 0\leq\theta\leq\gamma\}$ is considered, while for the last 2 rows the closed in the longitudinal direction fragment $\Omega=\{\varphi,\theta \mid \varphi_0\leq\varphi\leq\varphi_1;\ 0\leq\theta\leq 2\pi\}$ of torus is presented. The regular components $R_i=R_i\left(\varphi,\theta;\xi,\tau\right),\ i=\overline{1,6}$ are found as

$$R_1=\sum_{n=1}^{\infty}\frac{1}{2\pi n}\frac{\sinh\left(n\pi\left(\omega(\xi)-\omega(\varphi_1)\right)/\gamma\right)\sinh\left(n\pi\left(\omega(\varphi_0)-\omega(\varphi)\right)/\gamma\right)}{e^{2n\pi(\omega(\varphi_1)-\omega(\varphi_0))/\gamma}\sinh\left(n\pi\left(\omega(\varphi_1)-\omega(\varphi_0)\right)/\gamma\right)}\left(\cos n\eta-\cos n\kappa\right),$$

$$R_2=\sum_{n=1}^{\infty}\frac{1}{2\pi n}\frac{\sinh\left(n\pi\left(\omega(\xi)-\omega(\varphi_1)\right)/2\gamma\right)\sinh\left(n\pi\left(\omega(\varphi_0)-\omega(\varphi)\right)/2\gamma\right)}{e^{n\pi(\omega(\varphi_1)-\omega(\varphi_0))/\gamma}\sinh\left(n\pi\left(\omega(\varphi_1)-\omega(\varphi_0)\right)/2\gamma\right)}\left(\cos\frac{n\eta}{2}-\cos\frac{n\kappa}{2}\right),$$

$$R_3=\sum_{n=1}^{\infty}\frac{1}{2\pi n}\frac{\cosh\left(n\pi\left(\omega(\xi)-\omega(\varphi_1)\right)/\gamma\right)\sinh\left(n\pi\left(\omega(\varphi_0)-\omega(\varphi)\right)/\gamma\right)}{e^{2n\pi(\omega(\varphi_1)-\omega(\varphi_0))/\gamma}\cosh\left(n\pi\left(\omega(\varphi_1)-\omega(\varphi_0)\right)/\gamma\right)}\left(\cos n\eta-\cos n\kappa\right),$$

$$R_4=\sum_{n=1}^{\infty}\frac{1}{2\pi n}\frac{\cosh\left(n\pi\left(\omega(\xi)-\omega(\varphi_1)\right)/2\gamma\right)\sinh\left(n\pi\left(\omega(\varphi_0)-\omega(\varphi)\right)/2\gamma\right)}{e^{n\pi(\omega(\varphi_1)-\omega(\varphi_0))/\gamma}\cosh\left(n\pi\left(\omega(\varphi_1)-\omega(\varphi_0)\right)/2\gamma\right)}\left(\cos\frac{n\eta}{2}-\cos\frac{n\kappa}{2}\right),$$

$$R_5 = \sum_{n=1}^{\infty} \frac{1}{2\pi n} \frac{\sinh\left(n\left(\omega(\xi) - \omega(\varphi_1)\right)\right) \sinh\left(n\left(\omega(\varphi_0) - \omega(\varphi)\right)\right)}{e^{2n(\omega(\varphi_1)-\omega(\varphi_0))} \sinh\left(n\left(\omega(\varphi_1) - \omega(\varphi_0)\right)\right)} \cos n\left(\theta - \tau\right),$$

and

$$R_6 = \sum_{n=1}^{\infty} \frac{1}{2\pi n} \frac{\cosh\left(n\left(\omega(\xi) - \omega(\varphi_1)\right)\right) \sinh\left(n\left(\omega(\varphi_0) - \omega(\varphi)\right)\right)}{e^{2n(\omega(\varphi_1)-\omega(\varphi_0))} \cosh\left(n\left(\omega(\varphi_1) - \omega(\varphi_0)\right)\right)} \cos n\left(\theta - \tau\right).$$

Considering the same geometry and the location of point sources, as in Figure 10, we show, in Figure 11, the potential field in the toroidal shell with one-side Dirichlet and three-side Nuemann boundary conditions imposed.

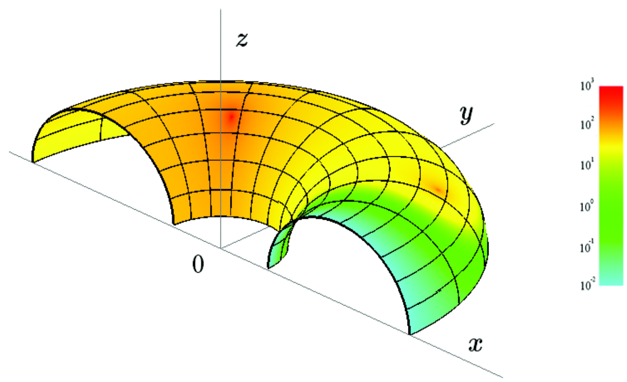

Figure 11: Potential field generated in toroidal region with Dirichlet and Neumann boundary conditions imposed

Potential fields generated by point sources in joint shell structures of various geometry will be considered in the next Chapter.

3 Potential fields in joint shell structures

3.1 Matrices of Green's type

Since a direct implementation of the Green's function formalism to the case of joint surfaces is problematic, the matrix of Green's type concept [49] comes to the picture instead. We begin our presentation in this chapter with introduction of the matrix of Green's type formalism for the case of two joint surfaces. In doing so, we target the potential field generated by a point source in a thin joint shell structure comprised of two fragments Ω_1 and Ω_2, with Γ_{in} representing their interface line. Assume that the lateral surfaces of the structure are insulated and the shell fragments are made of different homogeneous isotropic materials with their individual conductive properties spelled out by the constants λ_1 and λ_2.

In each of the surface fragments Ω_1 and Ω_2, that form the composed region $\Omega = \Omega_1 \cup \Omega_2$, we consider the Poisson equation

$$\nabla^2 u_i(P) = -f_i(P), \quad P \in \Omega_i, \quad i = 1, 2 \tag{3.1}$$

subject to the homogeneous boundary conditions

$$B[u_i(P)] = 0, \quad P \in \Gamma_{ex}, \quad i = 1, 2 \tag{3.2}$$

on the exterior component Γ_{ex} of Ω region's boundary. In addition, the conditions of ideal thermal contact

$$u_1(P) = u_2(P), \quad P \in \Gamma_{in} \tag{3.3}$$

and

$$\lambda_1 \frac{\partial u_1(P)}{\partial n_1} = \lambda_2 \frac{\partial u_2(P)}{\partial n_2}, \quad P \in \Gamma_{in} \tag{3.4}$$

are imposed on the interface line Γ_{in}. Here ∇^2 is the two-dimensional Laplace operator written in geographical coordinates that are specific for each surface fragment, while n_1 and n_2 represent the normal directions to Γ_{in} in Ω_1 and Ω_2, respectively.

Assume that the boundary-value problem in (3.1)–(3.4) is well-posed providing a unique solution. This implies that the corresponding homogeneous problem

$(f_i(P) \equiv 0)$ has only the trivial solution. To make the matrix of Green's type formalism applicable to the problem setting of (3.1)–(3.4), we introduce the two vector-functions

$$\mathbf{U}(P) = (U_i(P))_{i=1,2} \quad \text{and} \quad \mathbf{F}(P) = (F_i(P))_{i=1,2},$$

defined in Ω in the way that their components $U_i(P)$ and $F_i(P)$ are defined in pieces as

$$U_i(P) = \begin{cases} u_i(P), & P \in \Omega_i \\ 0, & P \in \Omega \backslash \Omega_i \end{cases}$$

and

$$F_i(P) = \begin{cases} f_i(P), & P \in \Omega_i \\ 0, & P \in \Omega \backslash \Omega_i \end{cases}$$

A specific strategy is required for obtaining the matrix of Green's type of the homogeneous boundary-value problem corresponding to that in (3.1)–(3.4). The strategy is based on the fact that if, for any integrable in Ω vector-function $\mathbf{F}(P)$, the solution-vector $\mathbf{U}(P)$ is expressed in the domain integral form

$$\mathbf{U}(P) = \iint_{\Omega} \boldsymbol{G}(P,Q)\,\mathbf{F}(Q)d\Omega(Q), \tag{3.5}$$

then the 2×2 kernel-matrix $\boldsymbol{G}(P,Q)$ in (3.5) represents the required matrix of Green's type.

Hence, in light of the above statement, it is crucial to aim at not just solving the problem in (3.1)–(3.4) by any means, but the objective must rather be in selecting such an approach that allows us to obtain the problem solution in the form of (3.5) that delivers an explicit expression for $\boldsymbol{G}(P,Q)$.

Note that the arguments of the element $G_{ij}(P,Q)$ of $\boldsymbol{G}(P,Q)$ belong to different fragments of Ω. That is, P and Q are the points in Ω_i and Ω_j, respectively, in the sense that in the element $G_{12}(P,Q)$, for example, P is the point in Ω_1, while Q belongs to Ω_2. Later in this chapter, we will describe our approach in full detail while obtaining the matrix of Green's type for one particular problem setting of the type in (3.1)–(3.4). The derivation of matrices of Green's type for other boundary-value problems is not presented but ultimate representations of their components are provided for a number of problem settings.

3.2 Matrix of Green's type for a sphere-torus structure

As an illustrative example, we consider a particular case of the boundary-value problem in (3.1)–(3.4). Let the region $\Omega = \Omega_1 \cup \Omega_2$ represent a compound surface of revolution, which is comprised of two coaxial fragments, one of which is spherical of radius a, occupying the region

$$\Omega_1 = \{(\phi, \theta) \mid 0 \leq \phi \leq \phi_0;\ 0 \leq \theta \leq 2\pi\},$$

while another fragment is circular toroidal of radii R and r, occupying the region

$$\Omega_2 = \{(\varphi, \theta) \mid \varphi_0 \leq \varphi \leq \varphi_1;\ 0 \leq \theta \leq 2\pi\}.$$

The axial cross-section of the considered compound thin-walled structure is presented in Figure 12. Clearly, the relation $a \sin\phi_0 + r\cos\varphi_0 = R$ holds for the radii of the structure.

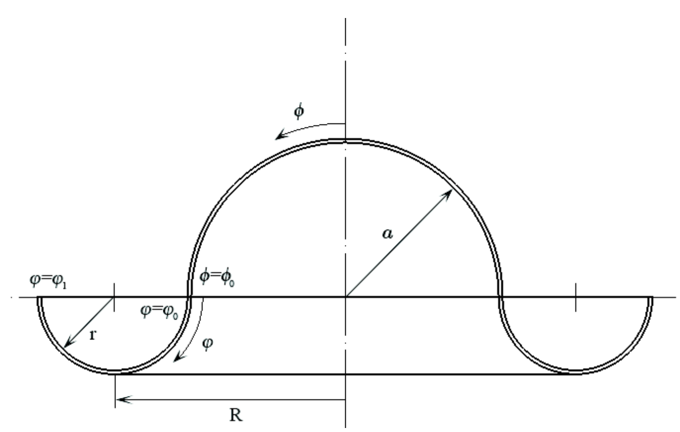

Figure 12: Axial cross-section of the sphere-torus assembly

The compound structure is set up in such a way that the parallel $\phi = \phi_0$ of the spherical fragment and the parallel $\varphi = \varphi_0$ of the toroidal fragment represent the same circle, which is, in fact, the interface line Γ_{in} of the two surfaces.

For the compound region $\Omega = \Omega_1 \cup \Omega_2$ just introduced, the problem setting in (3.1)–(3.4) reads explicitly as

$$\frac{1}{a^2 \sin\phi} \frac{\partial}{\partial \phi} \left(\sin\phi \frac{\partial u_1(\phi,\theta)}{\partial \phi} \right) + \frac{1}{a^2 \sin^2\phi} \frac{\partial^2 u_1(\phi,\theta)}{\partial \theta^2} = -f_1(\phi,\theta) \tag{3.6}$$

$$\frac{1}{D(\varphi)} \frac{\partial}{\partial \varphi} \left(D(\varphi) \frac{\partial u_2(\varphi,\theta)}{\partial \varphi} \right) + \frac{r^2}{D^2(\varphi)} \frac{\partial^2 u_2(\varphi,\theta)}{\partial \theta^2} = -f_2(\varphi,\theta) \tag{3.7}$$

$$\lim_{\phi \to 0} |u_1(\phi,\theta)| < \infty, \ u_2(\varphi_1,\theta) = 0 \tag{3.8}$$

$$u_1(\phi,0) = u_1(\phi,2\pi), \ \frac{\partial u_1(\phi,0)}{\partial \theta} = \frac{\partial u_1(\phi,2\pi)}{\partial \theta} \tag{3.9}$$

$$u_2(\varphi,0) = u_2(\varphi,2\pi), \ \frac{\partial u_2(\varphi,0)}{\partial \theta} = \frac{\partial u_2(\varphi,2\pi)}{\partial \theta} \tag{3.10}$$

$$u_1(\phi_0,\theta) = u_2(\varphi_0,\theta), \ \frac{\partial u_1(\phi_0,\theta)}{\partial \phi} = \lambda \frac{\partial u_2(\varphi_0,\theta)}{\partial \varphi} \tag{3.11}$$

where $D(\varphi) = R + r\sin\varphi$, and $\lambda = \lambda_2/\lambda_1$.

For notational convenience, we will use the single notation

$$\varsigma = \begin{cases} \phi & \text{in } \Omega_1 \\ \varphi & \text{in } \Omega_2 \end{cases}$$

for the latitudinal coordinate of a point in the compound surface structure.

Since the assembly is closed in the longitudinal direction, the conditions of (3.9) and (3.10) are included in the above setting to simulate the 2π-periodicity of the solution of the problem with respect to the variable θ. Given the above, the functions $u_i(\varsigma,\theta)$ and $f_i(\varsigma,\theta)$ can be expanded in the Fourier series

$$u_i(\varsigma,\theta) = \frac{1}{2} u_{i,0}(\varsigma) + \sum_{n=1}^{\infty} u_{i,n}^{(s)}(\varsigma) \sin n\theta + \sum_{n=1}^{\infty} u_{i,n}^{(c)}(\varsigma) \cos n\theta \tag{3.12}$$

and

$$f_i(\varsigma,\theta) = \frac{1}{2} f_{i,0}(\varsigma) + \sum_{n=1}^{\infty} f_{i,n}^{(s)}(\varsigma) \sin n\theta + \sum_{n=1}^{\infty} f_{i,n}^{(c)}(\varsigma) \cos n\theta \tag{3.13}$$

Upon substituting these into (3.6)–(3.11), we arrive at a three-point-posed boundary-value problem in the coefficients $u_{1,n}(\varsigma)$ and $u_{2,n}(\varsigma)$ of the series in (3.12). The governing differential equations of that problem appear in the self-adjoint form as

$$\frac{d}{d\phi} \left(\sin\phi \frac{du_{1,n}(\phi)}{\partial \phi} \right) - \frac{n^2}{\sin\phi} u_{1,n}(\phi) = -\widetilde{f}_{1,n}(\phi) \tag{3.14}$$

and

$$\frac{1}{r}\frac{d}{d\varphi}\left(D(\varphi)\frac{du_{2,n}(\varphi)}{\partial\varphi}\right)-\frac{rn^2}{D(\varphi)}u_{2,n}(\varphi)=-\widetilde{f}_{2,n}(\varphi), \tag{3.15}$$

where

$$\widetilde{f}_{1,n}(\phi)=a^2 f_{1,n}(\phi)\sin\phi,\ \text{and}\ \widetilde{f}_{2,n}(\varphi)=\frac{D(\varphi)}{r}f_{2,n}(\varphi),$$

while the boundary and contact conditions of (3.8) and (3.11) yield

$$\lim_{\phi\to 0}|u_{1,n}(\phi)|<\infty,\ u_{2,n}(\varphi_1)=0 \tag{3.16}$$

and

$$u_{1,n}(\phi_0)=u_{2,n}(\varphi_0),\ \frac{du_{1,n}(\phi_0)}{d\phi}=\lambda\frac{du_{2,n}(\varphi_0)}{d\varphi} \tag{3.17}$$

It is worth noting that at the current stage in the development the sine and the cosine components of the series in (3.12) can be treated similarly. That is why we omit the superscripts (s) and (c) on $u_{1,n}(\varsigma)$ and $u_{2,n}(\varsigma)$ in the setting of (3.14)–(3.17).

To approach the boundary-value problem in (3.14)–(3.17) for $n\geq 1$ (the case of $n=0$ will be considered specifically later), we proceed with the standard variation of parameters method which yields the general solutions to (3.14) and (3.15) in the form

$$u_{1,n}(\phi)=\frac{1}{2n}\int_0^{\phi}\left(\frac{\Phi_0^n(\phi)}{\Phi_0^n(\psi)}-\frac{\Phi_0^n(\psi)}{\Phi_0^n(\phi)}\right)\widetilde{f}_{1,n}(\psi)\,d\psi+L_1\Phi_0^n(\phi)+M_1\Phi_0^{-n}(\phi) \tag{3.18}$$

and

$$u_{2,n}=\frac{1}{n}\int_{\varphi_0}^{\varphi}\sinh n\sigma(\varphi,\xi)\,\widetilde{f}_{2,n}(\xi)\,d\xi+L_2e^{n\omega(\varphi)}+M_2e^{-n\omega(\varphi)} \tag{3.19}$$

where L_1, M_1, L_2, and M_2 represent arbitrary constants which will be determined by virtue of the uniqueness conditions of (3.16) and (3.17). The single-variable functions $\Phi_0(\alpha)$ and $\omega(\alpha)$ are defined as

$$\Phi_0(\phi)=\tan(\phi/2)\quad\text{and}\quad\omega(\varphi)=\frac{2r}{\sqrt{R^2-r^2}}\arctan\left(\frac{r+R\tan(\varphi/2)}{\sqrt{R^2-r^2}}\right),$$

while the double-variable function $\sigma(\alpha,\beta)$ reads as

$$\sigma(\alpha,\beta)=\omega(\alpha)-\omega(\beta).$$

The conditions of (3.16) and (3.17) transform the expressions for $u_{1,n}(\phi)$ and $u_{2,n}(\varphi)$ in (3.18) and (3.19) into

$$\begin{aligned}
u_{1,n}(\phi) &= \frac{1}{n\Delta}\int_0^{\phi}\frac{\Phi_0^n(\psi)}{\Phi_0^n(\phi_0)}\left[\left(\frac{\Phi_0^n(\phi)}{\Phi_0^n(\phi_0)}-\frac{\Phi_0^n(\phi_0)}{\Phi_0^n(\phi)}\right)QC_n(\varphi_1,\varphi_0)\right.\\
&\left.-\left(\frac{\Phi_0^n(\phi)}{\Phi_0^n(\phi_0)}+\frac{\Phi_0^n(\phi_0)}{\Phi_0^n(\phi)}\right)S_n(\varphi_1,\varphi_0)\right]\widetilde{f}_{1,n}(\psi)\,d\psi\\
&+\frac{1}{n\Delta}\int_0^{\phi}\frac{\Phi_0^n(\phi)}{\Phi_0^n(\phi_0)}\left[\left(\frac{\Phi_0^n(\psi)}{\Phi_0^n(\phi_0)}-\frac{\Phi_0^n(\phi_0)}{\Phi_0^n(\psi)}\right)QC_n(\varphi_1,\varphi_0)\right.\\
&\left.-\left(\frac{\Phi_0^n(\psi)}{\Phi_0^n(\phi_0)}+\frac{\Phi_0^n(\phi_0)}{\Phi_0^n(\psi)}\right)S_n(\varphi_1,\varphi_0)\right]\widetilde{f}_{1,n}(\psi)\,d\psi\\
&+\frac{2Q}{n\Delta}\int_{\varphi_0}^{\varphi_1}\frac{\Phi_0^n(\phi)}{\Phi_0^n(\phi_0)}S_n(\varphi_1,\xi)\,\widetilde{f}_{2,n}(\xi)\,d\xi
\end{aligned}\tag{3.20}$$

and

$$\begin{aligned}
u_{2,n}(\varphi) &= \frac{2}{n\Delta}\int_{\varphi_0}^{\varphi}S_n(\varphi_1,\varphi)\left[S_n(\varphi_0,\xi)-QC_n(\varphi_0,\xi)\right]\widetilde{f}_{2,n}(\xi)\,d\xi\\
&+\frac{2}{n\Delta}\int_{\varphi_0}^{\varphi}S_n(\varphi_1,\xi)\left[S_n(\varphi_0,\varphi)-QC_n(\varphi_0,\varphi)\right]\widetilde{f}_{2,n}(\xi)\,d\xi\\
&-\frac{2}{n\Delta}\int_0^{\phi_0}\frac{\Phi_n(\psi)}{\Phi_n(\phi_0)}S_n(\varphi_1,\varphi)\,\widetilde{f}_{1,n}(\psi)\,d\psi
\end{aligned}\tag{3.21}$$

where

$$Q=\frac{\lambda r}{D(\varphi_0)}\sin(\phi_0)\,,\quad \Delta=(1+Q)\,e^{n\sigma(\varphi_1,\varphi_0)}-(1-Q)\,e^{-n\sigma(\varphi_1,\varphi_0)},$$

$$S_n(\alpha,\beta)=\sinh n\sigma(\alpha,\beta)\,,\quad \text{and}\quad C_n(\alpha,\beta)=\cosh n\sigma(\alpha,\beta)\,,$$

In view of the development that follows, it appears convenient to reiterate the expressions from (3.20) and (3.21) in a more compact form

$$u_{1,n}(\phi)=\int_0^{\phi_0}g_{11,n}(\phi,\psi)\,\widetilde{f}_{1,n}(\psi)\,d\psi+\int_{\varphi_0}^{\varphi_1}g_{12,n}(\phi,\xi)\,\widetilde{f}_{2,n}(\xi)\,d\xi \tag{3.22}$$

and

$$u_{2,n}(\varphi)=\int_0^{\phi_0}g_{21,n}(\varphi,\psi)\,\widetilde{f}_{1,n}(\psi)\,d\psi+\int_{\varphi_0}^{\varphi_1}g_{22,n}(\varphi,\xi)\,\widetilde{f}_{2,n}(\xi)\,d\xi \tag{3.23}$$

with the kernel functions of the above integrals defined as

$$g_{11,n}(\phi,\psi)=\frac{1}{n\Delta}\begin{cases}\frac{\Phi_0^n(\psi)}{\Phi_0^n(\phi_0)}\left[\left(\frac{\Phi_0^n(\phi)}{\Phi_0^n(\phi_0)}-\frac{\Phi_0^n(\phi_0)}{\Phi_0^n(\phi)}\right)QC_n(\varphi_1,\varphi_0)\right. \\ \qquad \left.-\left(\frac{\Phi_0^n(\phi)}{\Phi_0^n(\phi_0)}+\frac{\Phi_0^n(\phi_0)}{\Phi_0^n(\phi)}\right)S_n(\varphi_1,\varphi_0)\right] & 0\le\psi\le\phi \\ \frac{\Phi_0^n(\phi)}{\Phi_0^n(\phi_0)}\left[\left(\frac{\Phi_0^n(\psi)}{\Phi_0^n(\phi_0)}-\frac{\Phi_0^n(\phi_0)}{\Phi_0^n(\psi)}\right)QC_n(\varphi_1,\varphi_0)\right. \\ \qquad \left.-\left(\frac{\Phi_0^n(\psi)}{\Phi_0^n(\phi_0)}+\frac{\Phi_0^n(\phi_0)}{\Phi_0^n(\psi)}\right)S_n(\varphi_1,\varphi_0)\right] & \phi\le\psi\le\phi_0\end{cases},\quad (3.24)$$

$$g_{12,n}(\phi,\xi)=\frac{2Q}{n\Delta}\frac{\Phi_0^n(\phi)}{\Phi_0^n(\phi_0)}S_n(\varphi_1,\xi),\quad g_{21,n}(\varphi,\psi)=-\frac{2}{n\Delta}\frac{\Phi_0^n(\psi)}{\Phi_0^n(\phi_0)}S_n(\varphi_{1,}\varphi),\quad (3.25)$$

and

$$g_{22,n}(\varphi,\xi)=\frac{2}{n\Delta}\begin{cases}S_n(\varphi_{1,}\varphi)\left[S_n(\varphi_0,\xi)-QC_n(\varphi_0,\xi)\right] & \varphi_0\le\xi\le\varphi \\ S_n(\varphi_{1,}\xi)\left[S_n(\varphi_0,\varphi)-QC_n(\varphi_0,\varphi)\right] & \varphi\le\xi\le\varphi_1\end{cases}\quad (3.26)$$

Note that the summation index n of the series in (3.12) and (3.13) appears as a parameter in the operators of the governing differential equations in (3.14) and (3.15) of the boundary-value problem of (3.14)–(3.17), affecting, subsequently, their fundamental sets of solutions.

As long as the solution to the problem in (3.14)–(3.17) is already obtained for the case of $n\ge 1$, we have to turn now to the particular problem setting of $n=0$, which ought to be considered separately, and in which case the governing differential equations as of (3.14) and (3.15) reduce to

$$\frac{d}{d\phi}\left(\sin\phi\frac{du_{1,0}(\phi)}{d\phi}\right)=-\widetilde{f}_{1,0}(\phi)$$

and

$$\frac{d}{d\varphi}\left(D(\varphi)\frac{du_{2,0}(\varphi)}{d\varphi}\right)=-\widetilde{f}_{2,0}(\varphi)$$

Following the standard procedure of the method of variation of parameters, we express the general solutions for the above equations as

$$u_{1,0}(\phi)=\int_0^{\phi}\ln\frac{\Phi_0(\phi)}{\Phi_0(\psi)}\widetilde{f}_{1,0}(\psi)\,d\psi+L_1\ln\Phi_0(\phi)+M_1\quad (3.27)$$

and

$$u_{2,0}(\varphi) = \int_{\varphi_0}^{\varphi} \sigma(\varphi, \xi) \widetilde{f}_{2,0}(\xi) \, d\xi + L_2 \omega(\varphi) + M_2 \tag{3.28}$$

Clearly enough, the boundary and contact conditions of (3.16) and (3.17) are not affected by the summation index n of the series in (3.12). Thus, applying these conditions to the forms in (3.27) and (3.28), we arrive at

$$u_{1,0}(\phi) = \int_0^{\phi_0} g_{11,0}(\phi, \psi) \widetilde{f}_{1,0}(\psi) \, d\psi + \int_{\varphi_0}^{\varphi_1} g_{12,0}(\phi, \xi) \widetilde{f}_{2,0}(\xi) \, d\xi \tag{3.29}$$

and

$$u_{2,0}(\varphi) = \int_0^{\phi_0} g_{21,0}(\varphi, \psi) \widetilde{f}_{1,0}(\psi) \, d\psi + \int_{\varphi_0}^{\varphi_1} g_{22,0}(\varphi, \xi) \widetilde{f}_{2,0}(\xi) \, d\xi \tag{3.30}$$

where the kernel-functions in the above integrals are expressed as

$$g_{11,0}(\phi, \psi) = \frac{1}{Q} \sigma(\varphi_0, \varphi_1) + \begin{cases} \ln \frac{\Phi_0(\phi)}{\Phi_0(\phi_0)} & 0 \leq \psi \leq \phi \\ \\ \ln \frac{\Phi_0(\psi)}{\Phi_0(\phi_0)} & \phi \leq \psi \leq \phi_0 \end{cases},$$

$$g_{12,0}(\phi, \xi) = -\sigma(\varphi_1, \xi), \quad g_{21,0}(\varphi, \psi) = \frac{1}{Q} \sigma(\varphi_1, \varphi),$$

and

$$g_{22,0}(\varphi, \xi) = \begin{cases} \sigma(\varphi, \varphi_1) & \varphi_0 \leq \xi \leq \varphi \\ \sigma(\xi, \varphi_1) & \varphi \leq \xi \leq \varphi_1 \end{cases}.$$

At this point in the development, we substitute the expressions for the functions $u_{i,n}(\varsigma)$, presented in (3.22), (3.23), (3.29), and (3.30), into (3.12), and express then the coefficients $f_{1,n}(\phi)$ and $f_{2,n}(\varphi)$ of the Fourier series from (3.13) in terms of the right-hand side functions $f_1(\phi, \theta)$ and $f_2(\varphi, \theta)$ of the governing differential equations of the boundary-value problem in (3.6)–(3.11). This allows us to ultimately obtain the solution of the problem in the vector form as

$$\mathbf{U}(P) = \iint_{\Omega} \boldsymbol{G}(P, Q) \, \mathbf{F}(Q) d\Omega(Q),$$

revealing, in light of (3.5), the matrix of Green's type

$$\boldsymbol{G}(\varsigma, \theta; \zeta, \tau) = [G_{ij}(\varsigma, \theta; \zeta, \tau)]_{2\times 2} \tag{3.31}$$

where

$$\zeta = \begin{cases} \psi & \text{in } \Omega_1 \\ \xi & \text{in } \Omega_2 \end{cases}$$

to the homogeneous boundary-value problem corresponding to that in (3.6)–(3.11). For the elements $G_{ij}(\varsigma, \theta; \zeta, \tau)$ of the above matrix we arrived at the series expansions

$$\begin{aligned} G_{ij}(\varsigma, \theta; \zeta, \tau) &= \frac{1}{2} g_{ij,0}(\varsigma, \zeta) + \sum_{n=1}^{\infty} g_{ij,n}(\varsigma, \zeta) \sin n\theta \sin n\tau \\ &\quad + \sum_{n=1}^{\infty} g_{ij,n}(\varsigma, \zeta) \cos n\theta \cos n\tau \\ &= \frac{1}{2} g_{ij,0}(\varsigma, \zeta) + \sum_{n=1}^{\infty} g_{ij,n}(\varsigma, \zeta) \cos(\theta - \tau) \end{aligned} \tag{3.32}$$

The form in (3.32) appears efficient for immediate computer implementations for the peripheral elements of $\boldsymbol{G}$, since the observation point (ς, θ) and the source point (ψ, τ) are, for the peripheral elements, located in different fragments of Ω. This implies that just some partial sums of the series can be used to attain an accuracy level required in this or that case. In the diagonal elements of $\boldsymbol{G}$, on the other hand, the observation and the source points belong to the same fragment of Ω, making the convergence of the series in (3.32) non-uniform due to the logarithmic singularity that these elements possess. Hence, the convergence of the representation in (3.32) ought to be improved, if the diagonal elements of $\boldsymbol{G}$ are to compute. We accomplish such an improvement by splitting apart the terms of the series that are responsible for logarithmic and regular components. Omitting details, we present just the ultimate expressions

$$\begin{aligned} G_{11}(\phi, \theta; \psi, \tau) &= \frac{1}{2} g_{11,0}(\phi, \psi) - \frac{1-Q}{1+Q} H_P\left(\frac{\Phi_0(\phi)\,\Phi_0(\psi)}{\Phi_0^2(\phi_0)}, \theta - \tau\right) \\ &\quad + H_P\left(\frac{\Phi_0(\phi)\,\Phi_0(\psi)}{\Phi_0^2(\phi_0)} e^{2\sigma(\varphi_0, \varphi_1)}, \theta - \tau\right) + R_{11}(\phi, \theta; \psi, \tau) \\ &\quad + \begin{cases} \frac{1-Q}{1+Q} H_P\left(\frac{\Phi_0(\psi)}{\Phi_0(\phi)} e^{2\sigma(\varphi_0, \varphi_1)}, \theta - \tau\right) - H_P\left(\frac{\Phi_0(\psi)}{\Phi_0(\phi)}, \theta - \tau\right) \\ \frac{1-Q}{1+Q} H_P\left(\frac{\Phi_0(\phi)}{\Phi_0(\psi)} e^{2\sigma(\varphi_0, \varphi_1)}, \theta - \tau\right) - H_P\left(\frac{\Phi_0(\phi)}{\Phi_0(\psi)}, \theta - \tau\right) \end{cases} \end{aligned}$$

and

$$G_{22}(\varphi,\theta;\xi,\tau) = \frac{1}{2}g_{22,0}(\varphi,\xi) + H_P\left(e^{\sigma(\varphi,\varphi_1)+\sigma(\xi,\varphi_1)},\theta-\tau\right)$$
$$+\frac{1-Q}{1+Q}H_P\left(e^{\sigma(\varphi_0,\varphi)+\sigma(\varphi_0,\xi)},\theta-\tau\right) + R_{22}(\varphi,\theta;\xi,\tau),$$
$$-\begin{cases} H_P\left(e^{\sigma(\xi,\varphi)},\theta-\tau\right) + \frac{1-Q}{1+Q}H_P\left(e^{\sigma(\varphi,\xi)+2\sigma(\varphi_0,\varphi_1)},\theta-\tau\right) \\ H_P\left(e^{\sigma(\varphi,\xi)},\theta-\tau\right) + \frac{1-Q}{1+Q}H_P\left(e^{\sigma(\xi,\varphi)+2\sigma(\varphi_0,\varphi_1)},\theta-\tau\right) \end{cases}$$

for the diagonal elements of $\boldsymbol{G}$. The two-variable function $H_P(x,a)$ was introduced earlier in Chapter 2 (see equation (2.38)).

The regular additive components $R_{ii}(\varsigma,\theta;\zeta,\tau)$, $i=1,2$ in the above representations for the diagonal elements are expressed in a form of the uniformly convergent series

$$R_{ii}(\varsigma,\theta;\zeta,\tau) = \sum_{n=1}^{\infty} \frac{\widetilde{g}_{ii,n}(\varsigma,\zeta)(1-Q)\,e^{n\sigma(\varphi_0,\varphi_1)}}{(1+Q)^2\,e^{2n\sigma(\varphi_1,\varphi_0)} - (1-Q^2)}\cos(\theta-\tau)$$

where $\widetilde{g}_{ii,n}(\varsigma,\zeta)$ are defined in terms of $g_{ij,n}(\varsigma,\zeta)$ available in (3.24) and (3.26) as

$$\widetilde{g}_{ii,n}(\varsigma,\zeta) = g_{ii,n}(\varsigma,\zeta)\,\Delta$$

This makes the representations just presented for the diagonal elements of the matrix of Green's type efficiently computable. To illustrate this point, in Figure 13 we show the field induced in the considered thin-walled structure by point sources acting at three distinct locations. The parameters specifying the problem setting are chosen as: $a=1.0$, $r=0.5$, $R=1.5$, $\phi_0=\pi/2$, $\varphi_0=0.0$, $\varphi_1=\pi$, the locations of the point sources are $(0.26\pi, 0.42\pi)$ in the spherical fragment, and $(1.05\pi, 0.5\pi)$ and $(0.6\pi, 1.82\pi)$ in the toroidal fragment.

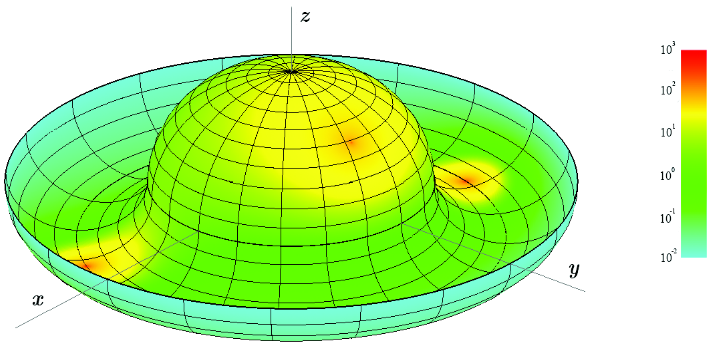

Figure 13: Multiple point sources in the sphere-torus structure

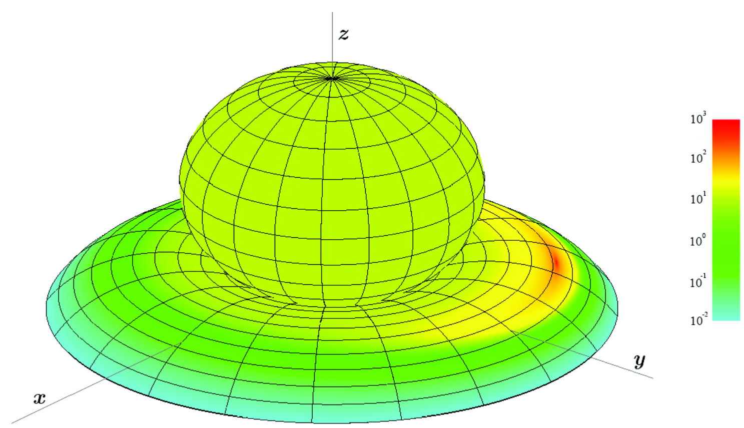

Figure 14: Field generated by a point source in the toroidal fragment of the structure

In Figure 14 we depict the potential field generated by two point sources where one is located in the spherical fragment of the sphere-torus shell structure, while another one is in its toroidal fragment. The parameters specifying the problem setting are chosen as: $a = 1.5$, $r = 1.4$, $\phi_0 = 0.8\pi$, $\varphi_0 = -0.2\pi$, $\varphi_1 = -0.8\pi$, $R = a\sin\phi_0 + r\cos\varphi_0 \approx 2.02$, the location of the point source is $(0.35\pi, 0.75\pi)$ in the toroidal fragment.

3.3 Cylindrical-toroidal shell structure

In this section, a thin-walled structure is considered as composed of two coaxial shells of revolution, one of which is semi-infinite cylindrical of radius a whilst another is toroidal of radii R and r. The axial cross-section of the structure is shown in Figure 15.

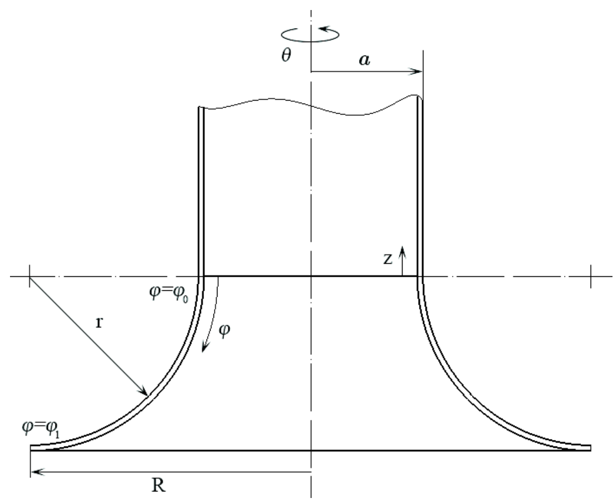

Figure 15: Axial cross-section of the cylinder-torus assembly

Middle surfaces of the shells are referenced to different geographical coordinates, and occupy the regions

$$\Omega_1 = \{(z, \theta)|\ 0 \leq z \leq \infty;\ 0 \leq \theta \leq 2\pi\}$$

and

$$\Omega_2 = \{(\varphi, \theta)|\ \varphi_0 \leq \varphi \leq \varphi_1;\ 0 \leq \theta \leq 2\pi\},$$

respectively. This problem setting gives rise to a set of two Laplace equations written in the corresponding coordinates as

$$\frac{\partial^2 u_1 (z, \theta)}{\partial z^2} + \frac{1}{a^2} \frac{\partial^2 u_1 (z, \theta)}{\partial \theta^2} = 0 \tag{3.33}$$

and

$$\frac{1}{r} \frac{\partial}{\partial \varphi} \left(D(\varphi) \frac{\partial u_2 (\varphi, \theta)}{\partial \varphi} \right) + \frac{r}{D(\varphi)} \frac{\partial^2 u_2 (\varphi, \theta)}{\partial \theta^2} = 0, \tag{3.34}$$

where $D(\varphi) = R + r\sin\varphi$. The above equations are subject to the following set of boundary and contact conditions

$$\lim_{z\to\infty} |u_1(z,\theta)| < \infty, \quad u_2(\varphi_1,\theta) = 0, \tag{3.35}$$

$$u_i(\varsigma,0) = u_i(\varsigma,2\pi), \quad \frac{\partial u_i(\varsigma,0)}{\partial\theta} = \frac{\partial u_i(\varsigma,2\pi)}{\partial\theta}, \ i = 1,2, \tag{3.36}$$

and

$$u_1(0,\theta) = u_2(\varphi_0,\theta) \quad \text{and} \quad \frac{\partial u_1(0,\theta)}{\partial z} = \lambda\frac{\partial u_2(\varphi_0,\theta)}{\partial\varphi} \ . \tag{3.37}$$

Similarly to the development in the previous section, we introduce the latitudinal coordinate

$$\varsigma = \begin{cases} z, & \text{in } \Omega_1 \\ \varphi, & \text{in } \Omega_2, \end{cases}$$

of the observation point for either fragment of the structure.

Upon implementing the procedure described in the previous section to the problem in (3.33)-(3.37), we obtain the matrix of Green's type

$$\boldsymbol{G}(\varsigma,\theta;\zeta,\tau) = [G_{ij}(\varsigma,\theta;\zeta,\tau)]_{2\times 2}$$

that we are looking for. The single variable ζ is introduced in the above as

$$\zeta = \begin{cases} s, & \text{in } \Omega_1 \\ \xi, & \text{in } \Omega_2, \end{cases}$$

to stay for the latitudinal coordinate of the source point for either fragment of the structure.

Skipping quite tedious but rather straightforward algebra, we present below just ultimate computer-friendly form of the elements $G_{ij}(\varsigma,\theta;\zeta,\tau)$ of $\boldsymbol{G}(\varsigma,\theta;\zeta,\tau)$. Its first main diagonal element was found as

$$\begin{aligned}G_{11}(z,\theta;s,\tau) &= \frac{1}{2}g_{11,0}(z,s)+\frac{Q-1}{Q+1}aH_P\left(e^{-(s+z)/a},\theta-\tau\right)\\&+\frac{2a}{Q+1}H_P\left(e^{2\sigma(\varphi_0,\varphi_1)-(s+z)/a},\theta-\tau\right)\\&+\sum_{n=1}^{\infty}\frac{a}{n}S_n(\varphi_1,\varphi_0)\,e^{-n(s+z)/a}P_n(\varphi_0,\varphi_1)\cos n(\theta-\tau)\\&-a\begin{cases}H_P\left(e^{(s-z)/a},\theta-\tau\right), & 0<s\le z\\ H_P\left(e^{(z-s)/a},\theta-\tau\right), & z\le s<\infty\end{cases}\end{aligned}$$

where, along with already accepted earlier $S_n(\alpha,\beta)$, we introduce some other shorthand notations. The parameter Q reads as $Q=\lambda r/a$, and the two-variable function $P_n(\alpha,\beta)$, which depends upon the summation index n of the series in the above expression, is introduced as

$$P_n(\varphi_0,\varphi_1)=\frac{(1-Q)\,e^{n\sigma(\varphi_0,\varphi_1)}}{(1+Q)^2\,e^{2n\sigma(\varphi_1,\varphi_0)}\,(1-Q^2)}\ ,$$

The function $g_{11,0}(z,s)$ reads as

$$g_{11,0}(z,s)=\frac{a}{Q}\sigma(\varphi_1,\varphi_0)-\begin{cases}s & 0<s\le z\\ z & z\le s<\infty.\end{cases}$$

For the second element of the first row of $\boldsymbol{G}(\varsigma,\theta;\zeta,\tau)$, we obtained

$$\begin{aligned}G_{12}(z,\theta;\xi,\tau) &= \frac{1}{2}g_{12,0}(z,\xi)-\frac{2Q}{Q+1}H_P\left(e^{\sigma(\varphi_0,\xi)-z/a},\theta-\tau\right)\\&+\frac{2Q}{Q+1}H_P\left(e^{\sigma(\varphi_0,\varphi_1)+\sigma(\xi,\varphi_1)-z/a},\theta-\tau\right)\\&+\sum_{n=1}^{\infty}\frac{Q}{n}S_n(\varphi_1,\xi)\,e^{-nz/a}P_n(\varphi_0,\varphi_1)\cos n(\theta-\tau)\,,\end{aligned}$$

where

$$g_{12,0}(z,\xi)=\sigma(\xi,\varphi_1)\,.$$

The first element of the second row of $\boldsymbol{G}(\varsigma,\theta;\zeta,\tau)$ was found as

$$\begin{aligned}
G_{21}(\varphi,\theta;s,\tau) &= \frac{1}{2}g_{21,0}(\varphi,s)+\frac{2a}{Q+1}H_P\left(e^{\sigma(\varphi_0,\varphi)-s/a},\theta-\tau\right)\\
&+\frac{2a}{Q+1}H_P\left(e^{\sigma(\varphi_0,\varphi_1)+\sigma(\varphi,\varphi_1)-s/a},\theta-\tau\right)\\
&+\sum_{n=1}^{\infty}\frac{a}{n}S_n(\varphi,\varphi_1)\,e^{-ns/a}P_n(\varphi_0,\varphi_1)\cos n(\theta-\tau),
\end{aligned}$$

where

$$g_{21,0}(\varphi,s)=\frac{\sigma(\varphi_1,\varphi)}{Q}\ .$$

And, finally, for the second main diagonal element of $\boldsymbol{G}(\varsigma,\theta;\zeta,\tau)$ we have

$$\begin{aligned}
G_{22}(\varphi,\theta;s,\tau) &= \frac{1}{2}g_{22,0}(\varphi,\xi)+H_P\left(e^{\sigma(\varphi,\varphi_1)+\sigma(\xi,\varphi_1)},\theta-\tau\right)\\
&+\frac{1-Q}{1+Q}H_P\left(e^{\sigma(\varphi_0,\varphi)+\sigma(\varphi_0,\xi)},\theta-\tau\right)+\sum_{n=1}^{\infty}\frac{P_nC_{22,n}}{2n}\cos n(\theta-\tau)\\
&-\begin{cases} H_P\left(e^{\sigma(\xi,\varphi)},\theta-\tau\right)+\frac{1-Q}{1+Q}H_P\left(e^{\sigma(\varphi,\xi)+2\sigma(\varphi_0,\varphi_1)},\theta-\tau\right)\\ H_P\left(e^{\sigma(\varphi,\xi)},\theta-\tau\right)+\frac{1-Q}{1+Q}H_P\left(e^{\sigma(\xi,\varphi)+2\sigma(\varphi_0,\varphi_1)},\theta-\tau\right),\end{cases}
\end{aligned}$$

where

$$g_{22,0}(\varphi,\xi)=\begin{cases}\sigma(\varphi,\varphi_1), & \varphi_0<\xi\leq\varphi\\ \sigma(\xi,\varphi_1), & \varphi\leq\xi<\varphi_1,\end{cases}$$

$$C_{22,n}=\begin{cases}\left[(Q+1)\,e^{\sigma(\xi,\varphi_0)}+(Q-1)\,e^{\sigma(\varphi_0,\xi)}\right]S_n(\varphi_1,\varphi),\\ \left[(Q+1)\,e^{\sigma(\varphi,\varphi_0)}+(Q-1)\,e^{\sigma(\varphi_0,\varphi)}\right]S_n(\varphi_1,\xi),\end{cases}$$

As to the last additive term in the above expression for $G_{22}(\varphi,\theta;s,\tau)$, which is defined in two pieces, its upper component is valid for $\varphi_0<\xi\leq\varphi$, whilst the domain of the lower one is $\varphi\leq\xi<\varphi_1$.

To illustrate the computational potential of the expressions just presented for the elements of the matrix of Green's type, we depict in Figure 16 the field induced by a set of two point sources in the considered assembly of thin shells. The parameters specifying the problem setting are chosen as: $a=2.0$, $r=1.5$, $R=a+r=3.5$, $\varphi_0=0.0$, $\varphi_1=2\pi/3$, the locations of the point sources are $(0.01,0.2\pi)$ in the cylindrical fragment, and $(0.13\pi,0.5\pi)$ in the toroidal fragment.

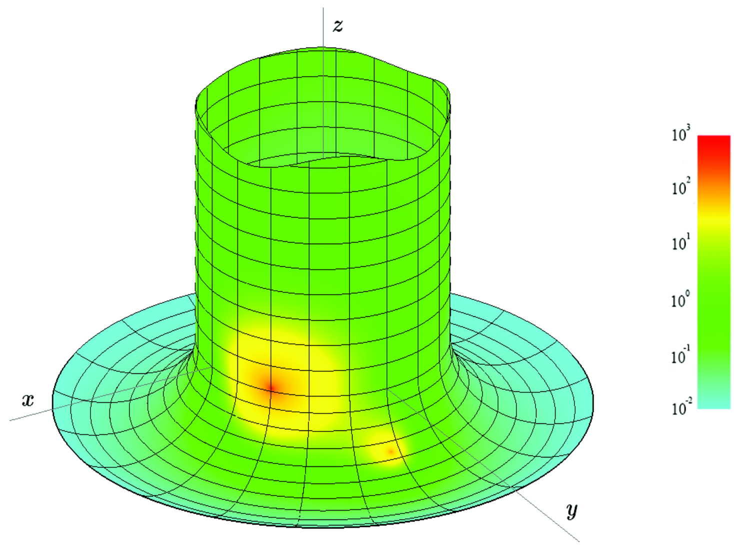

Figure 16: Field generated in the composition of cylindrical and toroidal shells

3.4 A three-fragment shell structure

The approach that we efficiently implemented so far to construct matrices of Green's type can readily be used for composition of more then two shell fragments. To illustrate this point, we consider the shell structure composed of three fragments each made of an individual material (λ_1, λ_2 and λ_3), whose axial cross-section is depicted in Figure 17. Set up Poisson equations each of which is posed in an individual region. These are, the cylinder

$$\Omega_1 = \{(z,\theta) \| \ 0 \leq z \leq \infty; \ 0 \leq \theta \leq \gamma\},$$

the toroidal shell

$$\Omega_2 = \{(\varphi,\theta) | \ \varphi_0 \leq \varphi \leq \varphi_1; \ 0 \leq \theta \leq \gamma\},$$

and the circular plate

$$\Omega_3 = \{(\rho,\theta) \, |0 \leq \rho \leq a_p; 0 \leq \theta \leq \gamma\}.$$

Clearly, the radii a_c, R, and a_p are equal each other.

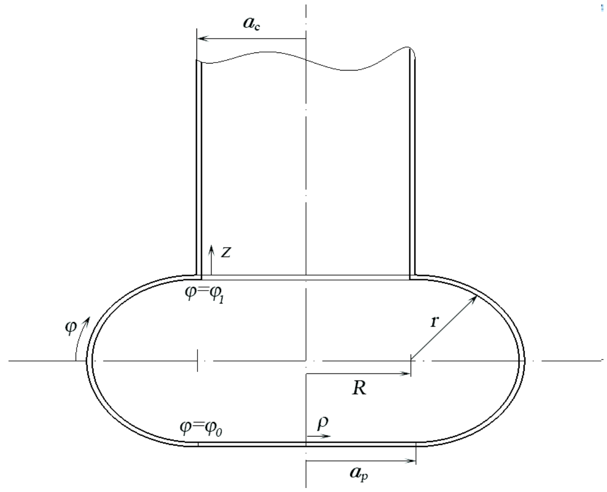

Figure 17: Cross-section of the cylinder-torus-plate composition

The three Poisson equations are considered in $\Omega = \Omega_1 \cup \Omega_2 \cup \Omega_3$ as

$$a_c \frac{\partial^2 u_1(z,\theta)}{\partial z^2} + \frac{1}{a_c}\frac{\partial^2 u_1(z,\theta)}{\partial \theta^2} = -\widetilde{f}_1(z,\theta), \quad \text{in } \Omega_1 \tag{3.38}$$

$$\frac{1}{r}\frac{\partial}{\partial \varphi}\left(D(\varphi)\frac{\partial u_2(\varphi,\theta)}{\partial \varphi}\right) + \frac{r}{D(\varphi)}\frac{\partial^2 u_2(\varphi,\theta)}{\partial \theta^2} = -\widetilde{f}_2(\varphi,\theta), \quad \text{in } \Omega_2 \tag{3.39}$$

$$\frac{\partial}{\partial \rho}\left(\rho \frac{\partial u_3(\rho,\theta)}{\partial \rho}\right) + \frac{1}{\rho}\frac{\partial^2 u_3(\rho,\theta)}{\partial \theta^2} = -\widetilde{f}_3(\rho,\theta), \quad \text{in } \Omega_3 \tag{3.40}$$

subject to the boundary conditions on the external boundary

$$\lim_{z\to\infty} |u_1(z,\theta)| < \infty \quad \text{and} \quad \lim_{\rho\to 0} |u_3(\rho,\theta)| < \infty, \tag{3.41}$$

$$u_i(\varsigma, 0) = 0 \quad \text{and} \quad u_i(\varsigma,\gamma) = 0, \; i = 1,2,3, \tag{3.42}$$

and ideal thermal contact conditions on the interfacial lines

$$u_1(0,\theta) = u_2(\varphi_1,\theta), \quad \frac{\partial u_1(0,\theta)}{\partial z} = \lambda_{12}\frac{\partial u_2(\varphi_1,\theta)}{\partial \varphi} \tag{3.43}$$

and

$$u_3(a_p,\theta) = u_2(\varphi_0,\theta), \quad \frac{\partial u_3(a_p,\theta)}{\partial \rho} = \lambda_{23}\frac{\partial u_2(\varphi_0,\theta)}{\partial \varphi} \tag{3.44}$$

where

$$\widetilde{f}_1(z,\theta) = a_c f_1(z,\theta), \quad \widetilde{f}_2(\varphi,\theta) = \frac{D(\varphi)}{r} f_2(\varphi,\theta), \quad \widetilde{f}_3(\rho,\theta) = \rho f_3(\rho,\theta)$$

$$\varsigma = \begin{cases} z, & \text{in } \Omega_1 \\ \varphi, & \text{in } \Omega_2 \\ \rho, & \text{in } \Omega_3 \end{cases}$$

$$\lambda_{21} = \frac{\lambda_2}{\lambda_1} \quad \text{and} \quad \lambda_{23} = \frac{\lambda_2}{\lambda_3}$$

Following the separation of variables procedure, one obtains a boundary-value problem for the following ordinary differential equations

$$a_c \frac{d^2 u_{1n}(z)}{dz^2} - \frac{\nu^2}{a_c} u_{1n}(z) = -\widetilde{f}_{1n}(z) \tag{3.45}$$

$$\frac{1}{r}\frac{d}{d\varphi}\left(D(\varphi)\frac{du_{2n}(\varphi)}{d\varphi}\right) - \frac{r\nu^2}{D(\varphi)} u_{2n}(\varphi) = -\widetilde{f}_{2n}(\varphi) \tag{3.46}$$

$$\frac{d}{d\rho}\left(\rho\frac{du_{3n}(\rho)}{d\rho}\right) - \frac{\nu^2}{\rho} u_{3n}(\rho) = -\widetilde{f}_{3n}(\rho), \quad \nu = \frac{n\pi}{\gamma} \tag{3.47}$$

in the Fourier series coefficients of the functions $u_1(z,\theta)$, $u_2(\varphi,\theta)$, and $u_3(\rho,\theta)$.

The general solutions for the equations in (3.45)-(3.47) are found in the form

$$u_{1n}(z) = \frac{1}{\nu}\int_0^h \sinh(\nu(z-s)/a_c)\,\widetilde{f}_{1n}(s)\,ds + D_{11}e^{\nu z/a_c} + D_{21}e^{-\nu z/a_c} \tag{3.48}$$

$$u_{2n}(\varphi) = \frac{1}{\nu}\int_{\varphi_0}^{\varphi} \sinh\nu(\omega(\varphi)-\omega(\xi))\,\widetilde{f}_{2n}(\xi)\,d\xi + D_{12}e^{\nu\omega(\varphi)} + D_{22}e^{-\nu\omega(\varphi)} \tag{3.49}$$

$$u_{3n}(\rho) = \frac{1}{2\nu}\int_0^{\rho}\left[\left(\frac{q}{\rho}\right)^{\nu} - \left(\frac{\rho}{q}\right)^{\nu}\right]\widetilde{f}_{3n}(q)\,dq + D_{13}\rho^{\nu} + D_{23}\rho^{-\nu} \tag{3.50}$$

For the sake of simplicity, we limit ourself to the case where the coefficients of thermal conductivity of the materials of which the fragments are made are related as

$$\lambda_1 = 2r\lambda_2 = \lambda_3$$

By satisfying the conditions resulting from (3.41) it can be shown that

$$D_{11} = -\frac{1}{2\nu}\int_0^{\infty} e^{-\nu s/a_c}\widetilde{f}_{1n}(s)\,ds \quad \text{and} \quad D_{23} = 0$$

The conditions that follow from (3.43) and (3.44) yield the system of linear algebraic equations

$$\begin{pmatrix} 1 & -e^{\nu\omega(\varphi_1)} & -e^{-\nu\omega(\varphi_1)} & 0 \\ -1 & -e^{\nu\omega(\varphi_1)} & e^{-\nu\omega(\varphi_1)} & 0 \\ 0 & e^{\nu\omega(\varphi_0)} & e^{-\nu\omega(\varphi_0)} & -a_p^\nu \\ 0 & e^{\nu\omega(\varphi_0)} & -e^{-\nu\omega(\varphi_0)} & -a_p^\nu \end{pmatrix} \begin{pmatrix} D_{21} \\ D_{12} \\ D_{22} \\ D_{13} \end{pmatrix} = \begin{pmatrix} M_1 \\ M_2 \\ M_3 \\ M_4 \end{pmatrix} \tag{3.51}$$

in D_{21}, D_{12}, D_{22}, and D_{13}, where

$$M_1 = \frac{1}{2\nu}\int_0^\infty e^{-\nu s/a_c}\widetilde{f}_{1n}(s)\,ds + \frac{1}{\nu}\int_{\varphi_0}^{\varphi_1} \sinh\left(\nu\left(\omega(\varphi_1) - \omega(\xi)\right)\right)\widetilde{f}_{2n}(\xi)\,d\xi$$

$$M_2 = \frac{1}{2\nu}\int_0^\infty e^{-\nu s/a_c}\widetilde{f}_{1n}(s)\,ds + \frac{1}{\nu}\int_{\varphi_0}^{\varphi_1} \cosh\left(\nu\left(\omega(\varphi_1) - \omega(\xi)\right)\right)\widetilde{f}_{2n}(\xi)\,d\xi$$

$$M_3 = \frac{1}{2\nu}\int_0^{a_p}\left[\left(\frac{q}{a_p}\right)^\nu - \left(\frac{a_p}{q}\right)^\nu\right]\widetilde{f}_{3n}(q)\,dq$$

and

$$M_4 = -\frac{1}{2\nu}\int_0^{a_p}\left[\left(\frac{q}{a_p}\right)^\nu + \left(\frac{a_p}{q}\right)^\nu\right]\widetilde{f}_{3n}(q)\,dq$$

Solving the system in (3.51), one obtains

$$\begin{aligned} D_{21} &= -\frac{1}{2\nu}\int_{\varphi_0}^{\varphi_1} e^{\nu(\omega(\xi)-\omega(\varphi_1))}\widetilde{f}_{2n}(\xi)\,d\xi \\ &\quad +\frac{1}{2\nu}e^{\nu(\omega(\varphi_0)-\omega(\varphi_1))}\int_0^{a_p}\left(\frac{q}{a_p}\right)^\nu \widetilde{f}_{3n}(q)\,dq \end{aligned}$$

$$\begin{aligned} D_{12} &= -\frac{1}{2\nu}e^{-\nu\omega(\varphi_1)}\int_0^\infty e^{-\nu s/a_c}\widetilde{f}_{1n}(s)\,ds \\ &\quad -\frac{1}{2\nu}\int_{\varphi_0}^{\varphi_1} e^{\nu(\omega(\varphi_0)-\omega(\xi))}\widetilde{f}_{2n}(\xi)\,d\xi \end{aligned}$$

$$D_{22} = \frac{1}{2\nu}e^{\nu\omega(\varphi_0)}\int_0^{a_p}\left(\frac{q}{a_p}\right)^\nu \widetilde{f}_{3n}(q)\,dq$$

and

$$\begin{aligned} D_{13} &= -\frac{1}{2\nu a_p^\nu}e^{\nu\omega(\varphi_0)-\nu\omega(\varphi_1)}\int_0^\infty e^{-\nu s/a_c}\widetilde{f}_{1n}(s)\,ds \\ &\quad +\frac{1}{2\nu a_p^\nu}\int_{\varphi_0}^{\varphi_1} e^{-\nu\omega(\xi)}\widetilde{f}_{2n}(\xi)\,d\xi \\ &\quad +\frac{1}{2\nu}\int_0^{a_p}\left(\frac{1}{q}\right)^\nu \widetilde{f}_{3n}(q)\,dq \end{aligned}$$

Substituting the above values into (3.48)-(3.50) we obtain

$$u_{1n}(z) = \int_0^h g_{11n}(z,s)\,\widetilde{f}_{1n}(s)\,ds + \int_{\varphi_0}^{\varphi} g_{12n}(z,\xi)\,\widetilde{f}_{2n}(\xi)\,d\xi + \int_0^{\rho} g_{13n}(z,q)\,\widetilde{f}_{3n}(q)\,dq$$

$$u_{2n}(\varphi) = \int_0^h g_{21n}(\varphi,s)\,\widetilde{f}_{1n}(s)\,ds + \int_{\varphi_0}^{\varphi} g_{22n}(\varphi,\xi)\,\widetilde{f}_{2n}(\xi)\,d\xi + \int_0^{\rho} g_{23n}(\varphi,q)\,\widetilde{f}_{3n}(q)\,dq$$

$$u_{3n}(\rho) = \int_0^h g_{31n}(\rho,s)\,\widetilde{f}_{1n}(s)\,ds + \int_{\varphi_0}^{\varphi} g_{32n}(\rho,\xi)\,\widetilde{f}_{2n}(\xi)\,d\xi + \int_0^{\rho} g_{33n}(\rho,q)\,\widetilde{f}_{3n}(q)\,dq$$

where $g_{ij}(\varsigma,\zeta)$ are the elements of the matrix

$$\mathbf{g}(\varsigma,\zeta) = \frac{1}{2\nu}\begin{pmatrix} g_{11n}(z,s) & g_{12n}(z,\xi) & g_{13n}(z,q) \\ g_{21n}(\varphi,s) & g_{22n}(\varphi,\xi) & g_{23n}(\varphi,q) \\ g_{31n}(\rho,s) & g_{32n}(\rho,\xi) & g_{33n}(\rho,q) \end{pmatrix} \tag{3.52}$$

and the parameter ζ is defined in different fragments of domain Ω as

$$\zeta = \begin{cases} s, & \text{in } \Omega_1 \\ \xi, & \text{in } \Omega_2 \\ q, & \text{in } \Omega_3 \end{cases}$$

The elements g_{ijn} of the matrix in (3.52) are found as

$$g_{11n}(z,s) = \begin{cases} e^{\nu(z-s)/a_c}, & 0 \le z \le s \\ e^{\nu(s-z)/a_c}, & s \le z < \infty \end{cases},$$

$$g_{12n}(z,\xi) = e^{\nu(\omega(\xi)-\omega(\varphi_1)-z/a_c)},$$

$$g_{13n}(z,q) = e^{\nu(\omega(\varphi_0)-\omega(\varphi_1)-z/a_c)}\left(q/a_p\right)^{\nu},$$

$$g_{21n}(\varphi,s) = -e^{\nu(\omega(\varphi)-\omega(\varphi_1)-s/a_c)},$$

$$g_{22n}(\varphi,\xi) = \begin{cases} e^{\nu(\omega(\xi)-\omega(\varphi))}, & \psi \le \varphi \le \varphi_1 \\ e^{\nu(\omega(\varphi)-\omega(\xi))}, & \varphi_0 \le \varphi \le \psi \end{cases},$$

$$g_{23n}(\varphi,q) = e^{\nu(\omega(\varphi_0)-\omega(\varphi))}\left(q/a_p\right)^{\nu},$$

$$g_{31n}(\rho,s) = -e^{\nu(\omega(\varphi_0)-\omega(\varphi_1)-s/a_c)}\left(\rho/a_p\right)^{\nu},$$

$$g_{32n}(\rho,\xi) = e^{\nu(\omega(\varphi_0)-\omega(\xi))}\left(\rho/a_p\right)^{\nu},$$

and

$$g_{33n}\left(\rho,q\right)=\begin{cases}\left(\rho/q\right)^{\nu}, & 0\le\rho\le q\\ \left(q/\rho\right)^{\nu}, & q\le\rho\le a_p\end{cases}.$$

The entries of the matrix of Green's type for the problem in (3.38)-(3.44)

$$\boldsymbol{G}\left(\varsigma,\theta;\zeta,\tau\right)=\left[G_{ij}\left(\varsigma,\theta;\zeta,\tau\right)\right]_{3\times3}$$

are found in the series form

$$G_{ij}\left(\varsigma,\theta;\zeta,\tau\right)=\sum_{n=1}^{\infty}g_{ij,n}\left(\varsigma,\zeta\right)\sin\nu\theta\sin\nu\tau,\quad i=\overline{1,3};\ j=\overline{1,3}$$

After substituting the expressions of $g_{ij,n}\left(\varsigma,\zeta\right)$ into the above series, transforming the product of sines into difference of cosines, and using the standard summation formula in (2.77) (see Chapter 2.) one obtains the following representations of the entries of $\boldsymbol{G}\left(\varsigma,\theta;\zeta,\tau\right)$

$$G_{ij}\left(\varsigma,\theta;\zeta,\tau\right)=H_D\left(\left(g_{ij,n}\left(\varsigma,\zeta\right)\right)^{1/n},\kappa,\eta\right)\tag{3.53}$$

where the function $H_D(x,\alpha,\beta)$ and the parameters κ, and η were defined in preceding chapters as

$$H_D(x,\alpha,\beta)=-\frac{1}{4\pi}\ln\left(\frac{1-2x\cos\alpha+x^2}{1-2x\cos\beta+x^2}\right)$$

and

$$\kappa=\frac{\pi}{\gamma}\left(\theta+\tau\right),\quad\eta=\frac{\pi}{\gamma}\left(\theta-\tau\right)$$

In what follows, we are going to present some illustrations of the computer-friendly nature of the form in (3.53). To do so, in Figure 18 we depict the potential field induced by multiple sources in the considered shell structure. Superposition of profiles of the matrix of Green's type in (3.53) is depicted as seen from two different view angles. The parameters specifying the problem setting are chosen as: $a_c=2.0$, $r=1.5$, $\varphi_0=-\pi/4$, $\varphi_1=\pi/2$, $R=a_c-r\cos\varphi_1=2.0$, $a_p=R+r\cos\varphi_0\approx3.06$, the locations of the point sources are $(1.25,0.83\pi)$ and $(0.5,0.12\pi)$ in the cylindrical fragment, $(0.01\pi,0.72\pi)$ in the toroidal fragment, and $(1.9,0.38\pi)$ in the plane fragment.

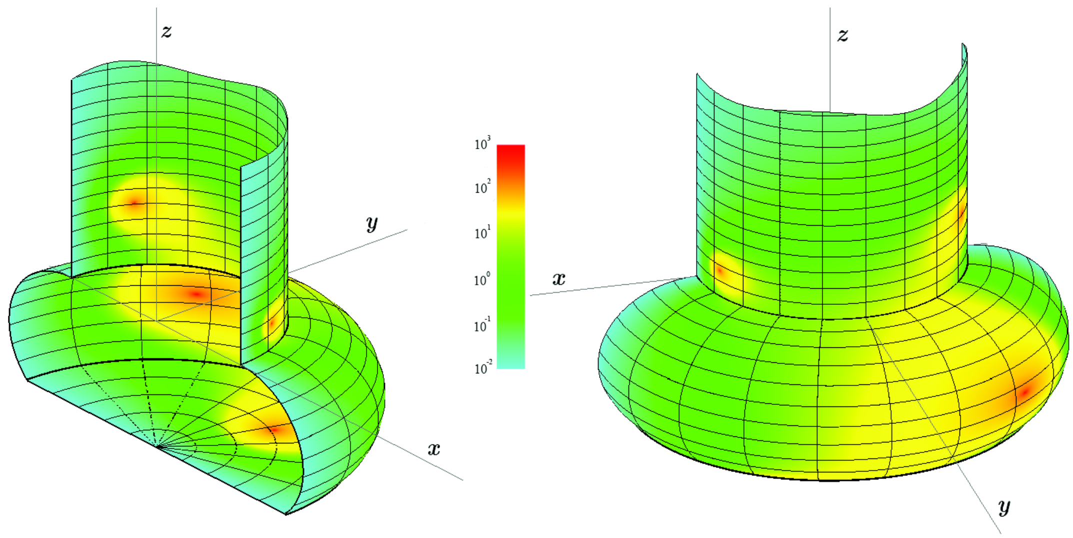

Figure 18: Multiple point sources in the three-fragment shell structure

The matrices of Green's type, which either have already been obtained in the current work or those which are potentially accessible within the scope of our approach, can be used in the development of efficient computational routines aiming at potential fields generated by point sources in joint shell structures weakened with apertures. Problems of that class will be investigated in the following chapter.

4 Green's functions for multiply-connected regions

4.1 Single fragments weakened with apertures

The Green's functions and matrices of Green's type constructed in Chapters 2 and 3, as well as many others, that could be similarly obtained, can be employed to accurately compute potential fields generated by point sources in perforated thin shell structures. This chapter is designed to describe an efficient semi-analytical procedure that allows us to do so. The procedure is based on the modification [12, 13, 47] of the classical [18] boundary integral equation method.

Let Ω represent a double-connected region on a spherical surface bounded with piecewise smooth closed contours S_1 (exterior) and S_2 (interior). On Ω, we consider the well-posed boundary-value problem

$$\frac{\partial}{\partial \phi}\left(\sin\phi \frac{\partial u(\phi,\theta)}{\partial \phi}\right) + \frac{1}{\sin\phi}\frac{\partial^2 u(\phi,\theta)}{\partial \theta^2} = 0, \quad \text{in } \Omega \tag{4.1}$$

$$B_1\left[u(\phi,\theta)\right] = 0, \quad \text{on } S_1 \tag{4.2}$$

$$u(\phi,\theta) = 0, \quad \text{on } S_2 \tag{4.3}$$

Let, also, $G_0(\phi,\theta;\psi,\tau)$ represent the Green's function to the problem in (4.1)-(4.2) set up on the simply-connected region bounded with S_1. The latter problem is also assumed well-posed. In what follows we will refer to $G_0(\phi,\theta;\psi,\tau)$ as the resolving Green's function.

If for an arbitrarily fixed location $(\psi^*,\tau^*) \in \Omega$ of the source point, the profile of the Green's function $G(\phi,\theta;\psi^*,\tau^*)$ of the problem setting in (4.1)-(4.3) is expressed as

$$G(\phi,\theta;\psi^*,\tau^*) = G_0(\phi,\theta;\psi^*,\tau^*) + g^*(\phi,\theta) \tag{4.4}$$

then the additive component $g^*(\phi,\theta)$ must be a solution of the governing equation in (4.1) that satisfies the boundary condition of (4.2). As far as the condition on S_2 is concerned, $g^*(\phi,\theta)$ has to nullify the trace of the resolving Green's function on S_2.

This implies that $g^*(\phi,\theta)$ has to represent the solution of the problem

$$\frac{\partial}{\partial\phi}\left(\sin\phi\frac{\partial g^*(\phi,\theta)}{\partial\phi}\right)+\frac{1}{\sin\phi}\frac{\partial^2 g^*(\phi,\theta)}{\partial\theta^2}=0, \quad \text{in } \Omega$$

$$B_1\left[g^*(\phi,\theta)\right]=0, \quad \text{on } S_1$$

$$g^*(\phi,\theta)=-G_0(\phi,\theta;\psi^*,\tau^*), \quad \text{on } S_2 \tag{4.5}$$

We express the solution of the above problem in the form

$$g^*(\phi,\theta)=\int_{\widetilde{S}_2} G_0(\phi,\theta;\psi,\tau)\,\mu(\psi,\tau)\,d\widetilde{S}_2(\psi,\tau), \quad (\phi,\theta) \text{ in } \Omega \tag{4.6}$$

where the kernel represents the resolving Green's function, and $\widetilde{S}_2$ is a smooth closed curve entirely embraced by S_2. This makes $\widetilde{S}_2$ laying out of Ω. We will refer to $\widetilde{S}_2$ as the fictitious contour. Note that the density function $\mu(\psi,\tau)$ in (4.6) is supposed to be integrable on $\widetilde{S}_2$.

It is evident that the two-variable function of ϕ and θ in (4.6) is harmonic in Ω and satisfies the boundary condition of (4.2) for any density function $\mu(\psi,\tau)$. To make the form in (4.6) complying with the boundary condition of (4.5), we take the limit as (ϕ,θ) approaches the actual interior contour S_2. This leads to the regular functional (of integral type) equation

$$\int_{\widetilde{S}_2} G_0(\phi,\theta;\psi,\tau)\,\mu(\psi,\tau)\,d\widetilde{S}_2(\psi,\tau)=-G_0(\phi,\theta;\psi^*,\tau^*) \tag{4.7}$$

in the density function $\mu(\psi,\tau)$.

The regularity of (4.7) follows from the fact that the curves S_2 and $\widetilde{S}_2$ have no common points. This makes a numerical solution of (4.7), for a fixed location of the fictitious contour $\widetilde{S}_2$, a routine procedure, for any location (ψ^*,τ^*) of the source point. From our experience, it also follows that the regularizing shape and location of the fictitious contour $\widetilde{S}_2$ can appropriately be determined through a straightforward numerical experiment conducted on a case-by-case basis. It appears, in particular, that the shape of $\widetilde{S}_2$ ought to somewhat resemble the shape of S_2. The fictitious contour has to be located close enough to S_2 to provide a required accuracy level. But, on the other hand, the fictitious contour should stay quite apart of the actual contour S_2, providing a stability of the process. We have determined that the distance between S_2 and $\widetilde{S}_2$ has to be within the range of 3-4% of the local radius of curvature of S_2.

To investigate the practicality of the proposed approach to the semi-analytical construction of Green's functions for regions of irregular configuration on spherical surfaces, and to justify its computational efficiency, we present some illustrative examples. For the first of those, we consider a double-connected region Ω_1 representing a quarter of the spherical surface of radius a (a spherical biangle)

$$\Omega_1 = \{(\phi, \theta) \,|0 \leq \phi \leq \pi, \; 0 \leq \theta \leq \pi/2\} \tag{4.8}$$

which is weakened with an aperture having a contour S. The latter is a circle which represents the intersection of the spherical surface and a circular cylinder of radius $0.25a$, whose axis passes through the center of the sphere.

Let the two-dimensional Laplace equation in (4.1) be considered in Ω_1 and subject to the Dirichlet boundary conditions

$$u\,(\phi, 0) = 0, \quad u\left(\phi, \frac{\pi}{2}\right) = 0 \tag{4.9}$$

$$u\,(\phi, \theta) = 0, \quad (\phi, \theta) \in S \tag{4.10}$$

in addition to which, the boundedness conditions

$$\lim_{\phi \to 0} |u\,(\phi, \theta)| < \infty, \quad \lim_{\phi \to \pi} |u\,(\phi, \theta)| < \infty \tag{4.11}$$

must be imposed at the poles of the spherical surface to make the above problem setting well-posed. The boundedness conditions are required due to the fact that the poles represent the points of singularity for the governing differential equation in (4.1).

The potential field depicted in the left fragment of Figure 19 is generated in Ω_1 by three unit sources located at $(0.3\pi, 0.2\pi)$, $(0.6\pi, 0.1\pi)$, and $(0.75\pi, 0.3\pi)$. The axis of the cylinder, that creates the aperture passes through the center of the sphere and the point $(0.5\pi, 0.25\pi)$ on it. Clearly, the shown potential field can be interpreted as the superposition of three profiles of the Green's function computed for the problem in (4.1), (4.9)-(4.11). To illustrate the effect that the aperture provides, we showed in the right fragment the field that would be generated by the same set of unit sources acting in the simply-connected region (see (4.8)).

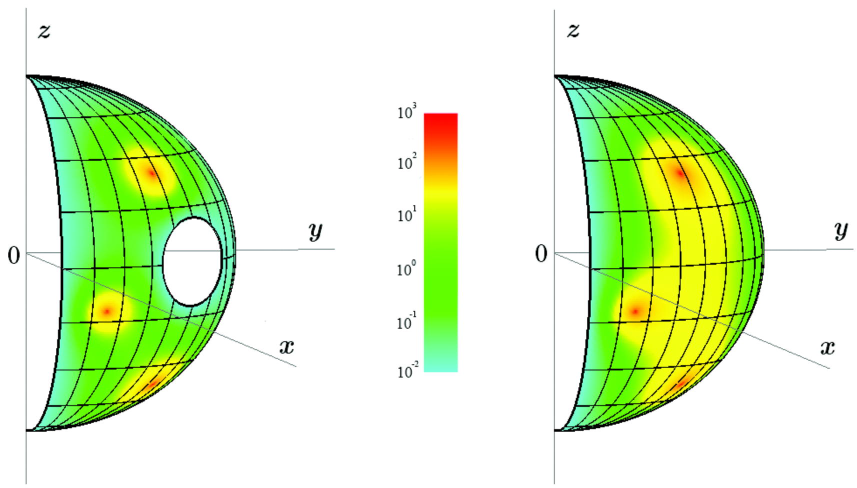

Figure 19: The fields induced by multiple sources in the perforated and the simply-connected spherical biangle

The developed approach can be applied to any boundary-value problem posed on a multiply-connected region, if the Green's function for the corresponding simply-connected region is known. For example, in Figure 20 and Figure 21 the potential fields generated by point sources are shown for other two spherical shells weakened with apertures. The corresponding resolving Green's functions are available in Table 1 (see Section 2.1). The parameters specifying the problem setting in Figure 20 are chosen as: $a = 1.0$, $\beta = \pi/2$, the circular aperture of radius 0.2 is located at $(0.4\pi, 0.3\pi)$. The locations of the point sources are $(0.33\pi, 0.25\pi)$, $(0.38\pi, 0.35\pi)$, $(0.28\pi, 0.47\pi)$, $(0.12\pi, 0.15\pi)$, and $(0.12\pi, 0.45\pi)$.

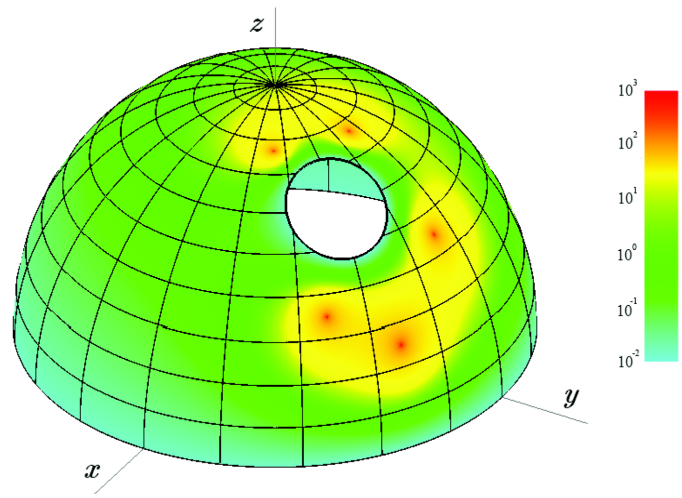

Figure 20: Multiple source points-generated field in a cap weakened with an aperture

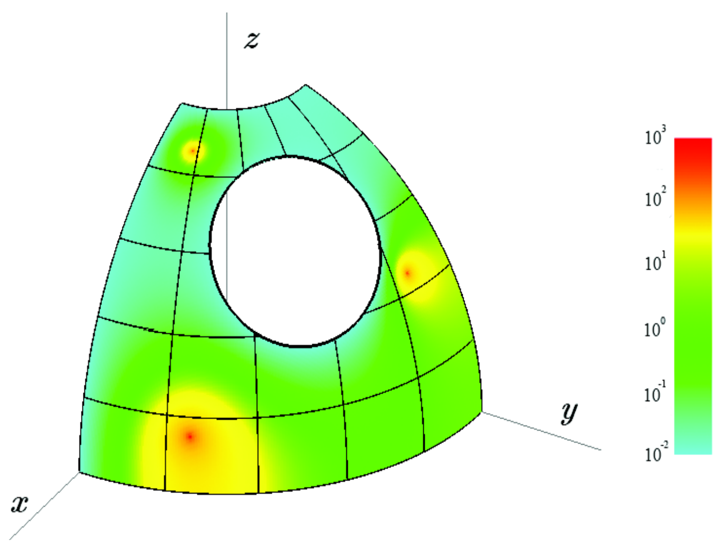

Figure 21: Potential field in a spherical quadrilateral with two-side Dirichlet and two-side Neumann boundary conditions imposed

The field generated in a spherical rectangle $\{\phi, \theta | 0.15\pi \leq \phi \leq 0.5\pi, 0 \leq \theta \leq 0.5\pi\}$ weakened with a circular aperture centered at $(0.3\pi, 0.3\pi)$ .The radius of the spherical surface 1.0, whilst the radius of the aperture is 0.4. Point sources are located at $(0.2\pi, 0.1\pi)$, $(0.45\pi, 0.12\pi)$, and $(0.33\pi, 0.42\pi)$.

So far in this section, we have dealt with Green's functions of boundary-value problems stated in multiply-connected regions. Note that by definition, Green's functions satisfy homogeneous boundary conditions on every piece of the boundary of the considered region. In many practical problems in engineering and science, potential fields are not, however, kept at zero level on each and every piece of the boundary.

The approach that has been used earlier to construct Green's functions can be efficiently implemented for computing potential fields occurring in multiply-connected thin-walled structures where some of the boundary pieces are not necessarily kept at zero potential. To illustrate this point we consider the following problem setting. Let a potential field be generated by N point sources located at points (s_i^*, τ_i^*) in a multiply-connected cylindrical region $\Omega = \Omega_0 \backslash \bigcup_{i=1}^{M} \Omega_i$ where

$$\Omega_0 = \{z, \theta \mid 0 \le z \le h;\ 0 \le \theta \le 2\pi\}$$

whilst the apertures' Ω_i contours S_i, $i = \overline{1, M}$, are smooth closed curves. Homogeneous boundary conditions are imposed on the outer boundary of Ω, whereas some non-homogeneous conditions are imposed on the contours S_i of the apertures.

The potential function $u(z, \theta)$ determined by the described problems setting can be obtained by the governing differential equation

$$\frac{\partial^2 u(z,\theta)}{\partial z^2} + \frac{1}{a^2}\frac{\partial^2 u(z,\theta)}{\partial \theta^2} = -\sum_{i=1}^{N} \delta\left(z - s_i^*, \theta - \tau_i^*\right), \quad \text{in } \Omega \tag{4.12}$$

subject to the boundary conditions

$$u(z,0) = u(z,2\pi), \quad \frac{\partial u(z,0)}{\partial \theta} = \frac{\partial u(z,2\pi)}{\partial \theta} \tag{4.13}$$

$$B_1\left[u(0,\theta)\right] = 0, \quad B_2\left[u(h,\theta)\right] = 0 \tag{4.14}$$

and

$$u(z,\theta) = w_j(z,\theta), \quad (z,\theta) \in S_j, \quad j = \overline{1, M} \tag{4.15}$$

where $w_j(z,\theta)$ represent continuous functions.

We look for the solution of the problem in (4.12)-(4.15) in the form

$$u(z,\theta) = \sum_{i=1}^{N} G_0\left(z,\theta; s_i^*, \tau_i^*\right) + g^*(z,\theta)$$

where $G_0(z,\theta;s_i^*,\tau_i^*)$ is the resolving Green's function (the one of the boundary-value problem in (4.12)-(4.14)), with the source points fixed at (s_i^*,τ_i^*). It can be found in Table 2 (Chapter 2). The corrector-function $g^*(z,\theta)$ will be expressed as

$$g^*(z,\theta)=\sum_{i=1}^{M}\int_{\widetilde{S}_i}G_0(z,\theta;s,\tau)\,\mu_i(s,\tau)\,d\widetilde{S}_i(s,\tau)\,,\quad (z,\theta)\in\Omega$$

where $\widetilde{S}_i$ are fictitious contours, one for the corresponding S_i located entirely within Ω_i, hence outside of Ω. The following system of functional equations

$$\begin{aligned}\sum_{i=1}^{M}\int_{\widetilde{S}_i}G_0(z,\theta;s,\tau)\,\mu_i(s,\tau)\,d\widetilde{S}_i(s,\tau) &= \\ w_j(z,\theta)-\sum_{i=1}^{N}G_0(z,\theta;s_i^*,\tau_i^*)\,,\quad (z,\theta) &\in S_j;\quad j=\overline{1,M}\end{aligned}\tag{4.16}$$

appears when we determine the density-functions $\mu_i(s,\tau)$, by means of the boundary conditions in (4.15).

The system of functional equations in (4.16) reduces to a system of linear algebraic equations by approximating the integrals in it by quadrature formulas. This system is supposed to have a unique solution for the fixed shape and location of the fictitious contours $\widetilde{S}_i$. Some numerical experiments are required to properly locate $\widetilde{S}_i$. These experiments have to be conducted on a case-by-case basis.

As an illustrative example for the problem setting in (4.12)-(4.15) we depict in Figure 22 (a) the potential field determined in Ω by the following set of initial data: $a=0.5$, $h=2$, $N=3$, $M=2$, $(s_1^*,\tau_1^*)=(0.8,0.25\pi)$, $(s_2^*,\tau_2^*)=(1.4,0.55\pi)$, $(s_3^*,\tau_3^*)=(0.2,0.4\pi)$, $w_1(z,\theta)\equiv 50.0$, and $w_2(z,\theta)\equiv 1.0$. The identity operators $B_1\equiv I$ and $B_2\equiv I$ define the boundary conditions on the outer contours $z=0$ and $z=h$. The apertures are circular of radii 0.1 and 0.2 centered at $(1.6,0.25\pi)$ and $(0.6,0.6\pi)$, respectively.

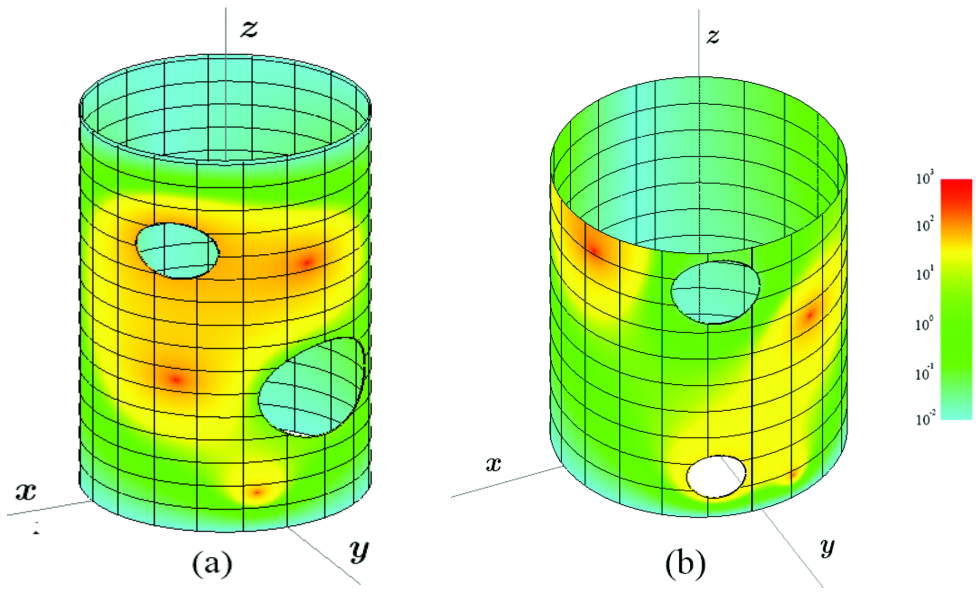

Figure 22: Potential fields induced by multiple point sources in perforated cylindrical shells

The potential field depicted in Figure 22 (b) is specified by another set of initial data in the problem setting of (4.12)-(4.15). That is $a = 2$, $h = 4$, $N = 3$, $M = 2$, $(s_1^*, \tau_1^*) = (3.65, 0.12\pi)$, $(s_2^*, \tau_2^*) = (0.25, 0.6\pi)$, $(s_3^*, \tau_3^*) = (2.6, 2\pi/3)$, $w_1(z, \theta) \equiv 1.0$, and $w_2(z, \theta) \equiv 10.0$. The boundary operators are: $B_1 \equiv I$ and $B_2 \equiv \partial/\partial z$. The apertures are circular of radii 0.5 and 0.3 centered at $(3.4, 0.45\pi)$ and $(0.6, 0.45\pi)$.

4.2 Assemblies of thin shells with apertures

The technique described in the preceding section could be extended for the case of assemblies of shells [14, 15]. Consider again the thin spherical-toroidal shell assembly similar to that we had earlier dealt with in Chapter 3 (see Figure 23).

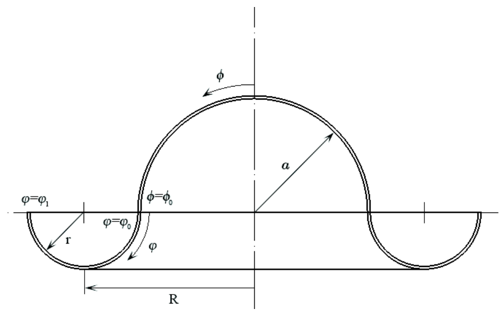

Figure 23: Axial cross-section of the sphere-torus assembly

Let the assembly be weakened with an aperture whose contour S represents intersection of the middle surface of the spherical fragment with a cylinder whose diameter is smaller than the radius of the sphere (see Figure 24).

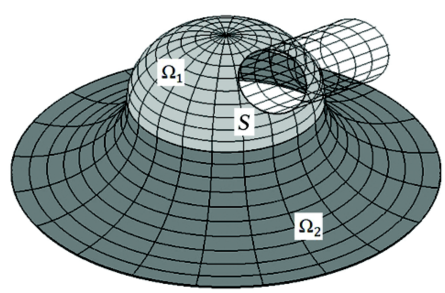

Figure 24: The assembly of spherical and toroidal fragments weakened with an aperture

This makes double-connected the fragment $\Omega_1(\phi, \theta)$ of the middle surface $\Omega = \Omega_1(\phi, \theta) \cup \Omega_2(\varphi, \theta)$ of the shell assembly, whereas the fragment Ω_2 remains simply-connected.

To determine a potential field generated by a point source acting in either Ω_1 or Ω_2, we consider the Laplace equations

$$\nabla^2 u_1(\phi, \theta) = 0, \qquad (\phi, \theta) \in \Omega_1 \tag{4.17}$$

and

$$\nabla^2 u_2(\varphi, \theta) = 0, \qquad (\varphi, \theta) \in \Omega_2, \tag{4.18}$$

referenced to the corresponding geographical coordinates and subject to the boundary and contact conditions

$$\lim_{\phi \to 0} |u_1(\phi, \theta)| < \infty, \; u_2(\varphi_1, \theta) = 0 \tag{4.19}$$

$$u_1(\phi, 0) = u_1(\phi, 2\pi), \quad \frac{\partial u_1(\phi, 0)}{\partial \theta} = \frac{\partial u_1(\phi, 2\pi)}{\partial \theta} \tag{4.20}$$

$$u_2(\varphi, 0) = u_2(\varphi, 2\pi), \quad \frac{\partial u_2(\varphi, 0)}{\partial \theta} = \frac{\partial u_2(\varphi, 2\pi)}{\partial \theta} \tag{4.21}$$

$$u_1(\phi_0, \theta) = u_2(\varphi_0, \theta), \quad \frac{\partial u_1(\phi_0, \theta)}{\partial \phi} = \lambda \frac{\partial u_2(\varphi_0, \theta)}{\partial \varphi} \tag{4.22}$$

In addition, let the function $u_1(\phi, \theta)$, whose domain is Ω_1, be subject to the condition

$$u_1(\phi, \theta) = 0, \quad (\phi, \theta) \in S \tag{4.23}$$

Clearly, the potential field generated by a point source, acting at a point $(\zeta^*, \tau^*) \in \Omega$ can be simulated with corresponding profiles of the elements of the matrix of Green's type $\widetilde{\boldsymbol{G}}(\varsigma, \theta; \zeta, \tau)$

$$\widetilde{\boldsymbol{G}}(\varsigma, \theta; \zeta^*, \tau^*) = \left[\widetilde{G}_{ij}(\varsigma, \theta; \zeta^*, \tau^*)\right]_{2\times 2} \tag{4.24}$$

of the problem in (4.17)–(4.23). Similarly to what was done in Chapter 3, we introduce the common notations

$$\varsigma = \begin{cases} \phi, & \text{in } \Omega_1 \\ \varphi, & \text{in } \Omega_2 \end{cases} \quad \text{and} \quad \zeta = \begin{cases} \psi, & \text{in } \Omega_1 \\ \xi, & \text{in } \Omega_2 \end{cases}$$

already accepted in (4.24) for the latitudinal coordinate of an observation and source points in either fragment of the structure.

To efficiently compute the elements of $\widetilde{\boldsymbol{G}}(\varsigma, \theta; \zeta, \tau)$ within the scope of the Green's function modification [47] of one of the versions of the boundary integral equation method, we take advantage of the matrix of Green's type

$$\boldsymbol{G}(\varsigma, \theta; \zeta, \tau) = [G_{ij}(\varsigma, \theta; \zeta, \tau)]_{2\times 2},$$

which was earlier obtained in (3.31) for the homogeneous boundary-value problem corresponding to (4.17)-(4.22) stated in the compound (simply-connected) region Ω. As we have already agreed on, $\boldsymbol{G}(\varsigma, \theta; \zeta, \tau)$ will be referred to as the resolving matrix.

For a fixed in Ω location (ζ^*, τ^*) of the source point, we express the matrix of Green's type $\widetilde{\boldsymbol{G}}(\varsigma, \theta; \zeta^*, \tau^*)$ in terms of the resolving matrix as

$$\widetilde{\boldsymbol{G}}(\varsigma, \theta; \zeta^*, \tau^*) = \boldsymbol{G}(\varsigma, \theta; \zeta^*, \tau^*) + \mathbf{W}^*(\varsigma, \theta). \tag{4.25}$$

Clearly, the resolving matrix, as an additive component to $\widetilde{\boldsymbol{G}}(\varsigma, \theta; \zeta^*, \tau^*)$, provides the latter with the logarithmic singularity. As to the second component in (4.25), it represents a two-by-two matrix

$$\mathbf{W}^*(\varsigma, \theta) = \begin{pmatrix} w_{11}^*(\phi, \theta) & w_{12}^*(\phi, \theta) \\ w_{21}^*(\varphi, \theta) & w_{22}^*(\varphi, \theta) \end{pmatrix},$$

implying that its elements $w_{11}^*(\phi, \theta)$ and $w_{12}^*(\phi, \theta)$ are defined in Ω_1, whereas the domain for the elements $w_{21}^*(\varphi, \theta)$ and $w_{22}^*(\varphi, \theta)$ is Ω_2. Hence, the elements of $\mathbf{W}^*(\varsigma, \theta)$ have to be harmonic in their domains. In addition, to make the first row elements of $\widetilde{\boldsymbol{G}}(\varsigma, \theta; \zeta^*, \tau^*)$ vanishing on S, the elements $w_{11}^*(\phi, \theta)$ and $w_{12}^*(\phi, \theta)$ of $\mathbf{W}^*(\varsigma, \theta)$ have to compensate the traces of the first row elements of the resolving matrix on S. All the elements of $\mathbf{W}^*(\varsigma, \theta)$ are to comply with the boundary and contact conditions of (4.19)–(4.22) that they are relevant to.

The Green's function version of the functional equation method, introduced earlier in Section 4.1, will be used to accurately compute the elements of $\mathbf{W}^*(\varsigma, \theta)$. To be specific, we focus on the potential field generated by a unit source placed at a point (ζ^*, τ^*) located in the double-connected spherical fragment of the considered shell structure. Since (ζ^*, τ^*) is located in Ω_1, the elements of the first column of the matrix in (4.25) simulate the required potential field. To efficiently determine them, we introduce the vector-function

$$\mathbf{V}(\varsigma, \theta) = \begin{pmatrix} V_1(\phi, \theta) \\ V_2(\varphi, \theta) \end{pmatrix},$$

with components defined in terms of the elements of $\mathbf{W}^*(\varsigma, \theta)$ as

$$V_1(\phi, \theta) = \begin{cases} w_{11}^*(\phi, \theta), & \text{in } \Omega_1 \\ 0, & \text{in } \Omega_2 \end{cases} \quad \text{and} \quad V_2(\varphi, \theta) = \begin{cases} 0, & \text{in } \Omega_1 \\ w_{21}^*(\varphi, \theta), & \text{in } \Omega_2 \end{cases}.$$

Introducing also the vector-function

$$\mathbf{M}(\zeta, \tau) = \begin{pmatrix} M_1(\psi, \tau) \\ M_2(\xi, \tau) \end{pmatrix},$$

whose components are defined as

$$M_1(\psi, \tau) = \begin{cases} \mu_1^*(\psi, \tau), & \text{in } \Omega_1 \\ 0, & \text{in } \Omega_2 \end{cases} \quad \text{and} \quad M_2(\psi, \tau) = \begin{cases} 0, & \text{in } \Omega_1 \\ \mu_2^*(\xi, \tau), & \text{in } \Omega_2 \end{cases},$$

we express the vector $\mathbf{V}(\varsigma, \theta)$ in a form of the line integral

$$\begin{pmatrix} V_1(\phi, \theta) \\ V_2(\varphi, \theta) \end{pmatrix} = \int\limits_{S_0} \begin{pmatrix} G_{11}(\phi, \theta; \psi, \tau) & G_{12}(\phi, \theta; \psi, \tau) \\ G_{21}(\varphi, \theta; \xi, \tau) & G_{22}(\varphi, \theta; \xi, \tau) \end{pmatrix} \begin{pmatrix} M_1(\psi, \tau) \\ M_2(\xi, \tau) \end{pmatrix} dS_0(\zeta, \tau), \qquad (4.26)$$

where the fictitious contour S_0 represents a smooth closed line embraced with the actual aperture contour S.

From (4.26), it follows that the first component of the vector-function $\mathbf{V}(\varsigma, \theta)$ reads

$$\begin{aligned} V_1(\phi, \theta) \;\; &= \int\limits_{S_0} G_{11}(\phi, \theta; \psi, \tau) M_1(\psi, \tau) dS_0(\psi, \tau) \\ &+ \int\limits_{S_0} G_{12}(\phi, \theta; \psi, \tau) M_2(\psi, \tau) dS_0(\psi, \tau), \quad (\phi, \theta) \text{ in } \Omega_1. \end{aligned} \qquad (4.27)$$

Due to the way the vector-functions $\mathbf{V}(\varsigma, \theta)$ and $\mathbf{M}(\zeta, \tau)$ were introduced, the above representation reduces to

$$w_{11}^*(\phi, \theta) = \int\limits_{S_0} G_{11}(\phi, \theta; \psi, \tau)\, \mu_1^*(\psi, \tau) dS_0(\psi, \tau), \quad (\phi, \theta) \in \Omega_1 \qquad (4.28)$$

It is evident that the integral form in (4.28) is a harmonic function of ϕ and θ in Ω_1 regardless of the density function $\mu_1^*(\psi, \tau)$, which is of course supposed to be integrable on S_0. Clearly, the harmonic nature of $w_{11}^*(\phi, \theta)$ in (4.28) is guaranteed by the kernel-function $G_{11}(\phi, \theta; \psi, \tau)$.

Taking the limit in (4.28) as the field point (ϕ, θ) approaches the actual contour S of the aperture, we arrive, in view of the boundary condition of (4.23) and the form of $\widetilde{\boldsymbol{G}}(\varsigma, \theta; \psi^*, \tau^*)$ in (4.25), at the regular functional equation

$$\int\limits_{S_0} G_{11}\left(\phi, \theta; \psi, \tau\right) \mu_1^*(\psi, \tau) dS_0(\psi, \tau) = -\, G_{11}\left(\phi, \theta; \psi^*, \tau^*\right), \quad (\phi, \theta) \in S, \tag{4.29}$$

in the density function $\mu_1^*(\psi, \tau)$. Due to the regular nature of the above equation, its numerical solution is not expected to be problematic (for a fixed fictitious contour S_0). But finding optimal shape and location of S_0 is another issue representing a regularizing stage of our algorithm. It has to be addressed on the case-by-case basis. Our experience provides us with data ensuring a confidence in the efficiency of the suggested approach.

Once an accurate approximation of the density function $\mu_1^*(\psi, \tau)$ is found, the form in (4.28) gives us an explicit expression for the component $w_{11}^*(\phi, \theta)$ of the potential field generated in the double-connected region Ω_1 by a unit source at a point (ψ^*, τ^*) also located in Ω_1. To obtain the second fragment $w_{21}^*(\varphi, \theta)$ of the potential field generated in the simply-connected region Ω_2 by the unit source located at $(\psi^*, \tau^*) \in \Omega_1$, we turn to the integral representation of (4.26), from which the second component of the vector-function $\mathbf{V}(\varsigma, \theta)$ appears in the form

$$V_2(\varphi, \theta) = \int\limits_{S_0} G_{21}(\varphi, \theta; \psi, \tau) M_1(\psi, \tau) dS_0(\psi, \tau)$$

$$+ \int\limits_{S_0} G_{22}(\varphi, \theta; \psi, \tau) M_2(\psi, \tau) dS_0(\psi, \tau), \quad (\varphi, \theta) \in \Omega_2,$$

which yields the integral representation

$$w_{21}^*(\varphi, \theta) = \int\limits_{S_0} G_{21}\left(\varphi, \theta; \psi, \tau\right) \mu_1^*(\psi, \tau) dS_0(\psi, \tau), \quad (\varphi, \theta) \in \Omega_2$$

for the required fragment of the potential field.

In Figure 25, one finds a potential field induced by point sources in the considered spherical-toroidal joint shell structure perforated with a circular aperture whose contour is held at zero potential. The field was accurately computed within the scope of the described numerical procedure. The parameters specifying the problem setting are chosen as: $a = 0.6$, $r = 0.7$, $\phi_0 = \pi/2$, $\varphi_0 = 0.0$, $\varphi_1 = \pi/2$, $R = a + r = 1.3$, the locations of the point sources are $(0.4\pi, 0.18\pi)$ in the spherical fragment, and $(0.45\pi, 0.52\pi)$ and $(0.42\pi, 0.28\pi)$ in the toroidal fragment. The circular aperture of radius 0.2 is centered at $(0.35\pi, 0.5\pi)$ of the spherical fragment.

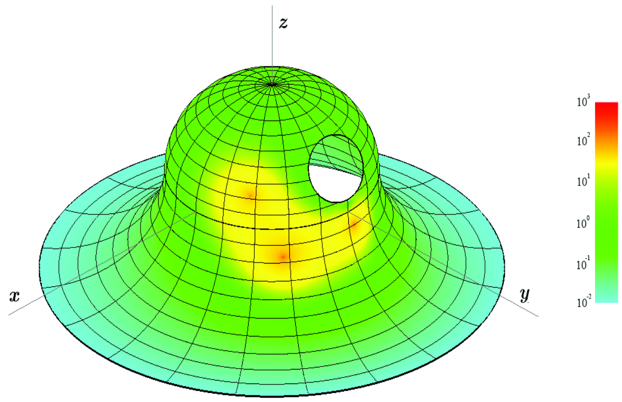

Figure 25: Potential field induced by multiple point sources in a double-connected compound shell structure

The following comments are appropriate as to the computational specifics making our procedure efficient:

- the regularizing effect is achieved by choosing the fictitious contour S_0 as a concentric with S circle of radius 0.98 of the latter;
- the functional equation in (4.29) was numerically solved by the quadratures method (the regular trapezoid rule with 40-50 grid points);
- the series-containing components of the matrix of Green's type were truncated to the tenth partial sum.

During the past several decades, the classical boundary integral equation method [18] is considered as one of the most efficient approaches to partial differential equations. Its key feature is the reduction of a considered boundary-value problem to boundary integral equations.

Our experience [16] reveals high computational potential of numerical schemes based on the incorporation of matrices of Green's type into the boundary integral equation method scheme. To illustrate this point, we are going to consider a problem simulating potential field that is induced in a thin-walled structure, comprised of two cylindrical shells shown in Figure 26. Both fragments (Ω_1 and Ω_2) represent closed finite cylindrical shells.

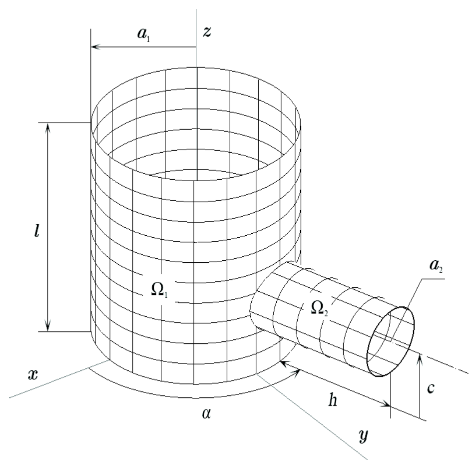

Figure 26: Geometry of the assembly of two cylindrical shells

Let λ_1 and λ_2 represent thermal conductivities of the materials of which the fragments Ω_1 and Ω_2 are made. Potential field induced by a point source acting in Ω_1, is simulated by a set of two Poisson equations each of which is written in the individual coordinate system (z_1, θ_1) and (z_2, θ_2). We write them in a vector form as

$$\frac{\partial^2 \mathbf{U}(z,\theta)}{\partial z^2} + \frac{1}{a_i^2}\frac{\partial^2 \mathbf{U}(z,\theta)}{\partial \theta^2} = -\mathbf{F}(z,\theta), \quad \text{in } \Omega, \quad i = 1, 2 \tag{4.30}$$

where

$$\mathbf{U}(z,\theta) = \begin{pmatrix} u_1(z_1,\theta_1) \\ u_2(z_2,\theta_2) \end{pmatrix}, \quad \mathbf{F}(z,\theta) = \begin{pmatrix} \delta(z_1 - s, \theta_1 - \tau) \\ 0 \end{pmatrix}$$

$$z = \begin{cases} z_1, & \text{in } \Omega_1 \\ z_2, & \text{in } \Omega_2 \end{cases} \quad \text{and} \quad \theta = \begin{cases} \theta_1, & \text{in } \Omega_1 \\ \theta_2, & \text{in } \Omega_2 \end{cases}$$

and a_i is the radius of the corresponding cylinder.

The boundary conditions are imposed on the outer boundary as

$$\mathbf{U}(z,0)=\mathbf{U}(z,2\pi), \quad \frac{\partial \mathbf{U}(z,0)}{\partial \theta}=\frac{\partial \mathbf{U}(z,2\pi)}{\partial \theta} \tag{4.31}$$

$$u_1(0,\theta_1)=0, \quad \frac{\partial u_1(l,\theta_1)}{\partial \theta_1}=0 \tag{4.32}$$

$$u_2(0,\theta_2)=0 \tag{4.33}$$

and the ideal contact conditions are imposed on the interfacial line L as

$$\begin{aligned} u_1(z_1,\theta_1) &= u_2(z_2,\theta_2), \quad \frac{\partial u_1(z_1,\theta_1)}{\partial \mathbf{n}_1}=-\lambda\frac{\partial u_2(z_2,\theta_2)}{\partial \mathbf{n}_2}, \\ (z_i,\theta_i) &\in L\subset\Omega_i, \quad i=1,2 \end{aligned} \tag{4.34}$$

where $\mathbf{n}_i$, $i=1,2$ is the normal vector to L in Ω_i, and $\lambda=\lambda_2/\lambda_1$. Note that the contour L has to be defined in two coordinate systems individually, i.e. $L(z_1,\theta_1)$ and $L(z_2,\theta_2)$. Before we proceed any further, let us pay special attention to the analytic geometry behind the shell configuration. First, we describe the contour L in both coordinate systems. As shown on Figure 26, the contour L appears as the intersection of two cylindrical surfaces with mutually perpendicular axes. In Ω_1 L is parametrically defined as

$$\begin{aligned} z_1(t) &= c+a_2\sin t \\ \theta_1(t) &= \begin{cases} \arctan(y(t)/x(t)) & y(t)/x(t)>0 \\ \pi+\arctan(y(t)/x(t)) & y(t)/x(t)<0 \end{cases} \end{aligned}$$

where

$$x(t)=\sqrt{a_1^2-a_2^2\cos^2 t}\cos\alpha-a_2\cos t\sin\alpha$$

$$y(t)=\sqrt{a_1^2-a_2^2\cos^2 t}\sin\alpha+a_2\cos t\cos\alpha$$

and $t\in[0,2\pi)$.

On the other hand, in Ω_2, L reads as

$$\begin{aligned} z_2(t) &= h+a_1-\sqrt{a_1^2-a_2^2\cos^2 t} \\ \theta_2(t) &= t \end{aligned}$$

Note that parameter t must be the same for both regions.

Next, the normal derivatives in (4.34) are defined in terms of the local coordinate systems as

$$\frac{\partial}{\partial \mathbf{n}_i} = \left(n_{z_i} \frac{\partial}{\partial z_i} + n_{\theta_i} \frac{\partial}{\partial \theta_i} \right), \quad i = 1, 2$$

The normal derivative in region Ω_2 is fairly trivial

$$\mathbf{n}_2 = (1, 0)$$

while in the case of $\mathbf{n}_1$, after some algebra, one obtains

$$\mathbf{n}_1 = \left(\frac{1}{|\mathbf{n}_1|}, \frac{1}{|\mathbf{n}_1|} \frac{dz}{d\theta} \right)$$

where

$$|\mathbf{n}_1| = \sqrt{1 + \left(\frac{dz}{d\theta} \right)^2}$$

and

$$\frac{dz}{d\theta} = \sqrt{a_1^2 - a_2^2 \cos^2 t} \cot t$$

Note that, when $\cot t$ is undefined, we have

$$\mathbf{n}_1 = \begin{cases} (0, 1), & t = 0 \\ (0, -1), & t = \pi \end{cases}$$

Clearly, the potential field generated by a point-source, located at a point (s^*, τ^*) in Ω_1, is simulated by the matrix of Green's type for the boundary-value problem in (4.30)-(4.34). Since the point-source is located in Ω_1, the 2×1 matrix

$$\boldsymbol{G}(z, \theta; s^*, \tau^*) = \begin{pmatrix} G_{11}(z_1, \theta_1; s^*, \tau^*) \\ G_{21}(z_2, \theta_2; s^*, \tau^*) \end{pmatrix}$$

is targeted, where $G_{i1}(z_i, \theta_i; s^*, \tau^*)$ represents the field induced in the corresponding region Ω_i, $i = 1, 2$. We look for the elements of the above matrix in the form

$$G_{11}(z_1, \theta_1; s^*, \tau^*) = G_0(z_1, \theta_1; s^*, \tau^*) + w_1^*(z_1, \theta_1)$$

$$G_{21}(z_2, \theta_2) = w_2^*(z_2, \theta_2)$$

where $G_0(z_1,\theta_1;s^*,\tau^*)$ is the Green's function for the boundary-value problem in (4.30)-(4.32) whose representation

$$G_0(z_1,\theta_1;s^*,\tau^*) = z_1 - aH_P\left(e^{(z_1+s^*-2h)/a},\theta_1-\tau^*\right) + aH_P\left(e^{-(z_1+s^*)/a},\theta_1-\tau^*\right) + R + \left\{\begin{array}{l} z_1 - aH_P\left(e^{(z_1-s^*)/a},\theta_1-\tau\right) + aH_P\left(e^{(-z_1+s^*-2h)/a},\theta_1-\tau^*\right) \\ s^* - aH_P\left(e^{(-z_1+s^*)/a},\theta_1-\tau\right) + aH_P\left(e^{(z_1-s^*-2h)/a},\theta_1-\tau^*\right) \end{array}\right.$$

can be found in Table 2 of Chapter 2. The upper branch of the last additive component in the above formula corresponds to $0 \le z_1 \le s^*$, while the lower branch takes place if $s^* \le z_1 \le l$. The regular component $R = R(z_1,\theta_1;s^*,\tau^*)$ reads as

$$R = \sum_{n=1}^{\infty} \frac{a}{2\pi n} \frac{\sinh(nz_1/a)\cosh(n(s^*-l)/a)}{e^{2nl/a}\cosh(nl/a)} \cos n(\theta_1-\tau^*)$$

The functions $w_i^*(z,\theta)$, $i=1,2$ are expressed as

$$w_1^*(z_1,\theta_1) = \int_{\widetilde{L}_1} G_0(z_1,\theta_1;s,\tau)\,\mu_1(s,\tau)\,d\widetilde{L}_1(s,\tau)$$

and

$$w_2^*(z_2,\theta_2) = \int_{\widetilde{L}_2} G_0(z_2,\theta_2;s,\tau)\,\mu_2(s,\tau)\,d\widetilde{L}_2(s,\tau)$$

So, our strategy in finding the regular components $w_1^*(z_1,\theta_1)$ and $w_2^*(z_2,\theta_2)$ is similar to that we used earlier. That is, the fictitious contours $\widetilde{L}_1$ and $\widetilde{L}_2$ are introduced, where each of them is defined in the corresponding coordinate system and lies outside of the corresponding region Ω_i. In order to find the density-functions $\mu_i(s,\tau)$ the conditions in (4.34) are to be employed. In doing so, we arrived at the system of functional equations

$$\begin{aligned} -G_0(z_1,\theta_1;s^*,\tau^*) = & \int_{\widetilde{L}_1} G_0(z_1,\theta_1;s,\tau)\,\mu_1(s,\tau)\,d_{s,\tau}\widetilde{L}_1 \\ & - \int_{\widetilde{L}_2} G_0(z_2,\theta_2;s,\tau)\,\mu_2(s,\tau)\,d_{s,\tau}\widetilde{L}_2 \end{aligned} \tag{4.35}$$

$$\begin{aligned} -D\left[G_0(z_1,\theta_1;s^*,\tau^*)\right] = & \int_{\widetilde{L}_1} D\left[G_0(z_1,\theta_1;s,\tau)\right]\mu_1(s,\tau)\,d_{s,\tau}\widetilde{L}_1 \\ & + \lambda \int_{\widetilde{L}_2} \frac{\partial}{\partial z_2} G_0(z_2,\theta_2;s,\tau)\,\mu_2(s,\tau)\,d_{s,\tau}\widetilde{L}_2 \end{aligned} \tag{4.36}$$

where

$$(z_i, \theta_i) \in L, \quad i = 1, 2$$

and

$$D \equiv n_{z_1} \frac{\partial}{\partial z_1} + n_{\theta_1} \frac{\partial}{\partial \theta_1}$$

After reducing the system in (4.35) and (4.36) to a system of linear algebraic equations (in the way described earlier in Section 4.1) and solving it numerically, one obtains elements of the matrix of Green's type for the problem in (4.30)-(4.34). To illustrate high computational potential of the proposed algorithm, we present in Figure 27 the potential field obtained for a particular problem setting.

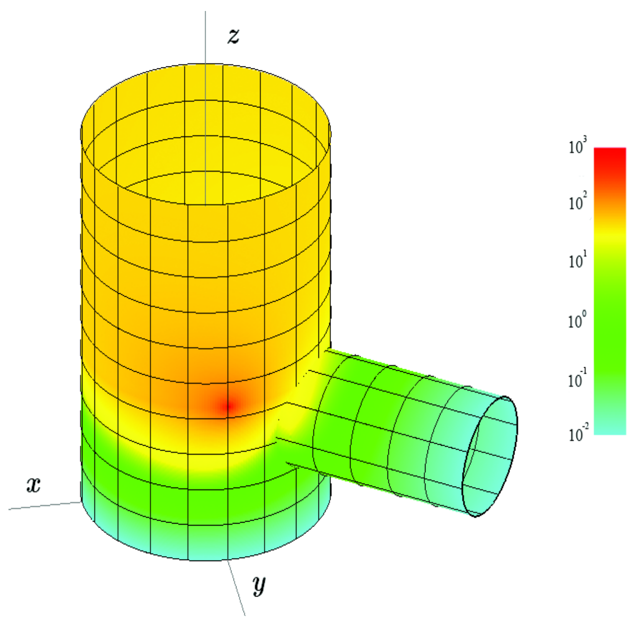

Figure 27: Potential field generated by a point-source in the shell structure

The parameters specifying the problem setting are chosen as: $a_1 = 1.0$, $a_2 = 0.3$, $l = 2.0$, $h = 1.2$, $c = 0.6$, $\alpha = 0.8\pi$, the location of the point source is $(0.7, 0.5\pi)$ in the first cylinder.

5 Computational Aspects

This Chapter is designed to highlight just a few aspects relevant to the computer algorithms created and repeatedly utilized in the present study. We plan to briefly discuss, in particular, the validation issue for the numerical methods used herein and present some arguments verifying actual results obtained. Parallelism in the computer routines developed in this manual represents another aspect which is supposed to be superficially discussed. In addition, as to the possibility of tackling inverse problem settings, we are going to bring to the readers attention the issue of potential implementation for this purpose of the algorithms that have been developed in the preceding Chapters for solution of direct boundary-value problems for partial differential equations.

5.1 Validation and verification

To make sure that the computational algorithms developed in the present study could form a solid and reliable background for implementation in engineering and science, they have to go through a process of validation and verification. Note, however, that as far as the materials of Chapters 2 and 3 are concerned, the validation and verification do not constitute pressing or urgent issues of any kind. Indeed, either closed forms or computer-friendly representations are obtained in those chapters for a vast number of Green's functions and matrices of Green's type for boundary-value problems simulating potential fields induced in thin shells and their assemblies. And since Green's functions deliver either exact analytical or easy-controlled approximate but still analytical solutions for considered problems, there is no need for special effort towards their verification.

A quite different situation takes place in Chapter 4, where we have developed and widely used some numerical algorithms based on our Green's function version of the classical boundary integral equation method for an important class of problems.

Those problems are stated in multiply-connected regions of irregular configuration, and this is why they do not allow exact analytical solution. Computational efficiency of our algorithms does really represent an issue for such problems and ought to be closely monitored.

To present some arguments and data verifying the results of Chapter 4, a particular problem setting is recalled of the type repeatedly analyzed over there. That is, consider a boundary-value problem where the two-dimensional Laplace equation, written in spherical coordinates,

$$\frac{1}{a^2 \sin\phi}\frac{\partial}{\partial\phi}\left(\sin\phi\frac{\partial u(\phi,\theta)}{\partial\phi}\right)+\frac{1}{a^2\sin^2\phi}\frac{\partial^2 u(\phi,\theta)}{\partial\theta^2}=0,\quad (\phi,\theta)\in\Omega \tag{5.1}$$

is posed in the region

$$\Omega=\{\phi,\theta|\,\alpha\le\phi\le\beta,\ 0\le\theta<2\pi\}$$

that represents a spherical belt. Let the governing equation be subject to the boundary conditions

$$u(\phi,0)=u(\phi,2\pi),\qquad \frac{\partial u(\phi,0)}{\partial\theta}=\frac{\partial u(\phi,2\pi)}{\partial\theta} \tag{5.2}$$

and

$$u(\alpha,\theta)=0,\quad u(\beta,\theta)=0 \tag{5.3}$$

The Green's function for the above problem setting was obtained in Section 2.1 of Chapter 2 (see equation (2.42)). It appears in the form

$$\begin{aligned} G(\phi,\theta;\psi,\tau) &= H_P\left(\frac{A_0^2}{\Phi_0(\phi)\,\Phi_0(\psi)},\theta-\tau\right)+H_P\left(\frac{\Phi_0(\phi)\,\Phi_0(\psi)}{B_0^2},\theta-\tau\right)\\ &+\begin{cases} \ln\frac{\Phi_0(\phi)}{B_0}\ln\frac{\Phi_0(\psi)}{A_0}-H_P\left(\frac{\Phi_0(\phi)}{\Phi_0(\psi)},\theta-\tau\right)-H_P\left(\frac{\Phi_0(\psi)A_0^2}{\Phi_0(\phi)B_0^2},\theta-\tau\right)\\ \ln\frac{\Phi_0(\psi)}{B_0}\ln\frac{\Phi_0(\phi)}{A_0}-H_P\left(\frac{\Phi_0(\psi)}{\Phi_0(\phi)},\theta-\tau\right)-H_P\left(\frac{\Phi_0(\phi)A_0^2}{\Phi_0(\psi)B_0^2},\theta-\tau\right)\end{cases}\\ &+R_{DD} \end{aligned} \tag{5.4}$$

where the uniformly convergent series term of the regular component reads as

$$R_{DD}=R_{DD}(\phi,\theta;\psi,\tau)=\sum_{n=1}^{\infty}\frac{1}{2\pi n}\frac{A_0^{2n}\left(\Phi_0^{2n}(\phi)-B_0^{2n}\right)\left(\Phi_0^{2n}(\psi)-A_0^{2n}\right)}{B_0^{2n}\Phi_0^n(\phi)\,\Phi_0^n(\psi)\left(B_0^{2n}-A_0^{2n}\right)}\cos n\,(\theta-\tau)$$

and the upper branch of the last additive term in (5.4) stays for $\alpha \leq \phi \leq \psi$, whereas for the lower branch we have $\psi \leq \phi \leq \beta$.

Clearly, the form in (5.4) is ready for immediate computer implementation. Thus, one can employ this form to accurately compute a potential field generated in Ω by either a single point concentrated source or a finite set of distinct point concentrated sources.

On the other hand, the formulation in (5.1)-(5.3) might be considered as a boundary-value problem posed in a double-connected region that arises if a circular aperture, whose contour L represents the coordinate line $\phi = \alpha$, is cut out from the spherical cap

$$\Omega_0 = \{\phi, \theta |\, 0 \leq \phi \leq \beta,\ 0 \leq \theta < 2\pi\}. \tag{5.5}$$

In this case a profile $G(\phi, \theta; \psi^*, \tau^*)$ of the Green's function shown in (5.4) could be expressed, for an arbitrary location (ψ^*, τ^*) of the source point, in the form

$$G(\phi, \theta; \psi^*, \tau^*) = G_0(\phi, \theta; \psi^*, \tau^*) + \int_{\widetilde{L}} G_0(\phi, \theta; \psi, \tau)\mu(\psi, \tau) d\widetilde{L}(\psi, \tau) \tag{5.6}$$

where $G_0(\phi, \theta; \psi, \tau)$ is the Green's function to the boundary-value problem

$$u(\phi, 0) = u(\phi, 2\pi), \quad \frac{\partial u(\phi, 0)}{\partial \theta} = \frac{\partial u(\phi, 2\pi)}{\partial \theta} \tag{5.7}$$

and

$$\lim_{\phi \to 0} u(\phi, \theta) < \infty, \quad u(\beta, \theta) = 0 \tag{5.8}$$

posed in Ω_0, and $\widetilde{L}$ is a fictitious contour embraced with the actual aperture boundary L. We refer to $G_0(\phi, \theta; \psi, \tau)$ as the resolving Green's function. Its closed analytical representation

$$G_0(\phi, \theta; \psi, \tau) = \frac{1}{4\pi} \ln \left(\frac{B_0^2 \left(\Phi_0^2(\phi) - 2\Phi_0(\phi)\Phi_0(\psi)\cos(\theta - \tau) + \Phi_0^2(\psi)\right)}{B_0^4 - 2B_0^2\Phi_0(\phi)\Phi_0(\psi)\cos(\theta - \tau) + \Phi_0^2(\phi)\Phi_0^2(\psi)} \right) \tag{5.9}$$

can be found in Section 2.1 (see equation (2.41)).

The density function $\mu(\psi, \tau)$ in (5.6) can be obtained upon satisfying the first boundary condition of (5.3) at $\phi = \alpha$. This yields the regular functional equation

$$\int_{\widetilde{L}} G_0(\phi, \theta; \psi, \tau)\mu(\psi, \tau) d\widetilde{L}(\psi, \tau) = -G_0(\phi, \theta; \psi^*, \tau^*), \quad (\phi, \theta) \in L \tag{5.10}$$

in $\mu(\psi, \tau)$.

Clearly, after a regularizing location of the fictitious contour $\widetilde{L}$ is found, and the functional equation in (5.10) is numerically solved, we substitute the density function $\mu(\psi, \tau)$ in (5.6). This completes our numerical procedure and provides us with approximate values of the profile $G(\phi, \theta; \psi^*, \tau^*)$ of the Green's function that we are looking for. Comparing then the found approximate values of $G(\phi, \theta; \psi^*, \tau^*)$ with their corresponding exact values directly computed by (5.4), we can obtain data that actually verify the efficiency of the used numerical procedure.

In Figure 28 and 29, we depicted the relative error for a particular problem setting with the parameter's values chosen as: $a = 1$, $\alpha = \pi/4$, $\beta = \pi/2$, $\psi^* = 3\pi/8$, $\tau^* = 2\pi/3$. Figure 28 shows the relative error in the entire domain Ω, whilst Figure 29 focuses on the relative error on the aperture's contour.

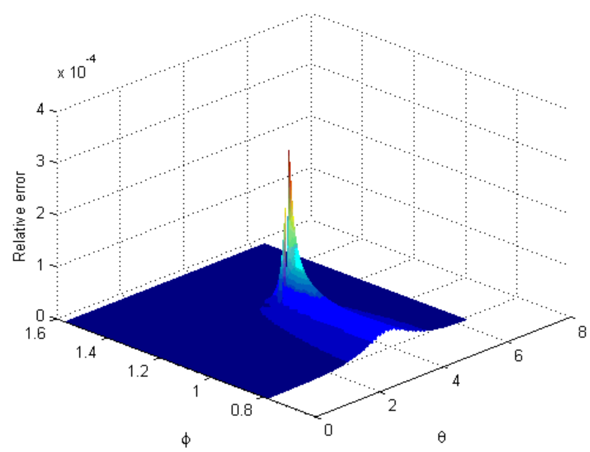

Figure 28: Relative error for the problem in (5.1)-(5.3) computed by (5.6) in Ω

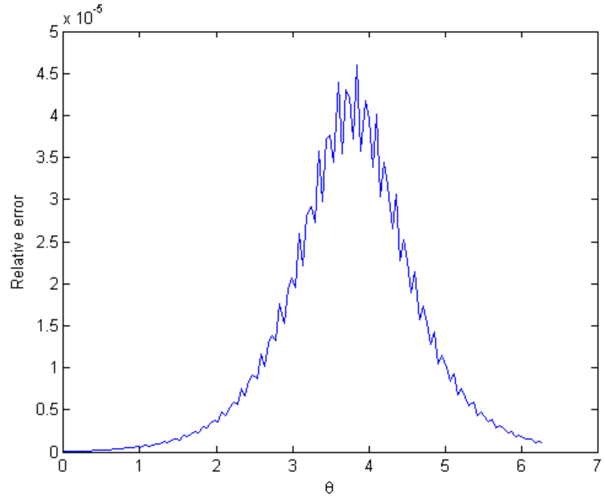

Figure 29: Relative error for the problem in (5.1)-(5.3) computed by (5.6) on L

To proceed further with our effort on collecting data that might be used to justify the results presented in our manual, another sample problem will be considered of the type that we have repeatedly dealt with. In doing so, we recall first, from Table 2 (see Chapter 2), the Green's function

$$\begin{aligned} G_0(z,\theta;s,\tau) &= aH_D\left(e^{\pi(z+s-2h)/a\gamma},\kappa,\eta\right) - aH_D\left(e^{\pi(z-s)/a\gamma},\kappa,\eta\right) \\ &\quad -aH_D\left(e^{\pi(-z+s-2h)/a\gamma},\kappa,\eta\right) + aH_D\left(e^{-\pi(z+s)/a\gamma},\kappa,\eta\right) + R \end{aligned} \tag{5.11}$$

of the boundary-value problem

$$\frac{\partial^2 u(z,\theta)}{\partial z^2} + \frac{1}{a^2}\frac{\partial^2 u(z,\theta)}{\partial \theta^2} = 0, \quad (z,\theta)\in\Omega_0 \tag{5.12}$$

$$u(0,\theta)=0, \qquad u(h,\theta)=0 \tag{5.13}$$

and

$$u(z,0)=0, \qquad u(z,\pi)=0 \tag{5.14}$$

posed in the rectangular region

$$\Omega_0 = \{z,\theta|\, 0\le z\le h,\ 0\le\theta\le\pi\}$$

which represents a finite fragment of a cylindrical surface of radius a and height h. The Green's function in (5.11) is presented for the case where $0 \leq z \leq s$, whilst the the case for $s \leq z \leq h$ could be obtained by interchanging variables z and s, the regular component $R = R\left(z, \theta; s, \tau\right)$ is defined as

$$R = R\left(z, \theta; s, \tau\right) = \sum_{n=1}^{\infty} \frac{a}{2\pi n} \frac{\sinh\left(n\pi z/\gamma a\right)\sinh\left(n\pi (s-h)/\gamma a\right)}{e^{2\pi n h/\gamma a}\sinh\left(n\pi h/\gamma a\right)} \left(\cos n\eta - \cos n\kappa\right)$$

where function $H_D\left(x, \alpha, \beta\right)$ and parameters η and κ where defined in Chapter 2 (see (2.23) and (2.21)).

Consider now the double-connected region Ω representing the just recalled Ω_0 weakened with a circular aperture whose contour is L. Let the Laplace equation in (5.12) be stated in Ω and subject to the boundary conditions in (5.13), (5.14), and the condition

$$u(z, \theta) = \Psi(z, \theta), \quad (z, \theta) \in L\ . \tag{5.15}$$

Let the right-hand side function $\Psi(z, \theta)$ in (5.15) represent trace that the profile $G_0(z, \theta; s^*, \tau^*)$ of the Green's function in (5.11) leaves on L (with the source point (s^*, τ^*) arbitrarily fixed inside of L). If so, then $G_0(z, \theta; s^*, \tau^*)$, as a function of z and θ, represents the exact solution to the boundary-value problem in (5.13)-(5.15) stated in Ω for the Laplace equation of (5.12).

So, with the exact solution $G_0(z, \theta; s^*, \tau^*)$ of the problem in (5.13)-(5.15) at hand, we can apply our version of the classical boundary integral equation method to compute its approximate solution $u_{aprx}(z, \theta)$. All the above creates a convenient situation where the accuracy level attained in computing $u_{aprx}(z, \theta)$ can be directly controlled. To illustrate the point, we depicted in Figures 30 and 31 the relative error for the boundary-value problem with the following parameter's values: $a = 1$, $h = 1$, $s^* = 0.35$, $\tau^* = 0.45\pi$, the aperture of radius 0.5 is located at $\left(0.35, 0.5\pi\right)$. Figure 30 shows the relative error in the entire domain Ω, whilst Figure 31 provides the relative error along the contour of the aperture.

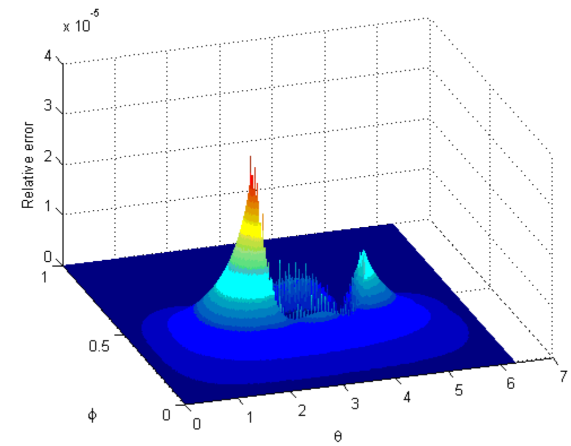

Figure 30: Relative error of the solution of the problem in (5.12)-(5.15) in Ω

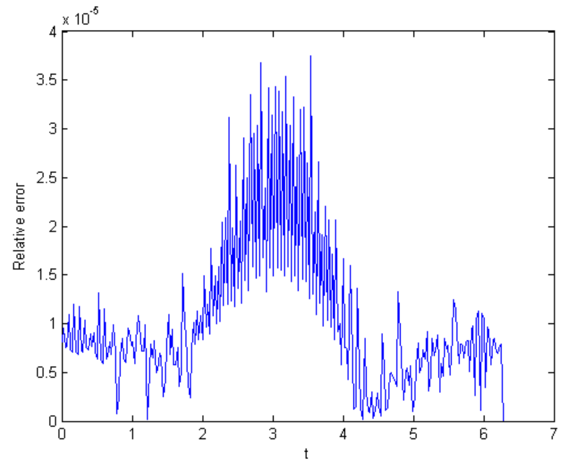

Figure 31: Relative error of the solution of the problem in (5.12)-(5.15) on L

The accuracy level shown in Figures 28-31 reveals computational efficiency of the technique proposed in this manual, and assures that our approach can be recommended for use in applied mathematics.

5.2 Parallelism in computer algorithms

Role of the parallelism in accelerating computational processes cannot be overestimated in nowadays, it has been recognized for decades. The scalable performance and lower cost of parallel algorithms is reflected in a vast variety of applications. The original desire for fast and efficient computation has been declared in a wide number of contexts involving initial and boundary-value problems for partial differential equations. This is so because there are heavy and extremely time consuming numerical computations that ought to be performed in this area of applied mathematics.

That is why, when an algorithm for solving a partial differential equation is designed in nowadays, it is highly desirable and recommended that it is parallelizable. We will show that our numerical routines based on the Green's function version of the boundary integral equation method represent a rather productive area for this contemporary and very efficient trend that in many cases allows to radically cut of the computational cost.

To illustrate the above mentioned point, we focus on just a single problem setting of a vast number of those we were dealing with in this volume. That is, we recall the boundary-value problem that has been tackled in Section 4.1. The problem is posed on a spherical biangle weakened with a circular aperture, and a potential field was computed in that region as induced by a set of point concentrated sources. It worth noting that the most expensive part of our computer algorithm was the image generation in high resolution depicted in Figure 19. To generate that figure, we were required to create, roughly saying, about one million images – one for each targeted grid-point (ϕ, θ) in the considered region. Taking into account that for each of those points, the Green's function $G(\phi, \theta; \psi^*, \tau^*)$ value (that simulates the field) is expressed in the integral-containing form

$$G(\phi, \theta; \psi^*, \tau^*) = G_0(\phi, \theta; \psi^*, \tau^*) + \int_{\widetilde{L}} G_0(\phi, \theta; \psi, \tau)\mu(\psi, \tau)d\widetilde{L}(\psi, \tau), \tag{5.16}$$

where the line integral has to be computed numerically after the density function is precomputed, the computational cost just for this part of our algorithm appears extremely high. Note, however, that, contrary to other numerical routines (based on the finite difference or the finite element methods, for instance, that could be considered as possible alternatives to our strategy), and where the field value at a single targeted grid-point (ϕ, θ) depends upon some information taken from a number of next-door grid-points, field values in our routine are completely independent and can be computed simultaneously. And this is what creates a perfect atmosphere for a possibility for the parallelism in, at least, this part of our algorithm.

The parallelism could be extended even further in our algorithm. Indeed, the integral operator in (5.16) might also be computed in parallel. To go this way, we parametrize first the fictitious contour $\widetilde{L}$ (introducing the polar angle parameter t), and transform then the line integral in (5.16) in the definite integral form as

$$\int_0^{2\pi} G_0(\phi, \theta; \psi(t), \tau(t))\mu(\psi(t), \tau(t))dt$$

At the next stage, an approximate value of the above definite integral, at each and every required field point (ϕ, θ) is computed by means of the standard trapezoid rule with N uniform grids. This yields

$$\begin{aligned} & \int_0^{2\pi} G_0(\phi, \theta; \psi(t), \tau(t))\mu(\psi(t), \tau(t))dt \\ \approx\ & \frac{\pi}{N} \sum_{i=0}^{N-1} [G_0(\phi, \theta; \psi(t_i), \tau(t_i))\mu(\psi(t_i), \tau(t_i)) \\ & + G_0(\phi, \theta; \psi(t_{i+1}), \tau(t_{i+1}))\mu(\psi(t_{i+1}), \tau(t_{i+1}))] \ . \end{aligned}$$

It is evident that each additive term in the above sum could potentially be computed independently in parallel. This implies that after all the additive terms in (5.12) are computed, a background for the ultimate summation is prepared and it can be conducted revealing the approximate value of the integral.

The chart in Figure 32 exhibits the speedup that we managed to achieve upon implementation of the parallelism strategy just described.

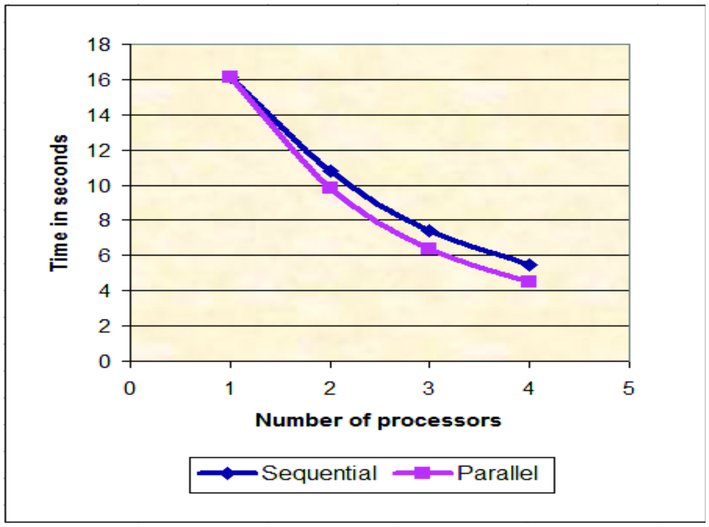

Figure 32: Computational speedup

Note that this brief section has not, of course, aimed at the detailed exploration of the possibility to parallelize all the numerical algorithms developed in the present study. Our goal was far less ambitious – we wanted to present just a single illustration of the fact that our algorithms represent a quite appropriate territory for that efficient computational modernism.

5.3 Inverse problems

Very important observation naturally arises from the analysis of our extensive research aiming at the incorporation of Green's functions and matrices of Green's type into traditional numerical algorithms of the classical boundary integral equation method and its numerous versions proposed more or less recently. From the available extensive data it follows that we can pretty much guarantee high accuracy level in solving direct boundary-value problems that simulate potential fields induced in complex thin-walled structures. And what sounds to users especially attractive and quite convincing that the Green's function-based numerical schemes, developed and intensively used in the preceding sections of this manual, allow us to obtain accurate enough solutions at a low computational expense.

All this creates a supportive atmosphere and opens a door to the realm of a certain class of inverse problems that are, on one hand, in huge demand in engineering and science, but represent, on another hand, extremely computationally expensive problem settings. Indeed, since one of the most widely implemented and efficient approaches to inverse problems is based on the method of successive approximations (where at each iteration we solve a direct problem, and the number of such iterations is often really massive counting in most cases hundreds and even thousands), a prospective of our approach to inverse problems looks really promising.

To provide some arguments verifying the above point, we are going to consider just one illustrative example of an inverse problem. That is, consider an inverse formulation of a boundary-value problem that arises as simulation of a potential field occurring in a thin shell. In doing so, consider a region Ω representing the fragment

$$\{\phi, \theta | \phi_0 \leq \phi \leq \phi_t; 0 \leq \theta < 2\pi\}$$

of the middle surface of a spherical shell of radius a weakened with a circular aperture whose contour is defined by intersection of the shell with a cylinder of radius r which is smaller than the shell diameter. The axis of the cylinder passes through the point $(\phi_c, 0)$ on the shell and the shell's center.

Let, in the triple-connected region Ω, $u(\phi, \theta)$ be the solution to the boundary-value problem

$$\frac{1}{a^2 \sin \phi} \frac{\partial}{\partial \phi} \left(\sin \phi \frac{\partial u(\phi, \theta)}{\partial \phi} \right) + \frac{1}{a^2 \sin^2 \phi} \frac{\partial^2 u(\phi, \theta)}{\partial \theta^2} = 0 \quad \phi, \theta \in \Omega \tag{5.17}$$

$$u(\phi, 0) = u(\phi, 2\pi), \qquad \frac{\partial u(\phi, 0)}{\partial \theta} = \frac{\partial u(\phi, 2\pi)}{\partial \theta} \tag{5.18}$$

$$\frac{\partial u(\phi_0, \theta)}{\partial \phi} = 0, \quad u(\phi_t, \theta) = 0 \tag{5.19}$$

and

$$u(\phi, \theta) = U, \quad (\phi, \theta) \in L \tag{5.20}$$

Here U is a given constant and L represents the aperture's contour.

The above formulation can, for instance, be interpreted as a simulation of the steady-state heat conduction field induced in the described fragment of a spherical belt-shaped shell perforated with a circular hole whose contour L is kept at a prescribed temperature level U. The edges $\phi = \phi_0$ and $\phi = \phi_t$ of the shell are kept at zero heat flux and zero temperature, respectively.

To present a possible inverse formulation of the problem in (5.17)-(5.20), we assume that some of its initial data are not available but ought to be determined to meet some constraints that are put on the solution we are looking for. To be more specific, let the size of the shell be given (implying that the parameters a, ϕ_0, and ϕ_t are fixed). Let also the value of U in (5.20) be fixed. Given that, we aim at the determination of the location and the size of the aperture (the values of r and ϕ_c are to be found) for which the following conditions hold

$$\max u\left(\phi_0, \theta\right) \leq A, \quad \max \frac{\partial u\left(\phi_t, \theta\right)}{\partial \phi} \leq B \tag{5.21}$$

where A and B are fixed constants.

It is not surprising that the above stated inverse problem is not, generally speaking, well-posed. Indeed, it quite might happen that for some combination of initial data it has no solution, and moreover in a case when existence is not an issue, the problem might allow multiple solutions. We leave, however, aside the existence and uniqueness issue and focus on the finding just a single possible solution of the problem. This kind of approach to inverse problems is quite customarily accepted and usually implemented in engineering practice.

Our strategy of handling the described inverse problem is based on an efficient Green's function-oriented algorithm to solve the direct problem in (5.17)-(5.20). First, with all the parameters (a, ϕ_0, ϕ_t, r, ϕ_c, and U), specifying the statement of the direct problem in (5.17)-(5.20) fixed, we follow the approach developed in Chapter 4. That is, recall the Green's function

$$G_0(\phi,\theta;\psi,\tau) = H_P\left(\frac{\Phi_0(\phi)\,\Phi_0(\psi)}{B_0^2},\theta-\tau\right) - H_P\left(\frac{A_0^2}{\Phi_0(\phi)\,\Phi_0(\psi)},\theta-\tau\right) + \begin{cases} \ln\frac{B_0}{\Phi_0(\phi)} - H_P\left(\frac{\Phi_0(\phi)}{\Phi_0(\psi)},\theta-\tau\right) + H_P\left(\frac{\Phi_0(\psi)A_0^2}{\Phi_0(\phi)B_0^2},\theta-\tau\right) \\ \ln\frac{B_0}{\Phi_0(\psi)} - H_P\left(\frac{\Phi_0(\psi)}{\Phi_0(\phi)},\theta-\tau\right) + H_P\left(\frac{\Phi_0(\phi)A_0^2}{\Phi_0(\psi)B_0^2},\theta-\tau\right) \end{cases} + R$$

where

$$R = R(\phi,\theta;\psi,\tau) = \sum_{n=1}^{\infty}\frac{1}{2\pi n}\frac{A_0^{2n}\left(\Phi_0^{2n}(\phi)-B_0^{2n}\right)\left(\Phi_0^{2n}(\psi)+A_0^{2n}\right)}{B_0^{2n}\Phi_0^{n}(\phi)\,\Phi_0^{n}(\psi)\left(B_0^{2n}+A_0^{2n}\right)}\cos n(\theta-\tau)$$

of the boundary-value problem in (5.17)-(5.19) that we dealt earlier in Section 4.1, and express the solution to the problem in (5.17)-(5.20) in terms of the modified potential

$$u(\phi,\theta) = \int_{\widetilde{L}} G_0(\phi,\theta;\psi,\tau)\,\mu(\psi,\tau)\,d\widetilde{L}(\psi,\tau), \quad (\phi,\theta)\in\Omega \tag{5.22}$$

where $\widetilde{L}$ is a fictitious contour embraced by L. The density function $\mu(\psi,\tau)$ for the representation in (5.22) can be found by satisfying the boundary condition in (5.20). Namely, if the field point (ϕ,θ) in (5.22) is taken to the actual contour L of the aperture, one arrives at the regular functional (of integral type) equation

$$U = \int_{\widetilde{L}} G_0(\phi,\theta;\psi,\tau)\,\mu(\psi,\tau)\,d\widetilde{L}(\psi,\tau), \quad (\phi,\theta)\in L \tag{5.23}$$

in $\mu(\psi,\tau)$.

Thus, the solution of the inverse problem just stated reduces to the system of non-linear equations

$$\begin{aligned} f_1(r,\phi_c) &= A \\ f_2(r,\phi_c) &= B \end{aligned} \tag{5.24}$$

in r and ϕ_c, where

$$f_1(r,\phi_c) \equiv \max u(\phi_0,\theta), \quad f_2(r,\phi_c) \equiv \max\frac{\partial u(\phi_t,\theta)}{\partial\phi}$$

The intricate point in solving the above system is that both functions $f_1(r,\phi_c)$ and $f_2(r,\phi_c)$ depend on their arguments implicitly. Hence, the standard techniques for solving systems of non-linear equations are problematic to directly apply. However, studying behavior of the functions $f_1(r, \phi_c)$ and $f_2(r, \phi_c)$, we discovered their remarkable properties that are helpful in the development of our strategy. That is, both of these functions increase if the variable r increases, whereas $f_1(r, \phi_c)$ decreases whilst $f_2(r, \phi_c)$ increases if the variable ϕ_c increases.

These properties allow us to use the following instruments in the iterative procedure to achieve an appropriate approximate solution of the system in (5.24):

1. if both $f_1(r, \phi_c)$ and $f_2(r, \phi_c)$ need to be increased, we increment the value of r;
2. if $f_1(r, \phi_c)$ has to be increased, whilst $f_2(r, \phi_c)$ must decrease, we decrement the value of ϕ_c;
3. if $f_1(r, \phi_c)$ is required to drop, and $f_2(r, \phi_c)$ has to go up, then the value of ϕ_c grows; and
4. if both $f_1(r, \phi_c)$ and $f_2(r, \phi_c)$ must decrease, then the value of r goes down.

The procedure should roll until a required accuracy level is achieved.

Following the described procedure, we solved the inverse problem stated earlier in this section. The parameters are set as $a = 1.0$, $\phi_0 = 0.1\pi$, $\phi_t = 0.5\pi$, $U = 1.0$, $A = 0.8$, $B = 2.0$. The recovered solution of the inverse problem is shown in Figure 33. The approximate values for the targeted parameters were found as $r \approx 0.1297$, $\phi_c \approx 1.0226$. It took 36 iterations with initial parameters' values of $r = 0.05$ and $\phi_c = 0.2\pi$ to achieve the accuracy level of order 10^{-4} for both parameters A and B.

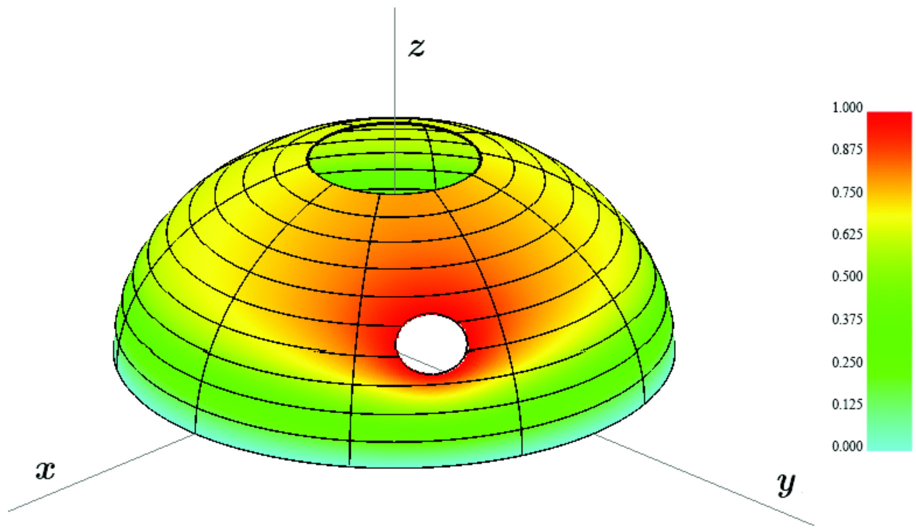

Figure 33: The recovered solution of the inverse problem

Our near future plan is to develop iterative procedures to tackle a wider class of inverse problems, where the computational algorithms created in the present study can be in help.

CONCLUDING REMARKS

An efficient half analytical-half numerical approach to the solution of boundary-value problems is proposed for the two-dimensional Laplace and Poisson equations stated in multiply-connected regions of irregular configuration on various surfaces of revolution. Solution of such problems is vitally critical for engineering and natural sciences because those mathematical problems simulate potential fields generated in thin shell structures made of conductive materials. The point is that shell structures represent widely used elements and fragments of contemporary machines and devices.

Governing differential equations in the boundary-value problems considered in the present work are written in geographical coordinates specific for every particular surface. This makes non-trivial the targeted problems which in turn requires the development of some non-trivial numerical schemes for their solution. Our approach to those problems implements a modification of the classical boundary integral equation method allowing us to achieve high potential of the developed computational algorithms.

The key stage of the approach to the solution of problems formulated on multiply-connected regions is the construction of readily computable representations of Green's functions and matrices of Green's type for some relevant simply-connected regions. Those functions and matrices are referred to as resolving Green's functions. They are utilized then to build up some integral representations of solutions of the targeted problems. A vast number of computer-friendly forms of resolving Green's functions and matrices is actually obtained, and their applicability is thoroughly tested.

Two important features stay behind the efficiency of our approach to problems stated in multiply-connected regions. First, since the resolving Green's functions are used as kernels in the integral representations of the solutions, the governing equations as well as most of boundary conditions in a considered problem are exactly satisfied prior to the computational stage of our algorithms. Second, all the factually required numerical work touches upon some regular one-dimensional functional equations where integral operators are to be approximated. This feature of our numerical algorithms provides a basis for attaining high accuracy level, which is repeatedly illustrated in this manual.

High computational potential of our Green's function-based approach to direct problems opened for us a door of inverse problems which we have proposed to tackle with the aid of iterative numerical procedures. At each successive approximation of the latter we run a corresponding algorithm developed in the present study for a relevant direct problem. Some explicit illustrations of the efficiency of the proposed strategy are presented.

To outline possible directions for extension of the present work, we focus on a few scenarios representing our objective in the near future. First, note that lateral surfaces of the shell structures considered herein are supposed to be thermally insulated which is not the case in many practical situations. Hence, development of workable algorithms for solution of problems simulating potential type fields induced in thin-walled structures whose lateral surfaces are not insulated looks quite promising if the reliable algorithms already tested in the present study are appropriately adjusted for that purpose. Another possible application of the results obtained herein could be associated with potential type phenomena occurring in thin shells made of either nonhomogeneous or anisotropic materials. One might also take a close look at an extension of the present study results to problems dealing with shells made of physically nonlinear materials.

LIST OF REFERENCES

1. Alzeer, I. and Qatanani, N., Numerical simulation of the steady state heat conduction equation, *International Journal of Mathematical Modeling, Simulation and Applications*, **2**, 1 (2008) 315-321

2. Andrews, M., Alternative separation of Laplace's equation in toroidal coordinates and its application to electrostatics, *Journal of Electrostatics*, **64**, 10 (2006) 664-672

3. Ang, D.D., Gorenflo, R., Le, V.K., and Trong, D.D., *Moment theory and some inverse problems in potential theory and heat conduction*, Springer-Verlag, Berlin, 2002

4. Antaki, P.J., Solution for non-Fourier dual phase lag heat conduction in a semi-infinite slab with surface heat flux, *International Journal of Heat and Mass Transfer*, **41**, 14 (1998) 2253-2258

5. Aster, R., Borchers, B., and Thurber, C., *Parameter estimation and inverse problems (2nd edition),* Elsevier Science & Technology, Oxford, 2012

6. Atluri, S.N., Kim, H.G., and Cho, J.Y., A critical assessment of the truly meshless local Petrov-Galerkin (MLPG), and local boundary integral equation (LBIE) methods, *Computational Mechanics*, **24**, 5 (1999) 348-372

7. Bag, S., Trivedi, A., and De, A., Development of a finite element based heat transfer model for conduction mode laser spot welding process using an adaptive volumetric heat source, *International Journal of Thermal Sciences*, **48**, 10 (2009) 1923-1931

8. Batycky, R.P. and Brenner, H., On the need for fictitious initial conditions in effective medium theories of transient nonconservative transport phenomena. Some elementary unsteady-state heat conduction examples, *Chemical Engineering Communications*, **153,** 3 (1996) 173-187

9. Bhattacharya, M.C., An explicit conditionally stable finite-difference equation for heat-conduction problems, *International Journal for Numerical Methods in Engineering*, **21**, 2 (1985) 239-265

10. Borodin, V.N., Construction of Green's functions for two-dimensional Laplace equation on spherical surface, In: *AMS sectional meeting*, Lincoln, NE, October 2011

11. Borodin, V.N., Recent advances in the construction of Green's functions for regions on surfaces of revolution, *Journal of Mathematical Sciences: Advances and Applications*, **15**, 1 (2012) 37-53

12. Borodin, V.N., A semi-analytic approach to the construction of Green's functions for the Laplace Equation posed in multiply-connected regions, In: *Ninth Mississippi state UAB conference*, Starkville, MS, October 2012

13. Borodin, V.N., A semi-analytical approach to Green's functions for problems in multiply-connected regions on a spherical surface, *Journal of Mathematics and System Science*, **3**, 12 (2013) 597-601

14. Borodin, V.N. and Melnikov, Yu.A., Matrices of Green's type for sets of Laplace equations posed on joint surfaces of revolution weakened with apertures, In: *Applied mathematical modeling and computational science '13 conference*, Waterloo, Canada, August 2013

15. Borodin, V.N. and Melnikov, Yu.A., Potential fields induced by point sources in assemblies of shells weakened with apertures, *Mathematical Methods in the Applied Sciences*, DOI: 10.1002/mma.3159, 2014

16. Borodin, V.N, Fields of potential induced by point sources in shell structures containing foreign inclusions, In: *The 37th annual meeting of the Texas partial differential equations conference*, Denton, TX, March 2014

17. Bourdin, E., Fauchais, P., and Boulos, M., Transient heat-conduction under plasma conditions, *International Journal of Heat and Mass Transfer*, **26**, 4 (1983) 567-582

18. Brebbia, C.A., *The boundary element method for engineers*, London, Pentech Press, New York, Halstead Press, 1978

19. Carslaw, H.S., Jaeger J.C., *Conduction of heat in solids*, Clarendon Press, Oxford, 1959

20. Chen, H.T. and Lin, J.Y., Numerical analysis for hyperbolic heat-conduction, *International Journal of Heat and Mass Transfer*, **36**, 11 (1993) 2891-2898

21. Chen, T.M., Numerical solution of hyperbolic heat conduction problems in the cylindrical coordinate system by the hybrid Green's function method, *International Journal of Heat and Mass Transfer*, **53**, 7-8 (2010) 1319-1325

22. Cheng, C.H. and Wu, C.Y., An approach combining body-fitted grid generation and conjugate gradient methods for shape design in heat conduction problems, *Numerical Heat Transfer Part B-Fundamentals*, **37**, 1 (2000) 69-83

23. Cruse, T.A., Ewing, A.P., and Wikswo, J.P., Green's function formulation of Laplace's equation for electromagnetic crack detection, *Computational Mechanics*, **23**, 5-6 (1999) 420-429

24. Dai, B., Zheng, B., Liang, Q., and Wang, L., Numerical solution of transient heat conduction problems using improved meshless local Petrov–Galerkin method, *Appl. Math. Comput.* **219**, 19 (2013) 10044–10052

25. Dramicanin, M.D., Ristovski, Z.D., Djokovic, V., and Galovic, S., Conduction of heat in inhomogeneous solids, *Applied Physics Letters*, **73**, 3 (1998) 321-323

26. Duffy, D.G., *Green's Functions with Applications*, Chapman&Hall/CRC, London, 2001

27. Fan, R., Jiang, Y.Q., Yao, Y., Shiming, D., and Ma, Z.L., A study on the performance of a geothermal heat exchanger under coupled heat conduction and groundwater advection, *Energy*, **32**, 11 (2007) 2199-2209

28. Fernandes, A.P., Sousa, P.F.B., Borges, V.L., and Guimaraes, G., Use of 3D-transient analytical solution based on Green's function to reduce computational time in inverse heat conduction problems, *Applied Mathematical Modeling*, **34**, 12 (2010) 4040-4049

29. Fosalba, P. and Gaztanaga, E., Measurement of the gravitational potential evolution from the cross-correlation between WMAP and the APM Galaxy Survey, *Monthly Notices of the Royal Astronomical Society*, **350**, 3 (2004) L37-L41

30. Gradshteyn, I.S. and Ryzhik, I.M., *Tables of integrals, series and products (7th edition)*, Academic Press, London, 2007

31. Haberman, R., *Applied partial differential equations (4th edition)*, Pearson Education Inc., New Jersey, 2004

32. Hào, D.N., *Methods for inverse heat conduction problems.* (English summary) Habilitationsschrift, University of Siegen, Siegen, 1996

33. Hon, Y.C. and Wei, T., A Fundamental solution method for inverse heat conduction problem, *Engineering Analysis with Boundary Elements,* **28**, 4 (2004) 489-495

34. Hu, J., Zhou, X.M., and Hu, G.K., Design method for electromagnetic cloak with arbitrary shapes based on Laplace's equation, *Optics Express*, **17**, 3 (2009) 1308-1320

35. Hu, L., Zou, J., Fu, X., Yang, H.Y., Ruan, X.D., and Wang, C.Y., Divisionally analytical solutions of Laplace's equations for dry calibration of electromagnetic velocity probes, *Applied Mathematical Modelling*, **33**, 7 (2009) 3130-3150

36. Huang, S.C. and Chang, Y.P., Heat-conduction in unsteady, periodic, and steady states in laminated composites, *Journal of Heat Transfer-Transactions of the ASME*, **102**, 4 (1980) 742-748

37. Huang, S.C., Unsteady-state heat-conduction in semi-infinite regions with mixed-type boundary-conditions, *Journal of Heat Transfer-Transactions of the ASME*, **107**, 2 (1985) 489-491

38. Iijima, K., Numerical solution of backward heat conduction problems by a high order lattice-free finite difference method, *Journal of the Chinese Institute of Engineers*, **27**, 4 (2004) 611-620

39. Jain, P.K. and Singh, S., An exact analytical solution for two-dimensional, unsteady, multilayer heat conduction in spherical coordinates, *International Journal of Heat and Mass Transfer*, **53**, 9-10 (2010) 2133-2142

40. Johnson, C. and Nedelec, J.C., On the coupling of boundary integral and finite-element methods, *Mathematics of Computation*, **35**, 152 (1980) 1063-1079

41. Kienle, A. and Patterson, M.S., Improved solutions of the steady-state and the time-resolved diffusion equations for reflectance from a semi-infinite turbid medium, *Journal of the Optical Society of America A-Optics Image Science and Vision*, **14**, 1 (1997) 246-254

42. Lee S.C., Cunnington G.R., Conduction and radiation heat transfer in high-porosity fiber thermal insulation, *Journal of Thermophysics and Heat Transfer*, **14**, 2 (2000) 121-136

43. Lewandowska, M. and Malinowski, L., An analytical solution of the hyperbolic heat conduction equation for the case of a finite medium symmetrically heated on both sides, *International Communications in Heat and Mass Transfer*, **33**, 1 (2006) 61-69

44. Liu, L., *Finite element analysis of nonlinear heat conduction problems.* Dissertation, University of Jyväskylä, Jyväskylä, 1997. Report, 75. University of Jyväskylä, Department of Mathematics, Jyväskylä, 1997

45. Llebot, J.E., Jou, D., and Casasvazquez, J., A thermodynamic approach to heat and electric conduction in solids, *Physica A*, **121**, 3 (1983) 552-562

46. McNabb, A., Wake, G.C., and Hossain Md.M., *Transition times between steady-states for heat conduction. Part I. General theory and some exact results.* Occasional Publications in Mathematics and Statistics, 20. Massey University, Departments of Mathematics and Statistics, Palmerston North, 1990

47. Melnikov, Yu.A., Some applications of the Green's function method in mechanics, *International Journal of Solids and Structures,* **13**, 5 (1977) 1045-1058

48. Melnikov, Yu.A., Green's function formalism extended to systems of differential equations posed on graphs, *Journal of Engineering Mathematics*, **34**, 3 (1998) 369-386

49. Melnikov, Yu.A., *Influence functions and matrices*, Marcel Dekker, New York, 1998

50. Melnikov, Yu.A. and Melnikov, M.Y., *Green's functions. Constructions and applications*, De Gruyter, Berlin/Boston, 2012

51. Meng, X.H. and Wang, P., Gravitational potential in the Palatini formulation of modified gravity, *General Relativity And Gravitation*, **36**, 8 (2004) 1947-1954

52. de Monte, F., Transient heat conduction in one-dimensional composite slab. A 'natural' analytic approach, *International Journal of Heat and Mass Transfer*, **43**, 19 (2000) 3607-3619

53. Morse, Ph. and Fechbach, H., *Methods of theoretical physics*, McGraw-Hill, New York, 1953

54. Peng, X.F., Wang, B.X., Peterson, G.P., and Ma, H.B., Experimental investigation of heat-transfer in flat plates with rectangular microchannels, *International Journal of Heat and Mass Transfer*, **38**, 1 (1995) 127-137

55. Pham, Q.T., A fast, unconditionally stable finite-difference scheme for heat-conduction with phase-change, *International Journal Of Heat And Mass Transfer*, **28**, 11 (1985) 2079-2084

56. Pham, Q.T., The use of lumped capacitance in the finite-element solution of heat-conduction problems with phase-change, *International Journal of Heat and Mass Transfer*, **29**, 2 (1986) 285-291

57. Press, W.H., Teukolsky, S.A., Vetterling, W.T., and Flannery, B.,P., *Numerical recipes: The art of scientific computing (3rd edition),* Cambridge University Press, New York, 2007

58. Prössdorf, S. and Schmidt, G., A finite element collocation method for singular integral equations, *Mathematische Nachrichten*, **100**, 1 (1981) 33–60

59. Pruess, K., Heat-transfer in fractured geothermal-reservoirs with boiling, *Water Resources Research*, **19**, 1 (1983) 201-208

60. Qin, M.H., Belarbi, R., Ait-Mokhtar, A., and Allard, F., Simulation of coupled heat and moisture transfer in air-conditioned buildings, *Automation In Construction*, **18**, 5 (2009) 624-631

61. Quaresma, J.N.N., Macedo, E.N., Da Fonseca, H.M., Orlande, H.R.B., and Cotta, R.M., An analysis of heat conduction models for nanofluids, *Heat Transfer Engineering*, **31**, 14 (2010) 1125-1136

62. Quillen, A.C., Frogel, J.A., and Gonzalez, R.A., The gravitational potential of the bar in NGC-4314, *Astrophysical Journal*, **437**, 1 (1994) 162-172

63. Ranganayakulu, C., Seetharamu, K.N., and Sreevatsan, K.V., The effects of longitudinal heat conduction in compact plate-fin and tube-fin heat exchangers using a finite element method, *International Journal of Heat and Mass Transfer*, **40**, 6 (1997) 1261-1277

64. Raudensky, M., Woodbury, K.A., Kral, J., and Brezina, T., Genetic algorithm in solution of inverse heat-conduction problems, *Numerical Heat Transfer Part B-Fundamentals*, **28**, 3 (1995) 293-306

65. Raynaud, M. and Bransier, J., A new finite-difference method for the nonlinear inverse heat-conduction problem, *Numerical Heat Transfer*, **9**, 1 (1986) 27-42

66. Seyidmamedov, Z.M. and Ozbilge, E., A mathematical model and numerical solution of interface problems for steady state heat conduction, *Mathematical Problems in Engineering*, Article Number: 20898, 2006

67. Skouras, E.D., Bourantas, G.C., Loukopoulos, V.C., and Nikiforidis, G.C., Truly meshless localized type techniques for the steady-state heat conduction problems for isotropic and functionally graded materials, *Engineering Analysis With Boundary Elements*, **35**, 3 (2011) 452-464

68. Sladek, J., Sladek, V., and Zhang, C., Transient heat conduction analysis in functionally graded materials by the meshless local boundary integral equation method, *Computational Materials Science*, **28**, 3-4 (2003) 494-504

69. Su, J. and Hewitt, G., Inverse heat conduction problem of estimating time-varying heat transfer coefficients, *Numerical Heat Transfer Part A: Applications,* **45**, 8 (2004) 777-789

70. Sun, K.H., Pyle, D.L., Fitt, A.D., Please, C.P., Baines, M.J., and Hall-Taylor, N., Numerical study of 2D heat transfer in a scraped surface heat exchanger, *Computers & Fluids*, **33**, 5-6 (2004) 869-880

71. Sun, K.H., Pyle, D.L., Fitt, A.D., Please, C.P., Baines, M.J., and Hall-Taylor, N., Heat transfer of nanofluids in a shell and tube heat exchanger, *International Journal Of Heat And Mass Transfer*, **53**, 1-3 (2010) 12-17

72. Tikhonov, A.N., Solution of incorrectly formulated problems and the regularization method. *Doklady Akademii Nauk SSSR* **151**, (1963) 501–504, (Translated in *Soviet Mathematics* **4**, (1973) 1035–1038)

73. Tikhonov, A.N. and Arsenin, V.Y., *Solutions of ill-posed problems,* Winston, New York, 1977

74. Tikhonov, A.N. and Goncharsky, A.V., *Ill-posed problems in the natural sciences,* Oxford University Press, Oxford, 1987

75. Tikhonov, A.N. and Samarskii, A.A., *Equations of mathematical physics*, Dover Publications, 1990

76. Tsirelman, N.M. and Zhiber, A.V., Solution of the unsteady-state heat-conduction problem for a two-dimensional region with a moving boundary, *International Journal Of Heat And Mass Transfer*, **30**, 7 (1987) 1259-1267

77. Tuan, P.C., Ji, C.C., Fong, L.W., and Huang, W.T., Am input estimation approach to on-line two-dimensional inverse heat conduction problems, *Numerical Heat Transfer Part B-Fundamentals*, **29**, 3 (1996) 345-363

78. Vadasz, P., Heat conduction in nanofluid suspensions, *Journal of Heat Transfer-Transactions of the ASME*, **128**, 5 (2006) 465-477

79. Wang, L., Zhou, X., and Wei, X., *Heat conduction. Mathematical models and analytical solutions.* Springer-Verlag, Berlin, 2008

80. Xiang, H.J. and Yang, J., Free and forced vibration of a laminated FGM Timoshenko beam of variable thickness under heat conduction, *Composites Part B-Engineering*, **39**, 2 (2008) 292-303

81. Yang, H.Q., Characteristics-based, high-order accurate and nonoscillatory numerical-method for hyperbolic heat-conduction, *Numerical Heat Transfer Part B-Fundamentals*, **18**, 2 (1990) 221-241

82. Yang, J.J., Huang, M., Yang, C.F., and Shi, J.H., Arbitrary shape electromagnetic transparent device based on Laplace's equation, *Radioengineering*, **20**, 1 (2011) 307-311

83. Yang, L., Yu, J.-N., Luo, G.-W., and Deng, Z.-C., Numerical identification of source terms for a two dimensional heat conduction problem in polar coordinate system. (English summary), *Appl. Math. Model.*, **37**, 3 (2013) 939–957

84. Yguel, F. and Peube, J.L., Combined effects of conduction, radiation and free-convection on the heat-transfer in a thick insulated wall, *Comptes Rendus De L Academie Des Sciences Serie* II, **292**, 13 (1981) 949-952

85. Young, G.W. and Chait, A., Steady-state thermal-solutal diffusion in a float zone, *Journal of Crystal Growth*, **96**, 1 (1989) 65-95

86. Yu, J.R. and Hsu, T.R., Analysis of heat-conduction in solids by space-time finite-element method, *International Journal for Numerical Methods in Engineering*, **21**, 11 (1985) 2001-2012

87. Zhang, Y.W. and Faghri, A., Vaporization, melting and heat conduction in the laser drilling process, *International Journal of Heat and Mass Transfer*, **42**, 10 (1999) 1775-1790

88. Zhu, T., Zhang, J.D., and Atluri, S.N., A local boundary integral equation (LBIE) method in computational mechanics, and a meshless discretization approach, *Computational Mechanics*, **21**, 3 (1998) 223-235

89. Zhu, T., Zhang, J., and Atluri, S.N., A meshless local boundary integral equation (LBIE) method for solving nonlinear problems, *Computational Mechanics*, **22**, 2 (1998) 174-186

90. Zhu, T.L., Zhang, J.D., and Atluri, S.N., A meshless numerical method based on the local boundary integral equation (LBIE) to solve linear and non-linear boundary value problems, *Engineering Analysis With Boundary Elements*, **23**, 5-6 (1999) 375-389

91. Zubair, S.M. and Chaudhry, M.A., Heat conduction in a semi-infinite solid due to ime-dependent laser source, *International Journal of Heat and Mass Transfer*, **39**, 14 (1996) 3067-3074